AD__________________

Award Number: DAMD17-99-1-9347

TITLE: Quantitative Image Quality Analysis of Soft Copy Displays

PRINCIPAL INVESTIGATOR: Dev P. Chakraborty, Ph.D.
Hans R. Roehrig, Ph.D.

CONTRACTING ORGANIZATION: University of Pennsylvania
Philadelphia, Pennsylvania 19104-3246

REPORT DATE: September 2002

TYPE OF REPORT: Final

PREPARED FOR: U.S. Army Medical Research and Materiel Command
Fort Detrick, Maryland 21702-5012

REPORT DOCUMENTATION PAGE

Form Approved
OMB No. 074-0188

1. AGENCY USE ONLY (Leave blank)

2. REPORT DATE
September 2002

3. REPORT TYPE AND DATES COVERED
Final (1 Sep 99 - 31 Aug 02)

4. TITLE AND SUBTITLE
Quantitative Image Quality Analysis of Soft Copy Displays

5. FUNDING NUMBERS
DAMD17-99-1-9347

6. AUTHOR(S)
Dev P. Chakraborty, Ph.D.
Hans R. Roehrig, Ph.D.

7. PERFORMING ORGANIZATION NAME(S) AND ADDRESS(ES)
University of Pennsylvania
Philadelphia, Pennsylvania 19104-3246

E-Mail: dchakraborty@mail.magee.edu

8. PERFORMING ORGANIZATION REPORT NUMBER

9. SPONSORING / MONITORING AGENCY NAME(S) AND ADDRESS(ES)

U.S. Army Medical Research and Materiel Command
Fort Detrick, Maryland 21702-5012

10. SPONSORING / MONITORING AGENCY REPORT NUMBER

11. SUPPLEMENTARY NOTES

12a. DISTRIBUTION / AVAILABILITY STATEMENT
Approved for Public Release; Distribution Unlimited.

12b. DISTRIBUTION CODE

13. ABSTRACT ***(Maximum 200 Words)***
The purpose of this work was to develop a computer based method for measuring the image quality of video displays used in digital mammography. The significance of this ability is that it will enable ready optimization of display image quality, and since the display is the weak link in digital mammography, this is expected to lead to better mammographer performance in detecting breast cancer. The original proposal involved application of the Computer Analysis of Mammography Phantom Images (CAMPI) algorithm to digital images of mammography phantom displayed on the monitor and images by a CCD camera. We have improved significantly on this idea and implemented an ideal-observer based method which is more suitable for display evaluation than CAMPI. This method has been applied to investigate the image quality of two digital mammography monitors with different phosphor types. The effect of CRYT luminance and pixel contrast has been evaluated. The measurements are of remarkable precision, allowing quantitative dependencies to be accurately demonstrated, no an extent never before possible. For example, the linear dependence of Signal-to-noise ratio on pixel contrast has been demonstrated to a high order or accuracy. We believe this method is novel and particularly advantageous for AMLCD displays that are being developed.

14. SUBJECT TERMS
Displays, CRT, Image Quality, CAMPI, Mammography, Phantoms, CCD

15. NUMBER OF PAGES
95

16. PRICE CODE

17. SECURITY CLASSIFICATION OF REPORT	18. SECURITY CLASSIFICATION OF THIS PAGE	19. SECURITY CLASSIFICATION OF ABSTRACT	20. LIMITATION OF ABSTRACT
Unclassified	Unclassified	Unclassified	Unlimited

NSN 7540-01-280-5500

Standard Form 298 (Rev. 2-89)
Prescribed by ANSI Std. Z39-18
298-102

Table of Contents

INTRODUCTION

The subject of this work is improving breast cancer detection via digital mammography. Breast cancer is potentially treatable if it is detected early. Digital mammography is widely believed to be a promising solution to problems faced by conventional mammography, but the advantages of digital are partially negated by the limitations of Cathode Ray Tube (CRT) displays.

The purpose of this work was to develop a computer based method (CAMPI – Computer Analysis of Mammography Phantom Images) for accurately measuring the image quality of video displays used in digital mammography. The significance of this ability is that it will enable optimization of display image quality. Since the display is the weak link in digital mammography, display optimization is expected to lead to better mammographer performance in detecting breast cancer. The scope of this research is developing efficient, accurate, and objective methodology for measuring display performance.

The original proposal involved application of the CAMPI algorithm, developed by the PI, to digital images of a mammography x-ray phantom that were displayed on the monitor and imaged by a Charge Coupled Device (CCD) camera. This approach turned out to be sub-optimal. We have improved significantly on this idea and implemented a method which is more suitable for display evaluation than the original CAMPI based idea. This method has been applied to investigate the image quality of two digital mammography monitors with different phosphors. Additionally the effect of CRT luminance and pixel contrast has been measured for both monitors. The measurements are remarkably precise, allowing quantitative dependencies to be accurately demonstrated, to an extent never before possible. We believe this method is novel and particularly advantageous for Advanced Matrix Liquid Crystal Display (AMLCD) displays that are being introduced for mammography, and plan to pursue this in future work.

The last annual report on this project was filed September 2001 and was accepted by the Army, with the recommendation that a revised SOW be included with future reports.

For convenience of reporting the numerical order of the tasks has been altered from the last report. The latter are referred to by their Original Task numbers. Indicated are the primary persons responsible for each task.

APPROVED TASKS / REVISED SOW

1. Acquire the CCD images (Roehrig)
2. Modify CAMPI software to analyze the CCD images and obtain SNR (Chakraborty)
3. Optimize the CCD acquisition method (Roehrig)
4. Quantify the image quality degradation due to the CCD acquisition (Roehrig)
5. Predict SNR measurements from available Fourier measurements and make bridging measurements (Chakraborty and Roehrig)

BODY OF REPORT

Personnel supported on Project

Dev Chakraborty, PhD, University of Pennsylvania
Hans Roehrig, PhD, University of Arizona
Mahesh Sivarudappa, MS, University of Arizona
Jiahua Fan MS, University of Arizona
Kunal Gandhi MS, University of Arizona
Amarpreet S. Chawla, University of Arizona

TASK: PERFORM IMAGE ACQUISITIONS

Use of CCD Camera for CRT and LCD evaluation

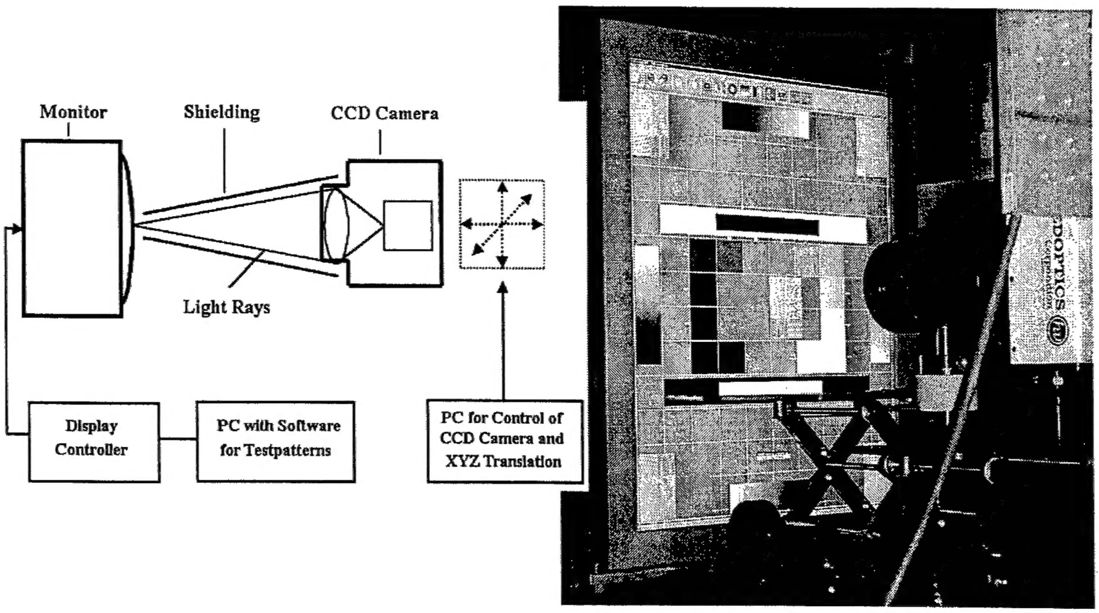

Fig. 1 Schematic of CCD acquisition of test-pattern images from a display.

Fig. 1 shows a schematic and a picture of the CCD camera ready to take a picture of the display. We setup the display on an optical table and mounted the CCD camera on an x-y-z translation stage. Then we stabilized, aligned and balanced the display and the camera with the help of an alignment laser, straight-edges and right-angle L-brackets. We also cleaned the display screen before the measurement, in order to remove finger prints.

Focusing the camera

Typically the camera is focused on the center of the display at the desired magnification ratio or pixel-ratio. Here the magnification ratio refers to the number of CCD pixels which cover (or "sample" the shape of) one display pixel.

In order to get a good focus, we use F# 2.8 for the relative lens aperture because the depth of focus at F# 2.8 is smaller than that at F# 16 and one finds the optimum focus position more easily. Once the optimum focus position is found the relative lens aperture is changed to F# 16 for taking the images of interest to this project. A relative lens aperture of F#16 is used in order to

reduce the veiling glare effect of the lens, and at the same time we achieve a larger depth of focus in case there are focusing errors.

The actual focusing procedure is a quantitative one and is as follows. First we display a vertical square wave pattern with a spatial frequency 1-vertical display line-on-1-vertical display line-off and then take an image of this pattern with the camera. In setting up the square wave pattern on the display, we make sure that the pattern fits easily into the field of view of the camera. We find the magnification ratio by counting the linear number of CCD pixels making up image of the square-wave test pattern on the CCD image in the horizontal direction and we relate this to the linear number of display pixels, making up the square-wave pattern in the horizontal direction. If the ratio of CCD pixels to CRT pixels is not the desired value, we change the camera to display distance, focus again and find the new value. This process is repeated until the desired pixel ratio is found. Notice that this procedure is very time consuming and was a big factor in finding the optimum pixel ratio!

We find the optimum focus position quantitatively by calculating the statistics of the CCD image, i.e., the sample standard deviation. Here the idea is, the higher the sample standard deviation, the sharper is the image and the better is the focus. We assume that the camera is well focused when the sample standard deviation reaches the maximum. From our experience, it is an objective and practical method to make very fine adjustments for the focus. When the optimum focus is reached, we switch the relative lens aperture to F# 16.

Images were acquired and transferred to CD ROM. Additional luminance calibration data was acquired, see Appendix 1, which allowed the analysis to account for the non-linear transfer characteristic of the display monitor. These are described later in connection with the analysis of these images. The CD-ROM was mailed to the PI. This procedure was repeated (using different test patterns) several times as needed.

TASK: MODIFY CAMPI SOFTWARE TO ANALYZE THE CCD IMAGES

The original plan called for CAMPI measurements of image quality using the ACR (American College of Radiology) phantom. CAMPI is a method developed by the PI (Chakraborty and Eckert 1995, Chakraborty 1997, Chakraborty, 1999), which enables accurate measurement of the image quality based on analysis of mammography phantom images. As outlined in the Year 1 and Year 2 reports, and as noted in the last review, we made major improvements over the originally proposed method by switching from phantom images to *test patterns*.

Test patterns are computer generated digital images with known pixel values. The use of test-patterns is impossible in the context of x-ray image quality measurement, where one wishes to include x-ray factors and therefore must use a phantom that interacts with the x-ray beam. CAMPI was originally developed for x-ray image quality measurements. The CRT/CCD-camera combination in Fig. 1 is a transducer that transforms an input pixel distribution (the Display Driving Levels, or DDLs) into an output pixel distribution (CCD pixel values). To evaluate the fidelity of this transducer it is only necessary to apply known input pixel distributions, measure the resulting output pixel distributions, and determine the image degradation by comparing the two distributions. Using a phantom, as originally planned, would have included extraneous noise (x-ray and other) and other degradations, which would have obfuscated effects due to the CRT that we wanted to measure.

By switching to test patterns we also made significant progress towards Original Task 4 (predicting measured SNR from the Fourier measurements). For a test pattern the targets, locations and background are all known exactly. In the jargon of Signal detection Theory the test-pattern task is a Signal Known Exactly, Background Known Exactly and Location Known Exactly Task, abbreviated to SKE/BKE/LKE. For such tasks the problem of calculating the SNR has been solved (Burgess, 1990). Indeed, several ideal observer models (Eckstein, Abbey, et al. 2000) are available to calculate the SNR in the SKE/BKE/LKE task. In this manner by switching to test-patterns we leveraged work done by other investigators. The down side of this, and other important changes described below, was that we had to essentially rewrite all of our CAMPI code, and spend much more time on this task than originally anticipated.

The CAMPI approach is based on an idea we had originally proposed[2] that signal detectability, as quantified by SNR of targets, chosen to resemble objects of clinical relevance on a uniform

background, be used as image quality metrics. For example, the object to be detected could be a disk similar to a microcalcification speck. One measures the cross correlation (the summed product of corresponding pixel values) of the image of the disk with a template (the idealized target pixel value distribution), when the template is aligned with the image of the disk[1]. Similarly, one measures the noise cross correlation when the template is positioned at non-target sites. The ratio of the target cross-correlation to the standard deviation of the noise cross correlation is the desired SNR for detection of the disk object on a uniform background.

A related idea was proposed by Tapiovaara and Wagner (Tapiovaara and Wagner, 1993) who showed that by using an appropriately blurred (via the system MTF – Modulation Transfer Function) target as the template one obtains the non-pre-whitening matched filter (NPWMF) SNR. The TW template determining procedure involves acquiring two images, with and without a target. If the images are registered so that the backgrounds structures line up, the difference image is an estimate of the template. They also developed methodology for calculating the SNR of the NPWMF ideal observer. This type of model observer is ideal (in the Bayesian sense) if the noise is white. (For non-white noise, the corresponding filter is the pre-whitening matched filter, implementation of which requires knowledge of the NPS – Noise Power Spectra - of the imaging system.) Besides their original application to fluoroscopic image quality (Tapiovaara, 1993), we know of only one other application of the method to medical imaging, namely the CAMPI method developed by us (while not identical to the TW method, see below, the CAMPI method is closely related to it).

As originally planned, the first experiment was done with images of the ACR phantom and slightly modified CAMPI software (see Reportable Outcomes: Chakraborty, Sivarudrappa and Roehrig, 1999). These measurements were restricted to one monitor and difficult to interpret quantitatively, as the input images were x-ray images, whose signal and noise characteristics were unknown.

When we realized that test patterns would be a superior approach, we designed appropriate patterns. We wished to maintain relevance to mammography, where relevant ACR phantom objects are microcalcifications, fibers and masses. The first-pass test-patterns consisted of 25 identical targets, each consisting of a periodic array of target elements, which were either dots or horizontal or vertical line-segments, or disk-shaped objects of varying radii. An image of a

[1] The alignment step is critical to achieving high-accuracy SNR measurements. A strong feature of CAMPI (as noted independently by Dr. Bob Jennings, FDA) is its high accuracy alignment routine.

horizontal line pattern is shown in Fig. 2. Three background values were used with DDL values of 55, 127 and 200, and each uniform field was imaged 15 times by the CCD camera. The pixel value difference between the target and the background was varied, as was the spacing between the target elements.

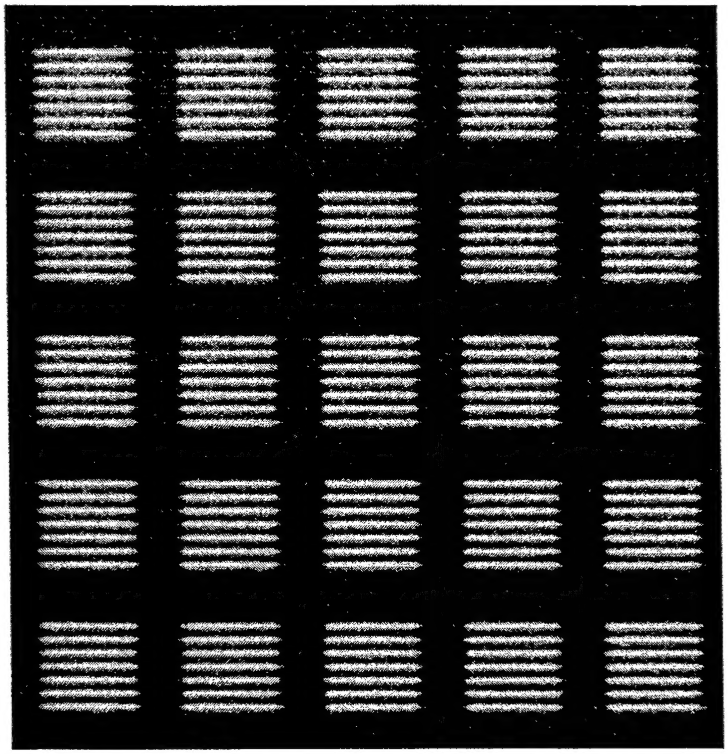

Fig. 2: example of a test-pattern with horizontal lines with a spacing of 2 pixels.

These images were analyzed by a modified CAMPI algorithm. The template used was the input test-pattern (in retrospect this was incorrect, as we should use the test-pattern appropriately blurred by the system MTF – this was corrected later, see below).

By this time we also started realizing that the CRT produces an image that is fundamentally different from a film image (produced by an x-ray machine, or digitized film, or direct digital images). A uniform object imaged by an x-ray machine will yield essentially uniform pixel values, apart from random noise. However, the image of a uniform test-pattern displayed on a monitor is not uniform, but contains superposed scan-lines. The scan-lines are readily evident in Fig. 2. This type of superimposed pattern is termed *stationary structured noise*. To suppress this effect a crude scan-line suppression algorithm was implemented (this is described in detail later). The SNR calculation consisted of calculating the cross-correlation of the template (one of the 25 identical targets in the input test pattern) with each of the 25 targets in the CCD image (as shown in Fig. 2). This was repeated for the 15 background only images, at 25 locations per background image. The 25 target samples and

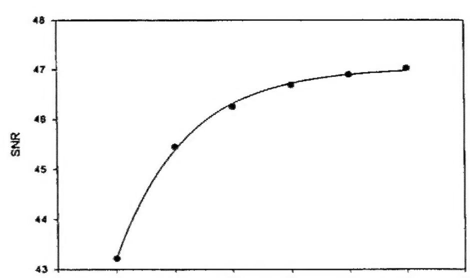

Fig. 3: non-linear dependence of SNR (y-axis) on dot-contrast. The solid line is an exponential fit.

the 375 (15 x 25) background samples were used to calculate the SNR in the manner described above. In all 162 target-containing CCD images and 45 (3x15) background images were analyzed. Two abstracts were submitted to the DOD conference (see Reportable Outcomes). We found that for high-contrast signals the P-45 phosphor did better than P-104, except at the highest luminance, where the reverse was true. We also noted that the dependence of SNR on target contrast was non-linear. An exponential function yielded a beautiful fit (see Fig. 3)! The SNR increased with contrast, but it appeared to level off, and in some cases (depending on the monitor or luminance) it even showed a maximum, beyond which SNR actually decreased with increasing dot contrast! This was very surprising.

Our criteria for "success" were repeatability, monotonic behavior and linearity of SNR with pixel contrast. Since SNR has signal in the numerator, it must scale linearly with contrast. The non-linear dependence raised our suspicion. Also some of the SNR values were noisy.

For a while we suspected imperfections in the critical alignment routines. This led to a redesigned test-pattern (shown in Fig. 4 for the special case of dot-targets) that included fiducial markers (high contrast single pixel dots positioned around the corners of each of the square signal areas, to aid in the alignment. This necessitated significant changes in the code, new images had to be acquired and analyzed, but it turned out that this did not solve the problem; in fact it made the alignment problem worse. In retrospect, to obtain good alignment one needs a lot of gray level information within the region that is used for alignment (so that mismatches in the information are easily noticed). One does better using the information within the target region itself to align it.

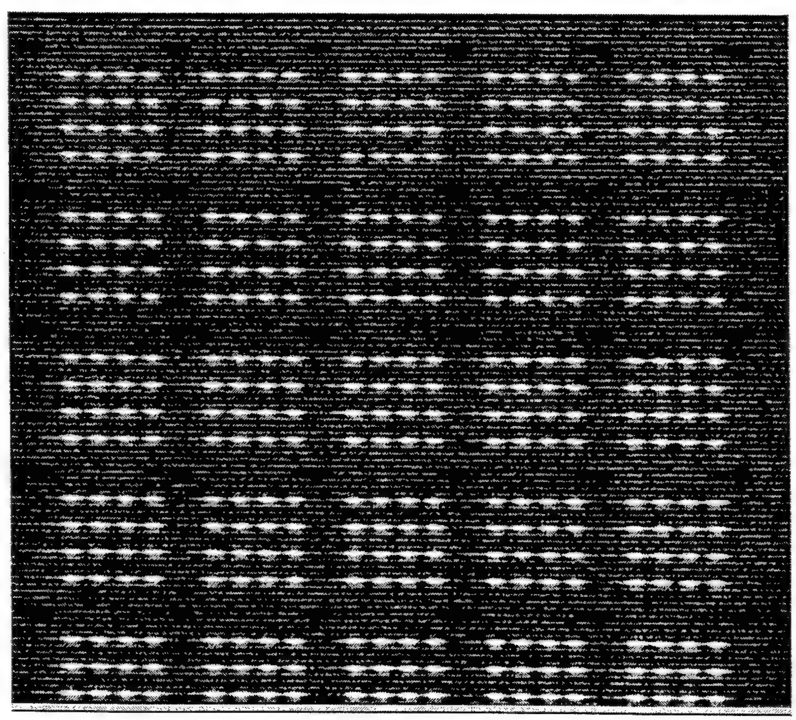

Fig. 4: redesigned test-pattern to reduce alignment errors. This was unsuccessful.

The preceding analysis used only 25 samples per target type. To reduce the noise we needed more samples. To obtain more samples we decided to concentrate on the dot–targets, Fig. 4, and regard each of the dots within each of the 25 target-groups as a target. This would only work for those images where the spacing between the dots was large; we used the 4-pixel spacing images already acquired. Now the number of signals (and noise) was larger by a factor of 16! The results from this test run were spectacular: the non-linear trend was still present, but the variability in the SNR values was much lower.

The logical conclusion of the success with the single dot measurements was to redesign the test pattern to consist only of dots, and to use a fairly large spacing (we compromised at 6-pixel spacing). Also instead of only one target image, we decided to use multiple number of target acquisitions and an equal number of background acquisitions. After some experimentation we decided on acquiring 3 targets and three background acquisitions for each test pattern. A typical test-pattern with the new design is shown in Fig. 5. Images are shown for both monitors and all three background values. No fiducial marks are needed, as each dot is individually aligned to the dot-template.

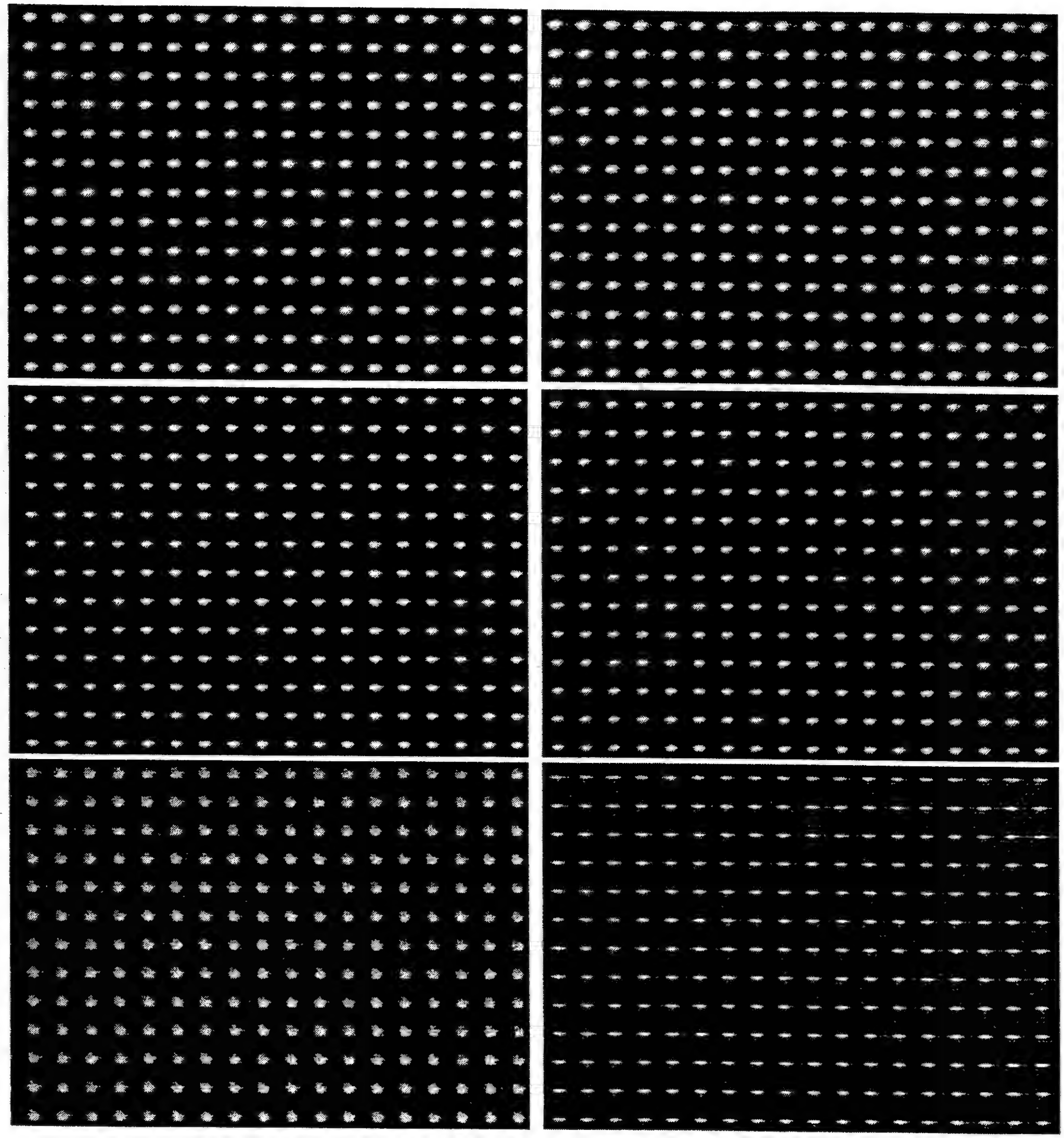

Figure 5: Shown are representative CCD images of the test patterns for the P-45 monitor (left column) and the P-104 monitor (right column) at three background pixel values: 55 (top row), 127 (middle row) and 200 (bottom row) respectively. The target test patterns consisted of single pixel "dots" spaced by 6 pixels in each direction and were imaged at a magnification of 8.

Scan-Line Registration

Another improvement came with our realization that the conventional TW method may not work for devices with significant stationary structured noise, e.g., scan-lines. *When scan-lines are present in the target and background images, care has to be taken before subtracting them by first aligning the scan-lines, and also normalizing them to equal amplitudes.* If this is not done then the scan-lines will not cancel and we will be left with a scan-line contaminated template. In hindsight, proper background alignment is implicit to a correct implementation of the TW method but the TW paper does not mention this point, as they were not dealing with raster-scan displays. We used one target image containing 600 single pixel dots, and a corresponding background test-pattern to estimate the template. The template is a single pixel dot (magnified by a factor of 8 by the CCD camera optics) and appears as a quasi-Gaussian blur as shown in the top-left figure of Fig. 7 (which is taken from Chakraborty, Fan et al, 2003, see Reportable Outcomes). Notice the ripples at the base of the diagram, due to imperfect subtraction of the scan-lines.

The contaminated template can give mysterious results depending on how well the residual-scan-lines in the template align with the scan-lines in the image whose SNR is to be measured. Therefore we developed a critical step to suppress the scan-lines in the template. The details are in the publication referred to, and we will merely show here that it works. The top-right figure in Fig. 7 shows the effect of the first step of the scan-line suppression procedure - note the significant reduction in the amplitude of the ripples. The bottom figure (Fig. 7) shows the final step of an iterative procedure - note the elimination of the scan-lines as a result of these steps. With this crucial change to the TW procedure, we obtained much better results.

Contrast Dependence of SNR and Image Linearization

We have noted above that we expected the SNR to be linear with contrast. The measurements had so far failed to yield the expected linearity. After a discussion with Bob Gagne (a scientist at the FDA Center for Devices and Radiological Health Laboratory in Twinbrook, MD), we realized that we needed to do the analysis in the DDL- value space, rather that the CCD-value space. In other words, we needed to linearize the pixel values.

As noted before, CRT calibration data was acquired by Dr. Hans Roehrig and Jiahua Fan (see Appendix 1 for a typical set of calibration data). This included measurements of CCD value vs. DDL values at different CCD-camera exposure times, MTF measurements, and the DICOM luminance calibration of the monitors (peak luminance was 500 Cd/m^2). This information was sent along with the CCD images on a CD-ROM to the PI. Figure 6 shows a typical dependence of CCD values per unit exposure time for an exposure time of 3 seconds (shown along the y-axis) on DDL values (shown along the x-axis). A polynomial fit is shown. This was not convenient, since to invert the function one would need to solve a cubic equation. SigmaPlot software was used to investigate different functions to fit DDL vs. CCD values (i.e., x and y are interchanged). We found that a three-parameter weighted exponential fit was sufficient. For the purpose of determining the weights we assumed 5% errors in the CCD values. All CCD images were linearized by transforming them via this function, which yielded DDL values. When the linearization correction was implemented, the results of the analysis were spectacular, see Figure 9 below.[2] This was a major turning point of the project.

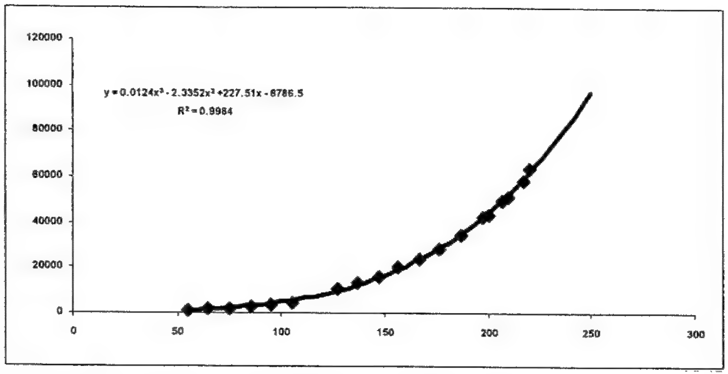

Fig. 6: Example of CRT calibration data used to linearize the data. X-axis is the DDL value, and y-axis is the CCD value.

[2] We had very helpful discussions at this point with Dr. Robert Gagne and Dr. Kyle Myers of the FDA/CDRH, in Twinbrook, MD. The PI made a one day trip to make a presentation of these results to the FDA group.

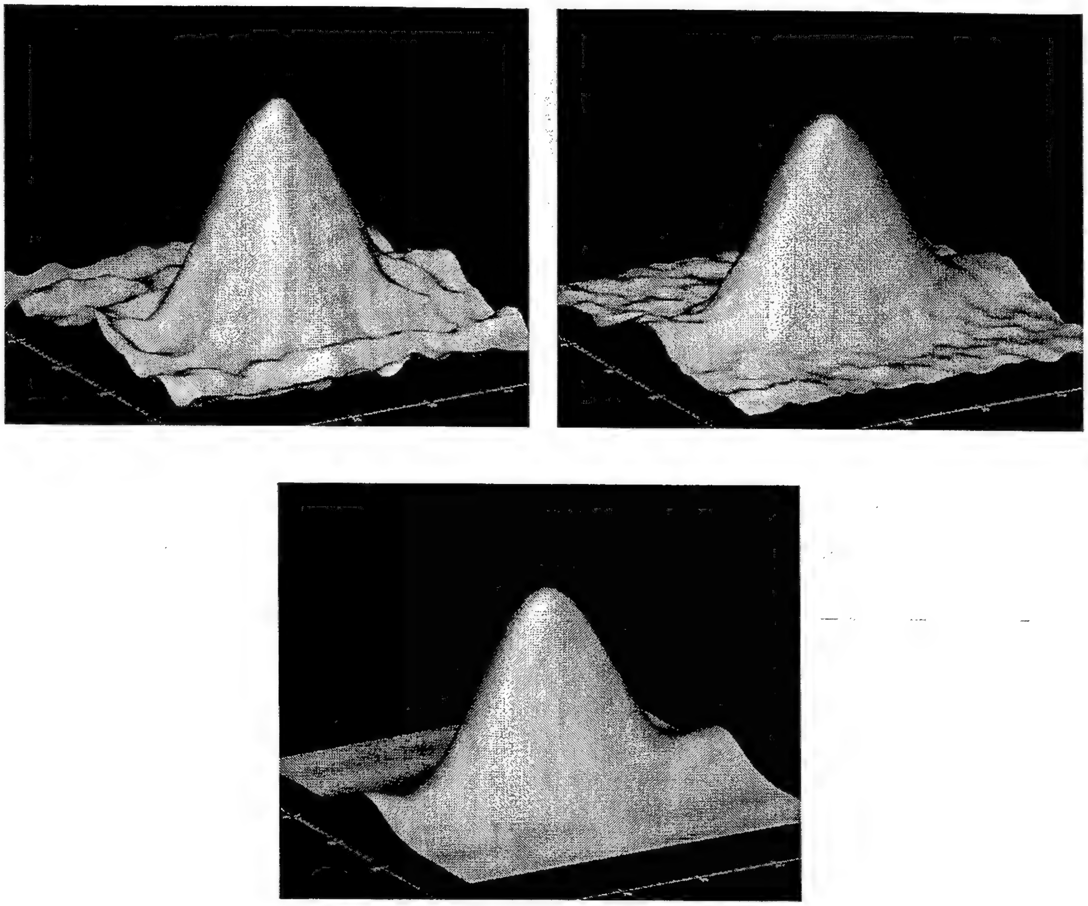

Figure 7: TW template estimation procedure: the top-left figure shows a 48 x 48 pixel region. The top-right figure shows the effect of aligning and subtracting the scan-lines from a background image – note the suppression of the scan-lines. The bottom figure shows the result of averaging 500-regions like the top-right figure – note the near elimination of the scan-lines.

SNR Analysis

As mentioned above, the template was determined from a pair of target-containing and background images. This pair of images is referred to as the "training set". The actual SNR measurement was done on two other pairs of images (testing set), yielding two SNR values. Note that no scan line suppression was used in this step, as we wished to measure the total detectability, which may be influenced by the presence of the scan-lines. All 3 pairs of images (3 target-containing and 3 backgrounds) were acquired under identical monitor conditions. The two SNR measurements were averaged. The procedure was repeated in "round-robin" fashion two more times, and we computed the grand mean and standard deviation of the 3 averaged SNR values. Only single pixel "dot" test-patterns were used in this work. The dots were on a 6-pixel grid (see Fig. 5). Most of the measurements were performed at the center of the CRT monitor at

a magnification of 8. The parameters varied were dot contrast (ten values), monitor luminance (3 values) and monitor type (P-45 vs. P-104). In a subset of measurements we varied the magnification and the location on the CRT where the test patterns were displayed (5 values: center plus 4-corners). The publication (see Reportable Outcomes: Chakraborty, Fan and Roehrig, 2003) describes the main set of measurements and will be summarized here.

Typical templates

These are shown in Fig. 8 for the P-45 monitor (left column) and P-104 (right column) for three display luminance values (DDL = 55, 127 and 200, corresponding to luminance of 9, 85, and 195 Cd/m^2 respectively). Note that each template is specific to a display condition – one cannot use a template determined for one condition to measure the SNR of a display in a different condition. This is an essential aspect of the TW methodology and allows effects such as focal spot blooming to be automatically included in the SNR analysis.

The 6 templates shown were for maximum dot-contrast. This was typically 100 DDL values (difference of pixel from surround), except when the background was at 200, when the maximum dot-contrast was 50 DDL values. (With an 8-bit display we cannot have test-pattern pixel values numbers greater than 255). The contrast was varied in steps of 10 starting from a minimum of 10. Not shown are templates at other contrast values.

General features evident from inspection of the templates

The template profiles are roughly two-dimensional Gaussian objects. We have successfully fitted them to such functions, in some cases with remarkable precision. If the fits were always reliable, then we could use the fitted templates instead of the actual templates for SNR determination. The advantage of this would be that the scan-lines (and other noise) are completely eliminated. However, the fitting procedure is not always reliable, especially for low-contrast dots, when there are residual scan line artifacts in the template and at high contrasts when the profile can be distinctly non-Gaussian. Residual scan line artifacts are visible in Fig. 8 in the P-104 image at 200 DDL. Non-gaussian behavior (double peak) is visible in Fig. 8 in the P-45 image at 200 DDL. To pursue this further we would need to model the scan-lines and the double peak nature of the template with additional parameters. While entirely feasible, due to time limitations we deferred this to a future investigation.

The scan direction is as indicated in the middle of Fig. 8 (see arrow). It is seen that the spot luminance profile is asymmetric in this direction – the luminance shows overshoot / undershoot effects beyond the dot. The reason for this is presently unclear.

The double peak evident in the P-45 image at 200 DDL is in the direction perpendicular to the scan-lines. Dr. Hans Roehrig has confirmed this general behavior with independent measurements. Note that the P-45 phosphor is not intended to be used at such high luminance, and this could be the reason for the non-Gaussian shape.

The importance of the templates cannot be over-emphasized. They are the major determinant of the accuracy of the SNR measurement. A faulty template (e.g., one with residual scan-lines) will lead to questionable SNR measurements. By visual inspection of the templates one can have a good idea of the reliability of a particular measurement.

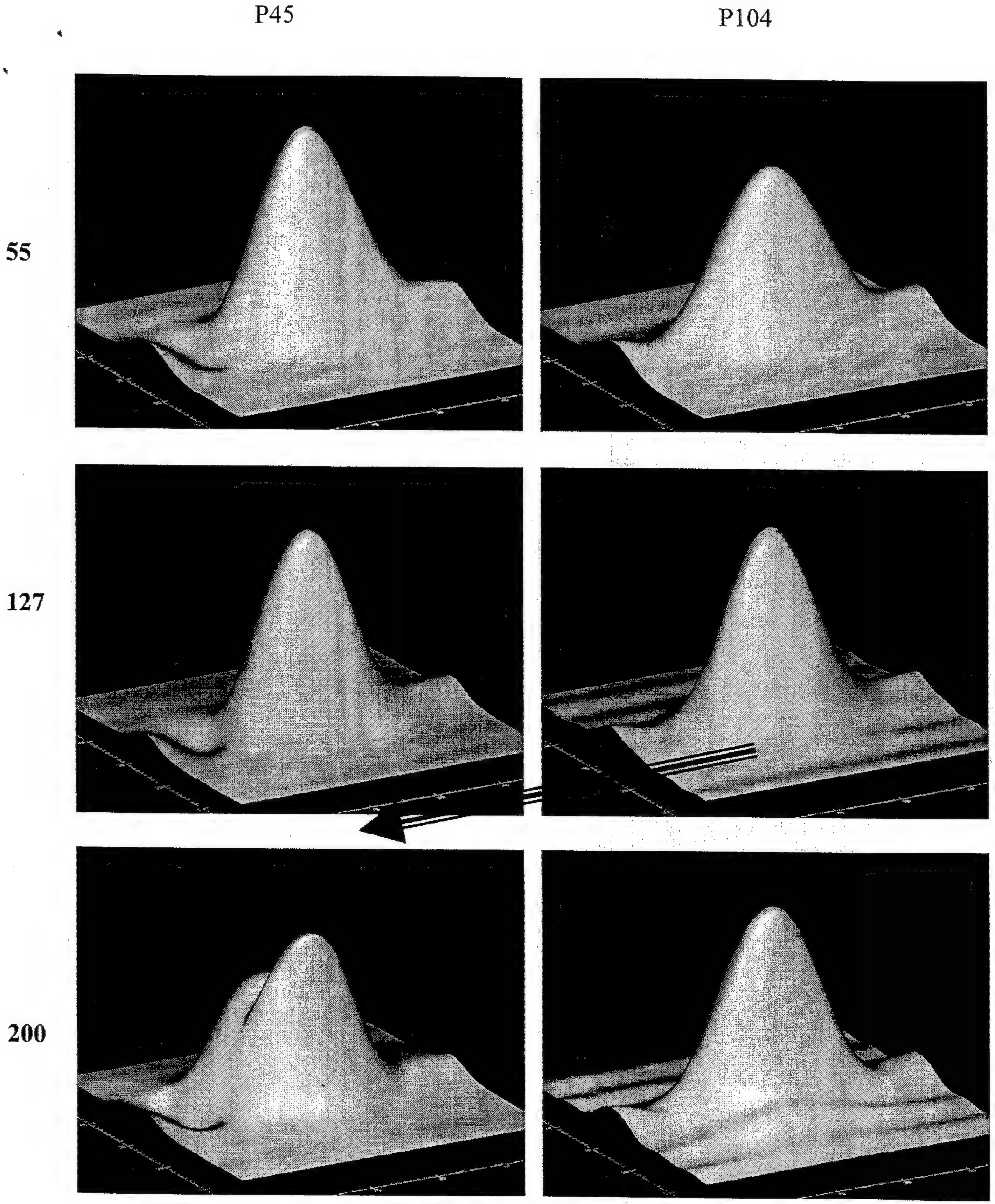

Figure 8: Typical templates; the scanning direction is as indicated. Note the deterioration in the template for the P-45 at the highest luminance.

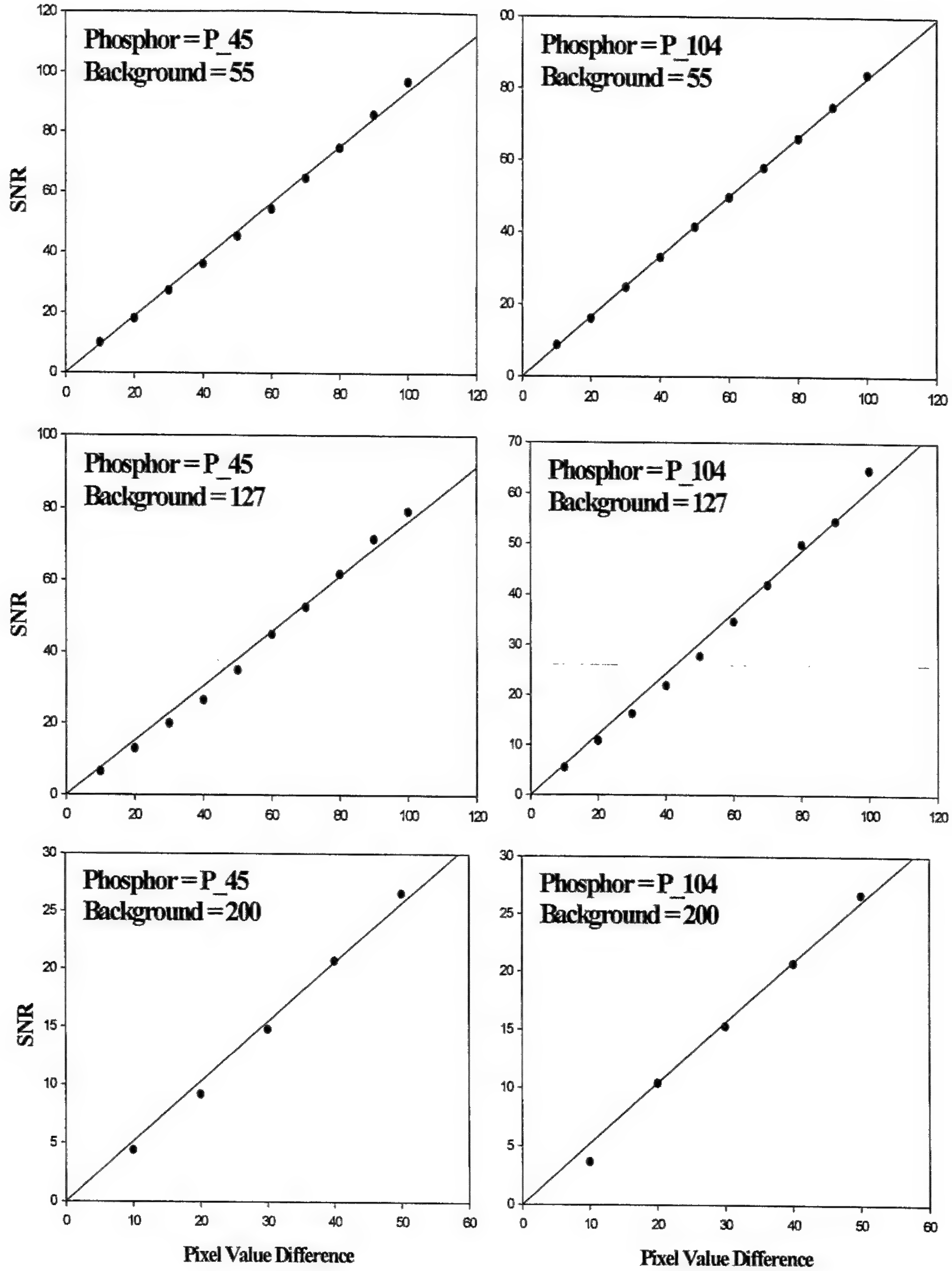

Figure 9: Contrast dependence of SNR: The left column shows the dependence of the measured SNR on dot-contrast, for the P-45 monitor, for three values of background pixel value, 55, 127 and 200 respectively. The right column shows corresponding plots for the P-104 phosphor.

Luminance and Phosphor Dependence of SNR

Fig. 9 is the spectacular result referred to earlier. The observed linear (r >= 0.997) dependence of SNR on dot contrast (labeled Pixel Value Difference in Fig. 9) means that one can use the slope of the straight line fit to define a normalized SNR per unit contrast, which is independent of dot-contrast, and depends only on luminance and the phosphor type. The slope of each regression straight-line, denoted by m and its standard deviation $\sigma(m)$ was calculated using a weighted least squares fitting procedure (REG in SAS) with weights $\sigma(SNR)$. The latter was available from the round-robin measurements. Fig. 10 shows a summary plot of the SNR of targets at equal Michelson contrasts – obtained by multiplying m by the corresponding pixel value. The multiplication is necessary as m represents the SNR per unit dot contrast and Michelson contrast equals dot-contrast per unit background pixel value. Note the superiority of the P-45 monitor at luminance below 100 Cd/m^2. Also note the overall increase of SNR with luminance, but a leveling off is observed. The reasons for this are presently unclear.

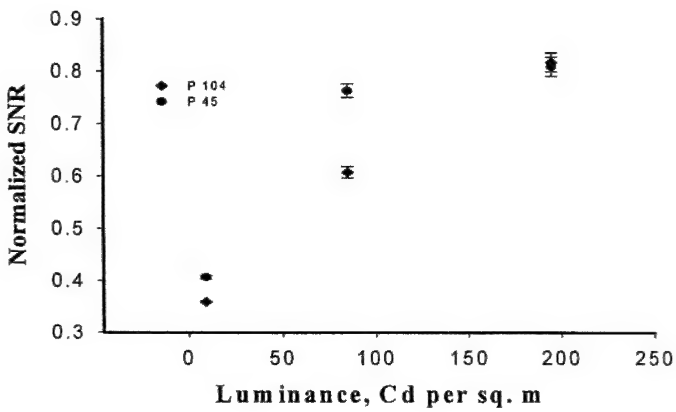

Figure 10: Luminance dependence of normalized SNR for the two phosphors.

Summary of the varying magnification CCD acquisitions

We acquired a set of images at different magnifications. Four values of magnification were investigated (mag = 3, 4, 6 and 8). At each magnification we acquired three target images and three background images of the dots-only test pattern (as in Fig. 5). These were analyzed as described above. In Fig. 11 is shown the SNR as a function of magnification. It shows a peak at about Mag = 6. This result can be understood qualitatively. Most imaging systems have multiple factors that limit image quality. These factors change differently with magnification, so that an optimal magnification exists when they are both acting together. See for example Sandrik, and Wagner, 1982. This paper shows that the detailed explanation of Fig. 11 will require calculations with measured MTF and NPS functions, along the lines of what was proposed for Original Task 4. This explanation is outside the scope of this work. For our purpose, the significant point is that the SNR depends in a qualitatively expected manner on magnification. Most importantly, it appears to vary smoothly. The calculations at Mag = 3 are much faster, as the images and template sizes all scale with the magnification. It appears that measurements at Mag = 3 may suffice for image quality measurements of the dots. This may be possible with inexpensive consumer grade digital cameras, rather than the expensive camera that we have. Whether this potential can be achieved cannot be answered at this point.

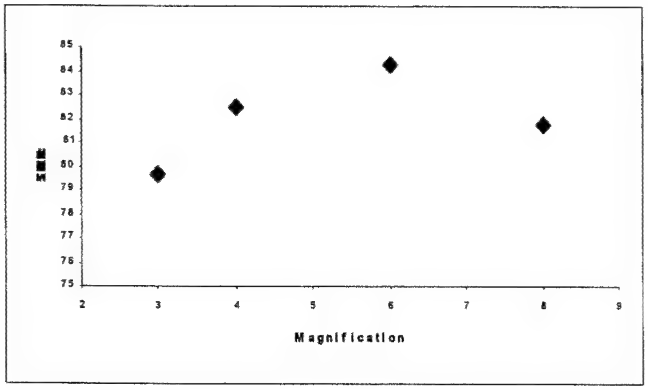

Fig. 11: Variation of SNR with magnification.

Summary of varying location CCD acquisitions

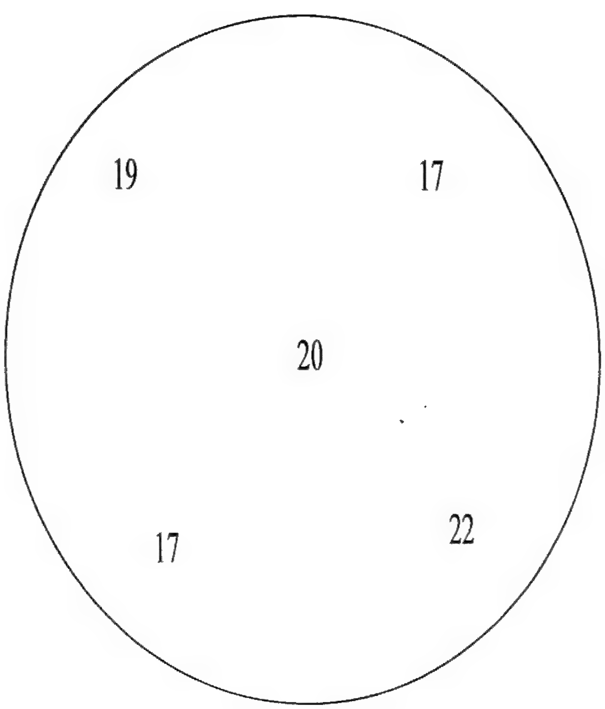

Fig. 12: SNR measurements at different locations on the P-45 monitor.

The measurements were made at the center, and four corners of the monitor. Results of these measurements are shown pictorially in Fig. 12. The mean SNR is 19.4 and the coefficient of variance is 10.5%. This result is another first – to our knowledge no one has measured the variation of signal detectability (SNR) over a medical monitor. The well known uniformity measurements performed for CRT displays in a PACS system consist of luminance measurements, only, which are insensitive to variations of MTF, contrast, and noise over the CRT faceplate. Our measurements include all these factors, to the extent that they affect signal detectability.

Investigation of variability of the method

While not on the original task list, it was considered essential to evaluate the variability of the new method, as this could impact its utility. Of coursed, if the same template is applied to the same set of testing images, it will always yield the same SNR value. Variability arises since the acquired images of each test-pattern are exhibit fluctuations (noise) in pixel values. We selected one horizontal line (HL) test-pattern, similar to that shown in Fig. 2, with background set to 127, and with 2-pixel spacing between the lines. Also generated was a blank test-pattern at background DDL = 127. We obtained ten (10) CCD images of each test-pattern under standard conditions (mag = 8). The ten image pairs (HL and background) are indexed 0, 1, 2, ..., 9.

To evaluate the variability due to our imperfect knowledge of the template, we constructed the template by training on pairs 0 and 1 (4 training images) and testing on pair 9. Similarly we re-determined the template by training on 2 and 3, and tested on 9. This was repeated 2 more times, each time training on a different pair of input images (specifically 4,5 and 6,7), and we always measured the SNR on pair 9. The observed variation must be due to template variability. The observed CV (coefficient of variance = standard deviation divided by the mean) of the measured SNR values was 3.3%. In another analysis we used the template obtained by training on image pairs 6,7 and testing on pairs 0, 1, 2, 3, 4, 5 and 9. The CV of the measurements was 6.8%.

These measurements were conducted on the HL pattern (as in Fig. 2), which has since been replaced by the dots (Fig. 5). Due to greater number of signal and noise samples, the errors are considerably smaller with the new design. Based on the fitting error in the linear fits of Fig. 9, the error is about 2%.

We end this section by showing what we proposed to do in the original application for this task, and explaining any discrepancies.

```
For Each Monitor (1 of 2) {
        Measure the Contrast Transfer Function;
        For Each LUT (1 of 9) {
                For Each Spot-Size (1 of 2) {
                        For Each Pre-processing (1 of 2) {
                                Measure MTF and NPS;
                                For Each Image (1 of 10) {
                                        Measure CCD/CAMPI indices;
                                }
                        }
                }
        }
}.
```

As noted in the Year1 report, the loops over LUT (Look-up tables) and pre-processing were eliminated by the switch to test patterns. This was stated in the two progress reports that have been submitted. As noted in the earlier report, we did not vary the focal spot size of the monitors, but rather concentrated on the P45 vs. P104 issue.

TASK: OPTIMIZE CCD IMAGING TECHNIQUE

Task: Optimize the CCD acquisition method. Determine the optimal optical magnification or, equivalently, the optimal pixel ratio, i.e., the number of CCD pixels to a CRT pixel. Determine necessary corrections to be made for CCD camera non-uniformity, vignetting of lens, CCD defects and CCD/lens MTF:

Sub-task 1: Optimal magnification or optimal pixel ratio.

We approached this sub-task from the point of view of Linear Systems Theory, which allows application of Fourier Transform Techniques. Here a linear system is a box with inputs and outputs. Most conveniently these inputs and outputs are sine-waves, representing the information from the display, which needs to be reproduced by imaging with the CCD camera. The optimal pixel ratio is that which reproduces the information displayed by the display accurately. Accordingly, the objective of the CCD camera is an accurate sampling of the various sine-waves making up the information displayed by the display. Insufficient sampling will lead to aliasing, a process which will transfer the power of a particular frequency into a lower frequency and consequently results in a wrong image and particularly in a wrong Noise Power Spectrum.

The information found on the face of a display consists of two parts. One part is that information which comes through the display's information channel, the highest frequency of which is given by the display's Nyquist frequency. The other part of the information consists of the display- or phosphor noise, the highest frequency of which is not precisely known. In fact it appears that the closer one gets to a display, particularly to a CRT (like with a microscope lens), the finer detail one observes. So it is very hard to avoid aliasing. A practical method to determine a cut-off frequency for a human observer is to find his MTF for the typical viewing distance of 0.5 m.

The accuracy in finding the desired information with the CCD camera is very much affected by the above mentioned sampling processes, but also by the spatial resolution of the CCD camera, specifically the Modulation Transfer Function of the combination lens-CCD.

For example if I(f) is the image produced by the CCD camera, and O(f) is the "object" displayed on the monitor, then:

$$I(f) = O(f) * P(f). \qquad (1)$$

Here P(f) is the CCD camera's Transfer Function. In particular, it is the Fourier Transform of the imaging system's Point-Spread Function (PSF) and f is the spatial frequency. P(f) is a complex quantity which can be written as

$$P(f) = |P(f)| \, e^{+i\phi} \qquad (2)$$

where |P(f)| is the modulus and ϕ is the phase. The modulus, normalized to unity at zero spatial frequency is called the MTF.

$$\mathrm{MTF}(f) = |P(f)|/P(0) \tag{3}$$

If the MTF of the CCD camera is known, then the digital data produced by the CCD camera can be processed with essentially the inverse of the MTF(f) to obtain:

$$O(f) = I(f)/\mathrm{MTF}(f). \tag{4}$$

There should be no degradation and the corrected CCD camera image should look just like the pattern on the display.

Clearly, one has to require that MTF(f) is never 0, but in a practical situation one will never use the exact inverse of the MTF(f). In addition, care must be taken in the consideration of: sampling conditions, positivity, and noise. The sampling enters because even if we could know the MTF of the system exactly, we have control over our compensating processing only at a discrete set of points. Those points are the pixel locations of the CCD. The positivity comes from the fact that we are using an incoherent imaging system whose point-spread function, PSF, is non-negative. Because both the MTF compensation and the MCE processing increase the relative strengths of signals

From these points of view, the optimum pixel ratio would be determined by the desire to accurately sample the information on the display and simply have a good MTF – possibly unity and the result would be that a large pixel ratio would be desirable, perhaps even values of 10 to 20 CCD-pixels per CRT pixel..

The sub-task of optimum pixel ratio can also be discussed from the point of view of the CCD pixel matrix size and display area to be analyzed, instead of from the point of view of Linear Systems Theory. The CCDs which we have in our labs have typically pixel matrices of 1317 x 1035 pixels, and frequently a display area of interest is subtending 100 x 100 display pixels. Consequently the maximum pixel ratio possible would then be 1035:100 = 10.35 CCD pixels / CRT pixel.

For one of our other research projects it is required to generate CCD camera images of CRT images subtending 250 x 250 CRT pixels. Here the pixel ratio can not be larger than 4:1. For that specific project the objective was to compare human observation of the images on a CRT with observation of these same images on the display by a computer model. Here the images on the display were imaged by the CCD camera and these CCD camera images were digitally fed to the computer model. It was estimated that for a pixel ratio of 4:1 pixel ratio, the cut-of frequency imposed by the CCD camera was the same as that of the human observer at a viewing distance of 0.50 m. Considering all points, it appeared that we should only work with magnification ratios of between 4 and 10.

Fig. 13 shows MTFs of the CCD Camera derived from the square-wave response for the 4 different magnification ratios 4, 6, 8 and 10. Note that as expected, as the magnification ratio increases, that means as the camera gets closer to the display and the lens focuses on more detail, the MTF of the camera is getting better. At a pixel ratio of 10:1 the MTF is about 95 % for most of the spatial frequencies of interest.

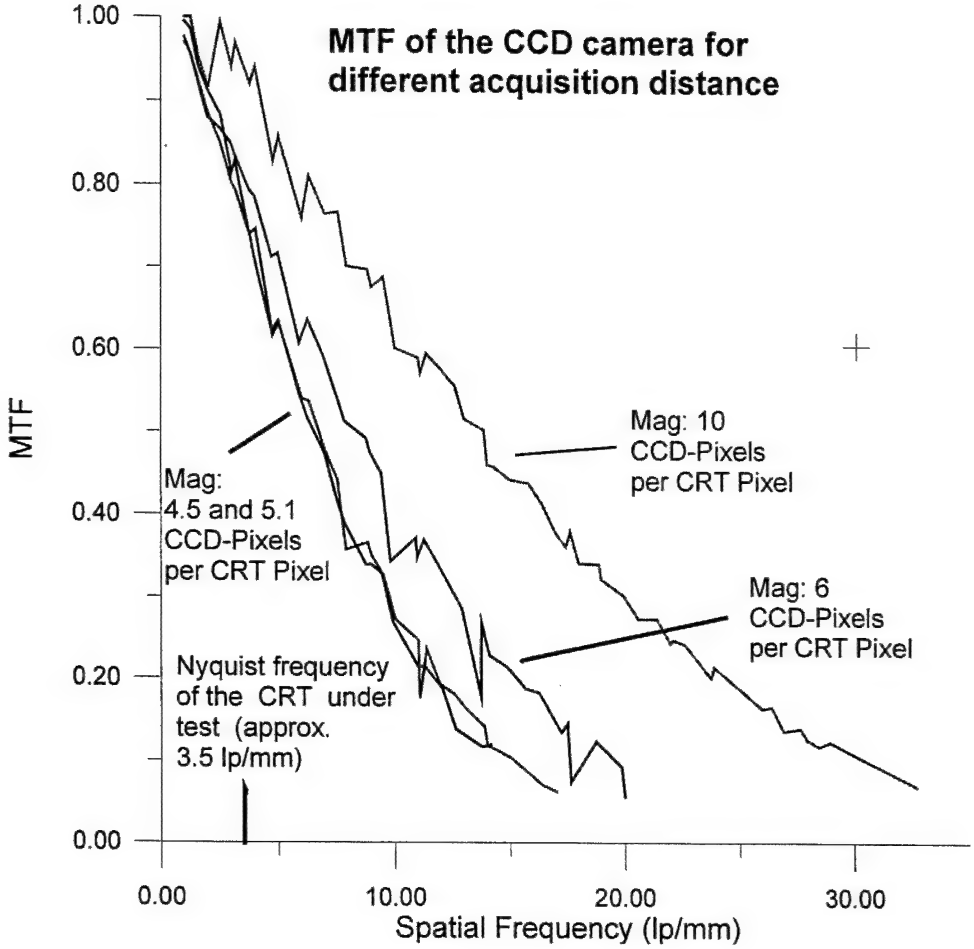

Fig. 13 MTFs of the CCD camera for pixel-ratios 4.5, 5.1, 6 and 10. The MTFs were derived from the camera's square-wave response

Fig. 14 shows Noise Power Spectra for the magnification ratios 53:1, 8:1 and 4:1 for two CRTs, one with a P45 phosphor and the other one with a P104 phosphor. It appears that the spatial frequencies displayed in the spectrum follow the principle that at high magnification (53:1) high frequencies are recorded (more detail), and at low magnification only lower spatial frequencies are recorded (less detail). Unfortunately, we were never able to systematically relate these power Spectra as they should following the respective MTFs of the CCD camera for the respective pixel ratios and the knowledge about aliasing caused by the CCD camera's sampling process.

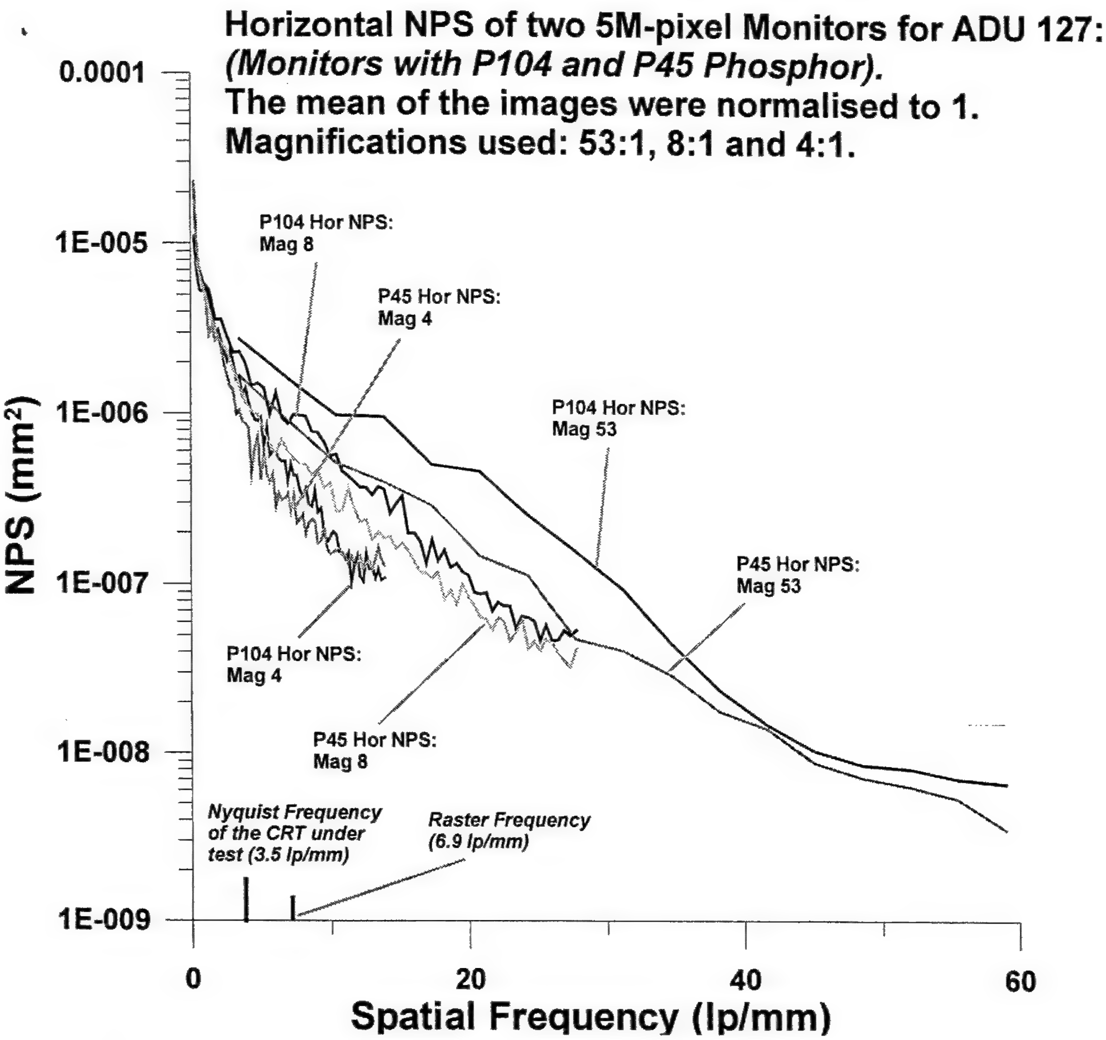

Fig. 14. NPS of two 5M-pixel CRTs, one with a P45 phosphor, and the other one with a P104 phosphor.

Sub-task 2: Corrections for CCD camera non-uniformity, vignetting of lens, and for CCD defects are made using the method of flat-field correction.

After the camera is focused, at the desired magnification ratio as described in under Task 3, we need to generate a flat-field image for the current setup. Flat-fielding is a common method to correct for non-uniformities and spatial noise of the CCD Camera and for vignetting of the lens. Here an image of a uniform field is taken by the CCD camera for the specific imaging geometry (i.e. magnification and lens F-stop). This image is stored in computer memory.

A simple and practical method has been adopted in our lab to get such a flat-field image. We put a high quality uniform opal glass in front of the display and direct the camera on it, but slightly defocused in order not to include non-uniformities of the opal glass. When displaying a uniform pattern with a high driving level, like DDL=255 on the display, the diffusing action of the opal glass provides a fairly uniform luminance. We take approximately 10 to 15 images of the practically uniform opal glass surface and average all "uniform" images. This averaged image is stored. Note that the temporal noise is reduced by averaging the individual images.

Next a dark image is generated, which represents the signal the CCD generates when it is in absolute darkness for some time and then read out. Finding the dark signal of the CCD is necessary, because despite the fact, that the CCD is cooled, every image with exposure to the scene also contains a certain amount of dark signal. This dark signal must be removed by subtraction if one wants to analyze the CCD's response to the exposure of the scene.

The dark image is found by running the camera without opening the camera shutter. Again we take many images (10 to 15) and average them in order to remove temporal noise. The resulting dark image is also stored in computer memory. Next the dark image is subtracted from the averaged light image; this difference image is called the "flat-field" and is stored in computer memory.

Now we are ready to take real images from the display and correct them for the camera's non-uniformities. The flat-fielding operation is as follows. We take an image of the desired scene and call it the raw image. Then the dark image from the computer memory is subtracted from the raw image. The resulting difference image is then devided by the flat-field pixel by pixel. Afterwards the devided image is multiplied by a factor proportional to the mean value of the flat-field to result in the corrected image of the desired scene.

This flat-fielding procedure has been incorporated in the software package, which runs the CCD camera. Flat-fielding is done automatically.

3. Sub-task 3: MTF of the combination Lens-CCD-Camera.

Two methods to determine the MTF of the combination Lens-CCD-Camera were explored: Using the square-wave response and the response due to a single point. The approach finding the MTF from the square-wave response was successful. The MTFs were shown in Fig. 13 above.

The approach finding the MTF from the point response has not been completed and will be continued under another research program. The experimental set-up is shown in Fig. 15. Fig. 16 shows as preliminary result a point-spread function (an Airy disk) for a relative aperture of F/# 16

Measurement of the MTF of a Lens-CCD combination (a CCD-Camera) using a "Spatial Filter" (a combination laser , microscope lens and a pinhole (a small aperture)).

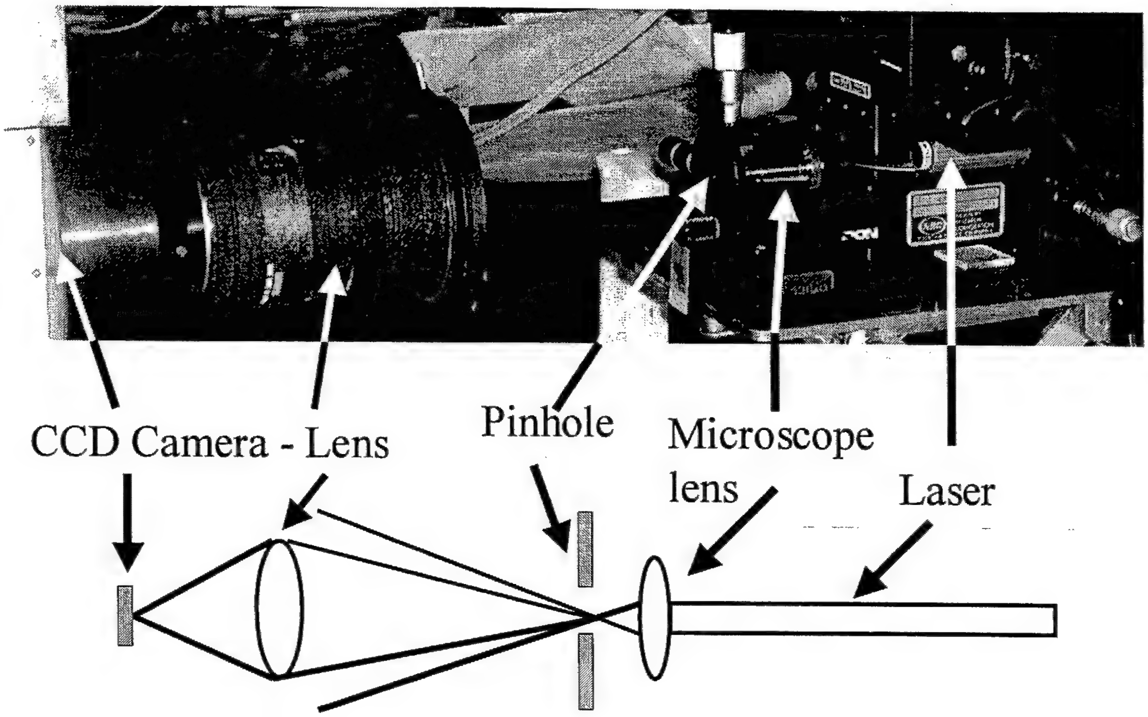

Fig. 15. Illustration of the method to find the MTF by imaging a pinhole

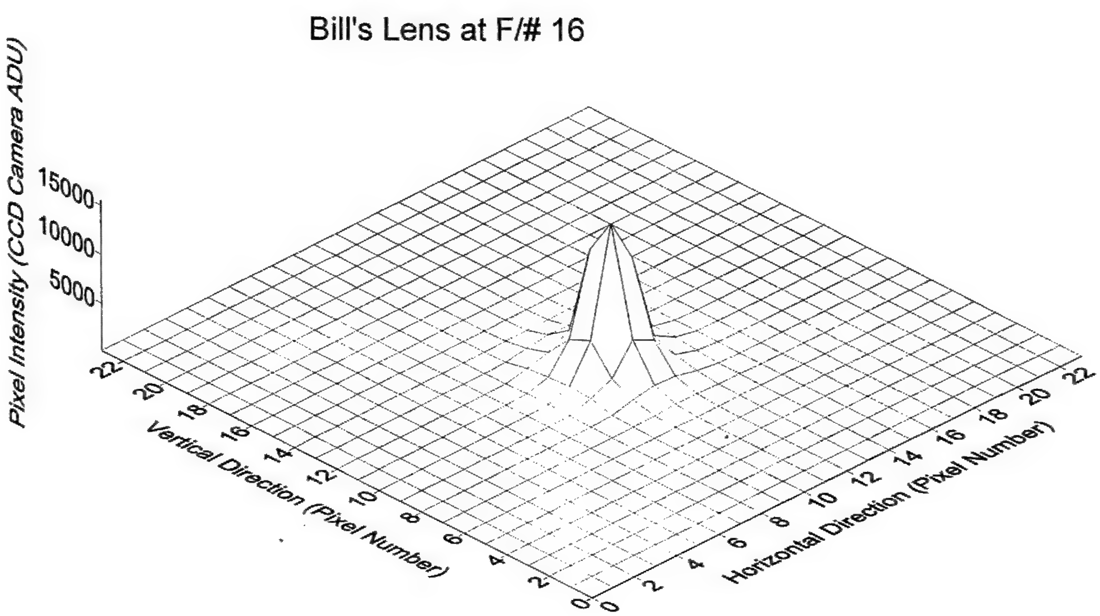

Fig 16: Point Spread Function of a lens with a relative aperture of F/#16.

Several presentations were made based on this work. These are included in Reportable Outcomes.

TASK: QUANTIFY THE DEGRADATION INTRODUCED BY THE CCD CAMERA

Image special films displayed on a high quality view-box, apply uniformity and distortion correction and measure physical image quality parameters.

The idea of this Task was to find a standard pattern representing a known amount of spatial noise, having a known shape of it power spectrum. The approach was to generate a digital image file consisting of noise only, having a known amount of spatial noise, having a white Noise Power Spectrum. This "image" was to be written on to typical clinically used film with a typical film printer. After development this film was to be imaged by the CCD camera. Subsequently the noise-Power-Spectrum of this image was to be generated.

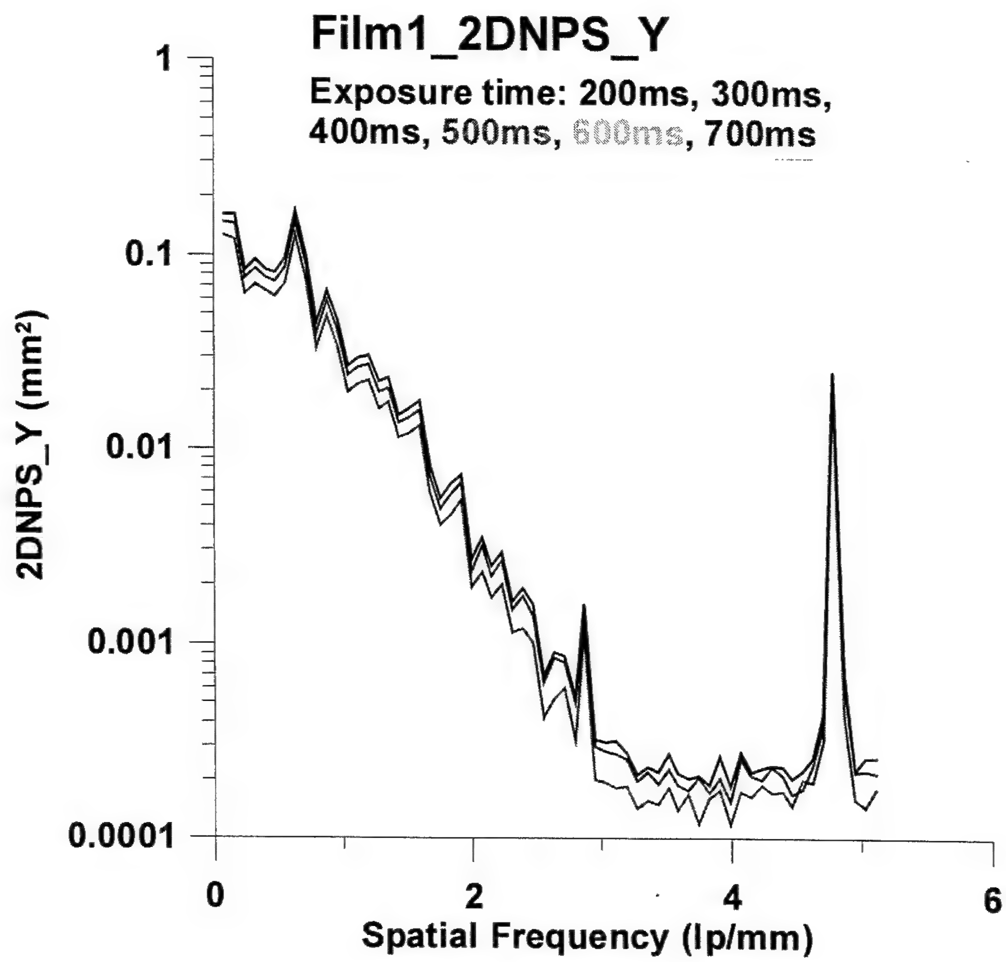

Fig. 17 a Noise Power Spectrum of film 1 in the y-direction.

Fig. 17 (a and b) are the result of a first try. Note that even though the image file displayed on the display had a white spectrum, the image captured by the CCD camera did not. An initial explanation has to consider the MTF of the film printer, but this could not be verified because no information on the properties of the film printer was available.

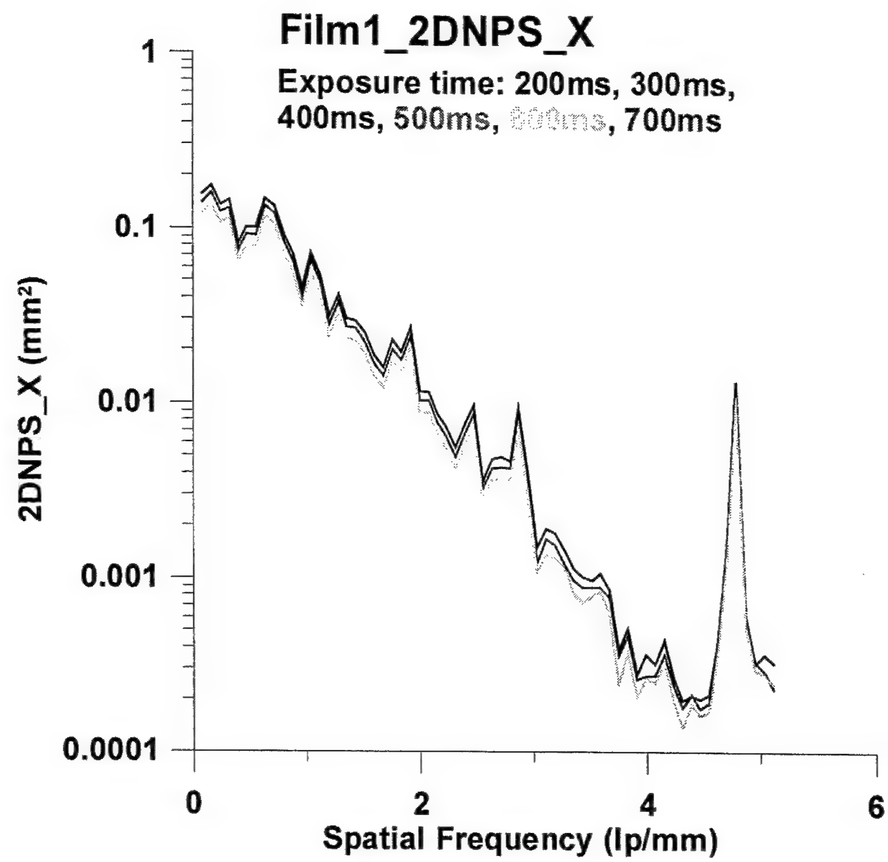

Fig. 17 b Noise Power Spectrum of film 1 in the x-direction

Since this experiment was not successful, it was decided in the middle of year three, to concentrate on measurements of physical image quality parameters as stipulated in the lower half of original Task 5. This slight modification was justified by the fact, that if indeed bridging attempts are to be successful, it is necessary to have a reliable method to find the MTF of the display.

Therefore we continued to improve the software for deriving CRT performance characteristics such as Modulation Transfer Functions (MTF) and Noise Power Spectra (NPS).

The accomplishments are summarized as follows.

1. **Generation and improvement of software.**

   a. **Improvement of the program to find the MTF from the square-wave response**

One of the refinements was an algorithm improved over the previous algorithm. In the previous one the Nyquist frequency was detected and depending on the ratio of the fundamental frequency and the Nyquist Frequency, the harmonics in the Fourier Transform data were picked up. This method was very sensitive to noise and consequently an erroneous value of the Nyquist Frequency was often calculated. With the improved algorithm the Nyquist Frequency

need not be calculated and the errors associated are avoided.

Fig. 18 is a block diagram, illustrating the various steps of the program. We worked on methods to standardize the determination of the Spatial Noise Power Spectrum such that measurements of the CRT Phosphor noise can be optimized.

The new program is described briefly in the following.

Operation:

The input to the program is a file of type *.img (with pixels of depth 14 bits and a 10 byte header. The header stores the size(rows and columns) of the image and also if the pixels are arranged in the little "ENDIAN" fashion). The image should be a square wave pattern(a one dimensional profile across the image should approximately be a square wave). The path and name of the files to be analyzed are written into the file "PROFILE.TXT"(in the form "D:\temp\new_siemens\ratio10\rotated\200_10.img") from which the program reads the images and writes the output into a file called "MTF.TXT" in the same directory.

When the program is run(the .exe file executed), it asks for the pixel's size of the CRT. The size of the pixel on a CRT is *1/(2*Nyquist Frequency)* i.e. the Nyquist frequency of the CRT. It also asks for the number of CCD pixels used for every CRT pixel which basically is the number of pixels with which a CRT pixel is oversampled (the above mentioned magnification value Mag).

The program senses the orientation of the bar patterns (horizontal or vertical) and accordingly calculates the vertical or horizontal MTFs. The program is "Windows 95/98,NT, 2000" compatible.

Block diagram of program for automatically finding the CRT MTF from a CCD image of several square patterns on a CRT

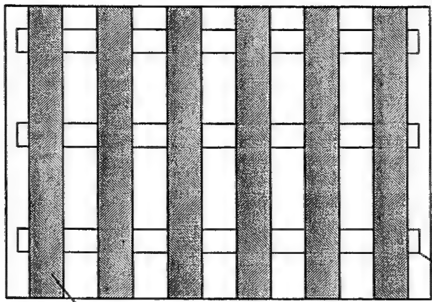

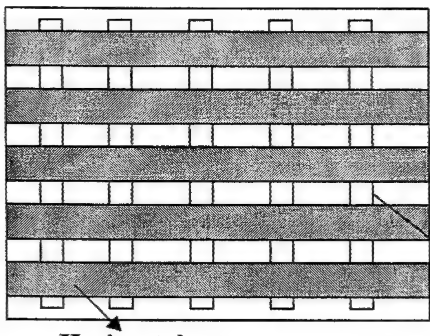

Step 1: Input an image of unknown spatial frequency and details like magnification on the CCD camera and pixel's size on the CRT.

Step 2: Make 1-D profiles depending on whether the input image has vertical or horizontal square waves.

Step 3: Detect the edges of the square wave to make a single profile with an exact integer number of square wave cycles.

Step 4: Perform the FFT of the resultant profile.

Step 5 : Determine the spatial frequency of the input square wave.

Step 6: Depending on the above parameters pick the relevant harmonics from the FFT.

Step 7: Calculate the MTF at each of these points. Club all of these points from various input files to get one MTF curve.

Fig. 18. Block diagram of the program for automatically finding the CRT MTF from the squarewave response.

ALGORITHM:

The value of pixels along five profiles taken across different cross sections of the image is averaged. The edges of the square waves in the profile are detected to ensure integral number of cycles are Fourier Transformed. Depending on the number of pixels detected within one cycle of the profile, the frequency of the input square wave is computed and all the resultant harmonics lying before the Nyquist frequency of the CRT are selectively picked up. This data once got from all the images is put into an array, sorted and finally written into MTF.txt.

b. Improvement of program to find the MTF from the line response.

The program continues to be MATLAB-based. The method to find the MTF from the line response continues to consider the CRT a non-linear device and uses small signals as stimuli (see Fig. 19). Here a single line is addressed with a digital driving level (DDL) slightly higher than the DDL of the background. And the program continues to

determine profiles across the CCD image of a CRT line, averages the profiles and takes a 1-D Fourier Transform of the averaged profile (the averaged profile represents the Line-Spread Function). Normalized to unity at the spatial frequency zero lp/mm, this Fourier Transform is the raw MTF. Corrections need to be made, in order to find the final MTF.

The improved program includes several mathematical manipulations and corrections.

- Before finding the profiles, a CCD image of the uniformly addressed CRT (same DDL as that used for the image with line and background) is taken, and this background image is subtracted from the CCD image with line and background. This procedure removes the stationary fixed pattern noise as well as part of the CRT raster lines and increases the signal-to-noise of the profiles.
- The user can review the profiles for any aberrations and make changes in the ROIs of the profiles
- A **polynomial curve fit** for the Fourier transform in the vicinity of zero spatial frequency aids in finding the normalization factor.
- Corrections were added for the MTF of the CCD camera, particularly for that of the lens (which is affected by the optical magnification), and for the width of the CCD-pixel.

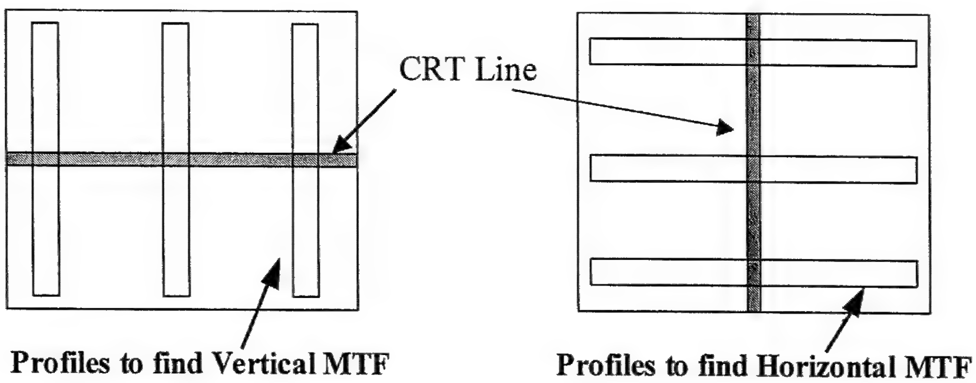

Fig. 19. Illustration for finding the MTF from the line response

c. Improvement of program to find the MTF from the response to Gaussian white noise.

The major part of the improvement consisted of a correction of the raw MTF for the finite size of the CRT pixel width. This correction is equivalent to the fact, that with a pixel width of finite size, like 0.145 mm, the spatial noise at the input to the CRT is not really white as it would be if the CRT pixel width was a delta-function.

Fig. 20 is a block diagram of the method to find the MTF from the response to Gaussian white noise.

Finding the CRT MTF from the NPS of that portion of white noise which is transmitted by the CRT, using 1 -D FFTs of the CCD image

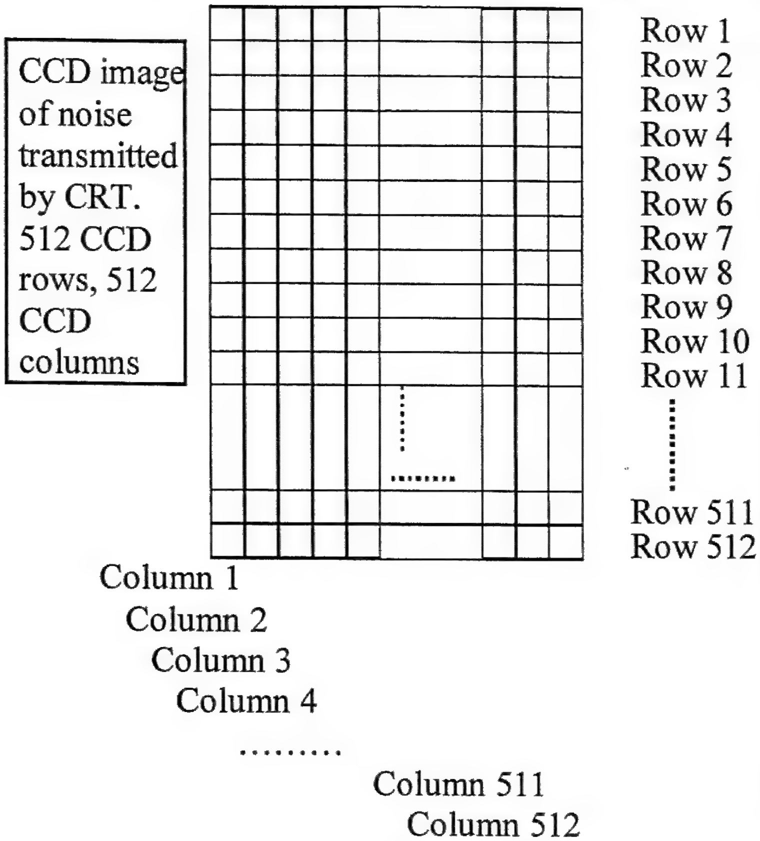

Step 1. Subtract background image from image of noise with background to remove CRT spatial noise.
Step 2. Perform FFT of individual rows.
Step 3. Calculate 1D NPS by squaring the 1D spectra.
Step 4. Average the 1D NPS over columns.
Step 5. Take the square root of the averaged 1D NPS.
Step 6. Correct for the finite size of CRT pixel width to get the horizontal MTF.
Step 7. Rotate the image by 90 degrees. Repeat step 2 to step 6 to get the vertical MTF.

Fig. 20 Block diagram for finding the MTF from the response to white noise.

d. Result of these improvements

Fig. 21 (a, b, c, and d) are MTFs of a 5-Mega-Pixel CRT, derived from the 3 methods discussed above. Notice that the MTFs are fairly close, much closer than reported in last year's report. But, particularly at high luminance levels, there is a slight but noticeable difference.

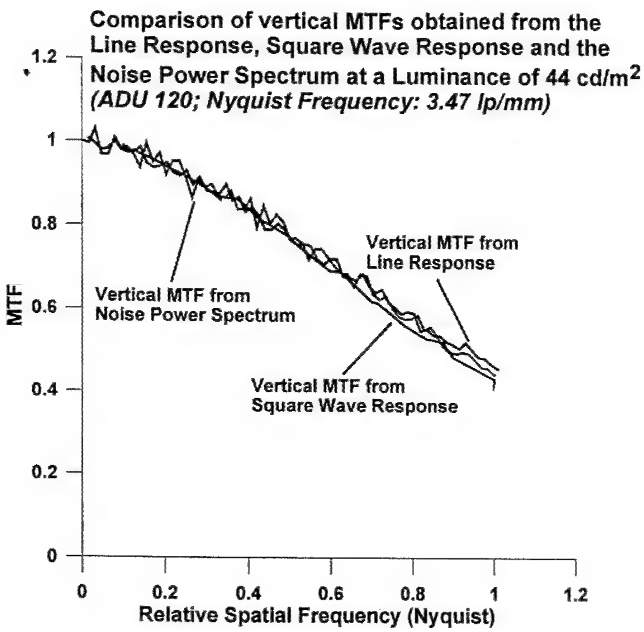

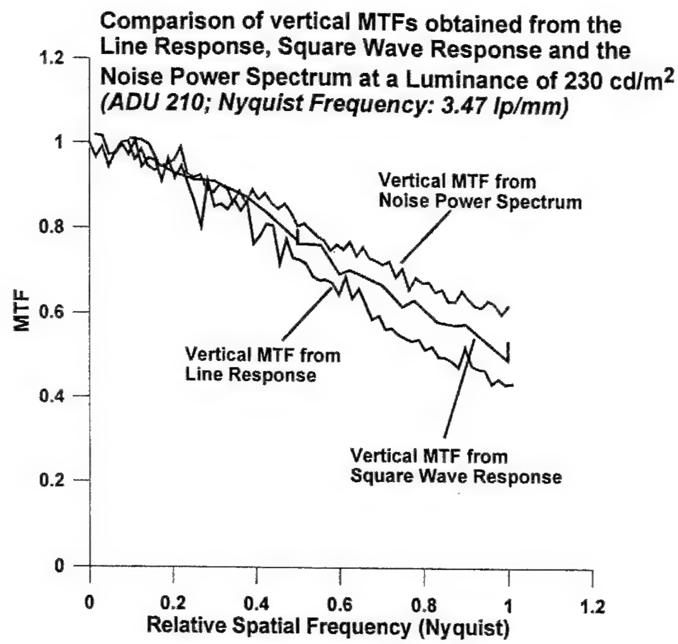

Fig. 21 a Vertical MTFs at luminance 44 cd/m^2

Fig. 21 b: Vertical MTFs at luminance 230 cd/m^2

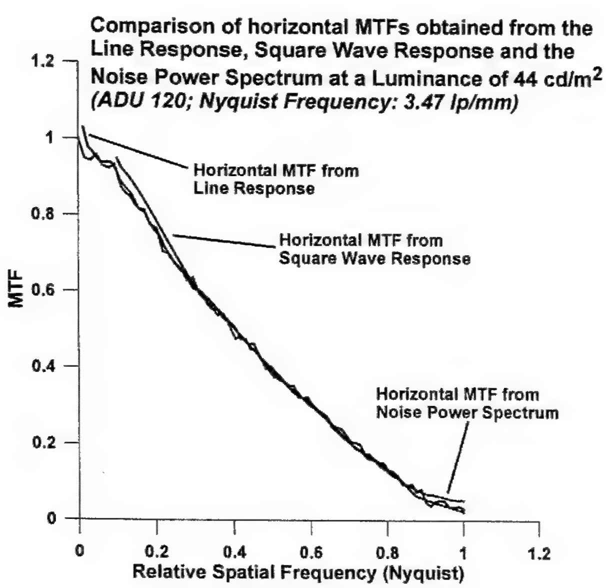

Fig. 21 c Horizontal MTFs at luminance 44 cd/m^2

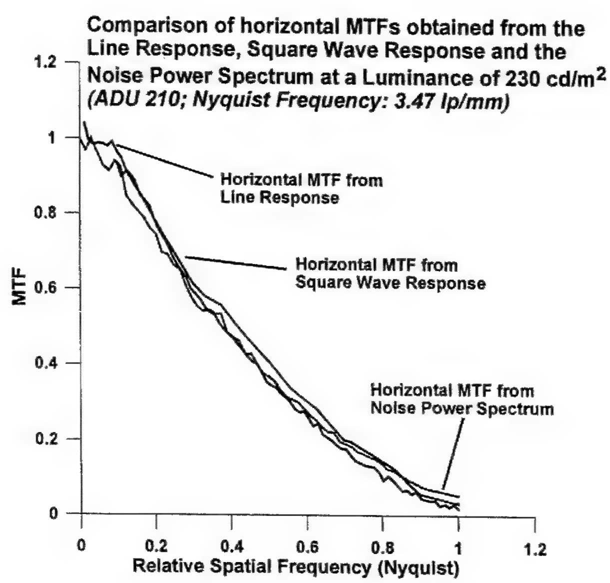

Fig. 21 d: Horizontal MTFs at luminance 230 cd/m^2

TASK: PREDICT SNR MEASUREMENTS FROM FOURIER MEASUREMENTS

As noted earlier, replacement of the CAMPI method by the modified TW method had the added benefit that we could leverage existing methodology to predict the measured results from the Fourier measurements. This led to some related work involving predicting ideal observer performance for detecting masses in mammographic images. The context for this was that in recent work (Burgess, et al, 2001) had showed that the noise power spectrum of mammograms was unusual, showing an approximate $1/f^3$ frequency-dependence down to very low frequencies. This dependence results in unusual effects: for example, *for equal contrasts, smaller masses are more visible that larger masses,* which is the opposite of the familiar contrast-detail behavior exhibited by the ACR phantom masses. Due to the importance of Burgess' observation, which impacts our own work (it necessitates extensions of the present method to include test patterns with anatomic background - see Future Directions Section), we performed related experiments in our laboratory. The results are reported in Reportable Outcomes (Chakraborty and Kundel, 2001). In this work we investigated the effect on the SNR of allowing differently shaped nodules, in particular nodules with sharper edges. The following types of nodules/disks were studied: Gaussian shaped nodules and blurred disks, the latter characterized by a radius and an independent edge sharpness parameter. In a second type of disk the edge blur was held proportional to the disk radius. Ideal Observer detection thresholds were calculated for different nodule/disk radii ranging from 1.5 to 15 mm and observer performance studies were conducted. Noise power spectra (NPS) measurements confirmed the frequency dependence previously reported, NPS $\propto 1/f^{3.1}$. For the Gaussian nodules we confirmed the reported behavior, with threshold contrast $\propto$ radius$^{0.2}$. However, for the disk nodules with fixed blur edges we observed different behavior (larger objects required less contrast), with threshold proportional to radius$^{0.28}$. For the disk nodules with variable blur the threshold contrast was almost independent of radius. In summary while we duplicated the reported CD diagrams for Gaussian nodules, different behavior was observed for nodules with edges. We conclude that in addition to considering the details of the noise, it is necessary to consider the signal properties in more detail.

As noted earlier, the difficulties with the MTF measurements of CRT displays necessitated extra efforts to resolve those issues. To predict SNR one needs the MTF and NPS measurements. Partly for this reason we could not complete this task entirely (we would also need to model the scan lines and the non-Gaussian template behavior noted previously). It is significant that for displays with a raster structure it may be easier to directly measure SNR by our method, than to conduct the Fourier measurements.

KEY RESEARCH ACCOMPLISHMENTS

- Adaptation and major improvements of CAMPI methodology to analyze CRT display images
- Validation of the method by checking a key prediction, namely linearity of SNR with contrast
- Development of software to produce the test patterns and software to perform the necessary calculations
- The software has a high degree of automation and flexibility; it will run on any platform that supports IDL – i.e., practically all computer systems.
- Application of the measurement of image quality of two monitors.
- Results showing the superiority of the P-45 design over the P-104 design for moderate luminance.
- Implementation of a method for measuring SNR of imaging systems with strong structure noise (e.g., scan lines)
- Measurements of SNR of two monitors (P-45 and P-104) as a function of contrast and background luminance
- Development of capability to measure SNR to high accuracy in CRT displays.
- Measurement of variability of SNR over the CRT.
- The intrinsic sampling variability of the method has been evaluated.
- Measurement of magnification dependence of the SNR.
- Improved on MTF measurement methodology.
- Determined optimal imaging parameters for the CCD images.
- Applied a SNR calculation methodology to predict observer performance of mass detection on mammographic backgrounds.

REPORTABLE OUTCOMES

1. DP Chakraborty, M Sivarudrappa and H Roehrig, "Computerized measurements of mammographic display image quality"; SPIE, 3659, page 131-141, 1999.

2. Chakraborty DP, Kundel HL: Anomalous nodule visibility effects in mammographic images, Proc. SPIE Vol. 4324, p. 68-76, Medical Imaging 2001: Image Perception and Performance, Elizabeth A. Krupinski; Dev P. Chakraborty; Eds., Publication Date: 6/2001.

3. Roehrig,H, Fan JH: "CRTs for Medical Imaging: Operation, Performance and Calibration". Invited Talk presented at the Annual Meeting of the Japanese Radiological Society, April 7, 2001, Kobe, Japan.

4. Roehrig H, Fan JH: "Performance Evaluation of CRT for Medical Application". Invited Talk, presented on April 10, 2001at the weekly Seminar of Gifu-University, Gifu, Japan.

5. Chakraborty, D. P., J. Fan, et al. (2003), "COMPUTERIZED CRT SNR MEASUREMENTS: EFFECT OF PHOSPHORS" DOD conference, Orlando, Fla, 2002.

6. Roehrig H, Chakraborty DP, Fan J-H, Chawla A, Gandhi K: "The Modulation Transfer Function (MTF) of CRT displays", DOD conference, , Orlando, Fla, 2002.

7. Chakraborty DP, Fan J-H, and Roehrig H: "A Methodology for Evaluating Display Monitor Performance", RSNA conference, Chicago, ILL, 2002, p 311, 2002.

8. Roehrig H, Blume H, Fan J-H, Chakraborty DP (2002), "Image Quality Control and Image Quality Measurements for Display Systems", RSNA conference, Chicago, ILL, 2002, p 770.

9. Roehrig H., Fan J., Chawla A., Gandhi K.: The Liquid Crystal Display (LCD) for Medical Imaging in Comparison with the Cathode Ray Tube Display (CRT). SPIE Vol. 4786, p. 114-131, 2002

10. Roehrig H, Fan J-H, Furukawa T, Ohashi M, Chawla A and Gandhi K: Performance evaluation of LCD displays Proceedings CARS 2002, pp 461-466, 2002

11. Chakraborty, D. P., J. Fan, et al. (2003). "Measuring CRT display image quality: effects of phosphor type, pixel contrast and luminance." SPIE Proc, Medical Imaging **5034**.

12. Three graduate students were trained in advanced measurement and analysis as part of this program. Their names are Jiahua Fan MS, Kunal Gandhi MS, and Amarpreet S. Chawla, MS. Their CVs are included in the Appendix.

CONCLUSIONS

Overall: We developed a new method for measuring the image quality of CRT displays, or any display with a structured pixel pattern, such as AMLCD displays. The method appears to have advantages over the conventional Fourier based approaches. We established the superiority of the P45 phosphor over the P104 for moderate luminance. We showed that normalized SNR increases with luminance, but appears to level off. We improved the methods for measuring MTF and NPS of displays. At a theoretical level we connected the SNR and Fourier measurements, but were unable to connect them experimentally.

Methodological developments during the project: A lot of papers (see almost any issue of SPIE Proceedings on Physics of Medical Imaging) have been published on image quality measurements on devices with structured noise (such as CRTs, AMLCDs, digital printers, etc.). They invariably adopt the well-known Fourier approach, which involves determining quantities such as the Modulation Transfer Characteristic (MTF), the Noise Power Spectrum (NPS), and the Detective Quantum Efficiency (DQE). The Fourier approach generally works well for devices with negligible structured noise (film, digitized film, direct digital acquisition, etc). However, they are not as easy to use for devices with large structured noise. A 1988 SPIE paper by Bunch and Van Metter (volume 914) sounded a warning. In the abstract of the paper, titled "Interpreting noise power spectra of digitally printed images", they noted:

> *The resulting spectra are significantly more complex than those generally estimated for uniformly exposed film. This complexity is manifested in the combination of narrow line and continuous spectral components, and in the highly anisotropic nature of the spectra. Simple models ... do not adequately describe our data.*

We have developed a method that may have advantages over the Fourier method for devices with large structured noise. The linear plots in Fig. 9 provide compelling evidence that this method potentially represents a breakthrough. <u>We know of no Fourier image quality measurements on CRTs that have demonstrated the expected linearity of SNR and contrast to such high precision</u>.

Task-specific image quality measure: The widely accepted Fourier method that is used for assessing the physical image quality of a general imaging system involves determining quantities characterizing the Modulation Transfer Characteristic (MTF), the Noise Power Spectrum (NPS), and the Detective Quantum Efficiency (DQE). Manufacturers of imaging equipment rely heavily on these measurements for system design and optimization, but these measurements are usually difficult to implement for clinical use or quality control, since they require significant laboratory resources and expertise in interpreting the data. Even if standardized software is made available (e.g., an AAPM Task Group, TG 16, is working on standards for Noise Power Spectrum analysis) it can be difficult to predict the effect on clinical performance of MTF and NPS data. For example, if the MTF curves of two imaging systems cross, then for small objects the system with the higher limiting resolution will be better, whereas for larger objects the opposite may be true. With raster scan displays there are additional problems as noted above. <u>For these reasons it is desirable to use a task-specific figure of merit</u>. The advantage of the method we have developed is that it explicitly includes the task. In the experiments we conducted the target objects we measured were single pixel dots. The targets could just as easily have been fiber like objects, or mass like objects, such as are present in the ACR phantom, or alternate objects, whose visibility is deemed to be critical.

Accuracy and efficiency of the method: Each of the data points shown in Fig. 9 was the result of analysis of 6 images – 3 with target and 3 with background. We do not know of any measurements on CRT displays with comparable precision and obtained with so few images.

P45 vs P104 phosphor: The P104 is mostly used where high luminance output is required (> 480 cd/m^2). P45 is predominantly used where long CRT lifetime and lower phosphor noise are required and lower luminance can be accepted. There is much interest in developing brighter displays for digital image interpretations. This is because a dim display requires low ambient lighting conditions in order that subtle features are visible. This is often hard to achieve in the clinics, where the mammographer is engaged in other activities besides looking at the image on the CRT. Consequently there has been a push towards developing brighter displays for digital image interpretations. This study has allowed us to make definitive image quality measurements of two monitors that are identical in all respects except for the phosphor. This has allowed the effect of the phosphor to be clearly identified. The results of this study, that the P-45 is still a superior choice for medical imaging applications implies that there is more work to be done on the monitor development side to increase brightness without sacrificing image quality. In the absence of these measurements there could have been a hasty move to introduce brighter displays.

Recommended Changes / Problems / Future Directions / SO WHAT

The scientific issues have been already described in context, see in particular the report for Original Task 2. One problem that affected us was the breakdown of one of our monitors – the Siemens P45. This developed an instability had to be sent back to the manufacturer for repairs. This invalidated some of the acquisitions and analysis and they had to be repeated. As is often the way with science, the course of this research was not linear. Rather, we had to take several detours, and do a fair amount of work before we found the answers to our problems. The PI believes that this effort was well justified, even though it took time away from other aspects of this project. Before we started this project, the ability to accurately measure image quality on CRT displays was non-existent (the difficulties with the Fourier method are evident from this report). The original plan to simply apply CAMPI was naïve. However, it led to something that surpassed our expectations for this project. The reviewer may wish to compare the accuracy of the measurements shown in the linearity plots of Fig. 9 to published CAMPI papers (Chakraborty, 1999). The present measurements exceed the precision of all CAMPI results that the PI has published to date. The PI is proud of achievements in this project. A fundamental advance in display measurements was made. Other researchers have expressed interest in our methods, and we fully expect more results to emerge from the foundation that we have laid as a result of this Army supported project.

Due to administrative issues there was an 8-month delay before funds became available for work on this project. [The grant was approved effective 9/1/99. The contract agreement between the University of Pennsylvania and the contractor (University of Arizona) was not reached until April 19, 2000. Funds for Dr. Roehrig were not released until late April 2000. Since Dr. Roehrig 's work and the Dr. Chakraborty's work are mutually dependent, this delayed the start of work by 8-months. The delay also prevented Dr. Roehrig from using the services of a trained student, who

graduated from the program, on this project.] Due to the delayed start in Year 1, we requested and received a one-year extension on this contract.

The effort expended on Original Task 2 (CAMPI modifications) was larger than originally anticipated. In the original plan we budgeted only 12% of time for the PI, as this task was supposed to be a relatively straightforward application of existing CAMPI code, with at most minor modifications.

The scientific issues were compounded by the environmental difficulties the PI was having, namely getting adequate departmental resources at his institution (e.g., space, secretarial support). The PI acknowledges that the institution was having severe financial difficulties at that time, and that he was not the only one who was affected. In addition, much time was lost due to two office moves: one from the original laboratory in Stemmler Hall to 3600 Market Street, another from the PIs office in HUP to 3600 Market Street. These moves happened in the final year of the project, when the scientific issues had been resolved, and we lost time during a particularly productive period. We could have sought another no-cost extension to sort out these issues. However, this was precluded with the PI's change of employment, which resulted in a delay in filing this report, as detailed in the cover letter.

The geographical separation of the two principal scientists created some inevitable communication issues, which were exacerbated by the administrative issues noted above. However, on the whole the collaboration was fruitful.

Application to AMLCD display evaluation: this project opens up the possibility of evaluating AMLCD displays. The problem with structured background is quite acute for AMLCD displays, where the pixels have a "Chevron" fine-structure. This structure creates strong peaks in the NPS at frequencies higher than the Nyquist frequency and makes it difficult to interpret the NPS measurements. The work done in this project makes it possible to approach AMLCD displays with our alternate real-space based approach. AMLCDs are of great interest in radiology because of their high luminance and high resolution. A number of manufacturers have introduced such display devices, and we intend to pursue this issue further.

Anatomic Background: While the measurements in this project were done with uniform background test-patterns, they are in principle extensible to test-patterns with realistic anatomic noise. The reason for seeking such an extension is that the closer the test-pattern is to real patient anatomy, the less likely that some unforeseen observer-background interaction might skew the results. For example, it is possible that this interaction might lead to one modality being judged superior when using uniform background test pattern, but the opposite result might apply with realistic backgrounds. The methodology for handling the more complex anatomic noise is being developed by other investigators (Eckstein and Whiting 1996; Eckstein, Ahumada et al. 1997; Barrett, Abbey et al. 1998; Eckstein and Whiting 1998; Eckstein, Wickens et al. 1998; Bartroff, Morioka et al. 1999; Bochud, Abbey et al. 1999; Eckstein, Abbey et al. 1999; Eckstein, Bartroff et al. 1999; Morioka, Eckstein et al. 1999; Bochud, Abbey et al. 2000; Eckstein, C.K. et al. 2000) and in a future project we hope to utilize some of their methods, just as we borrowed from the classic TW work for this project. In fact Art Burgess has already shown us how to predict the effects on mass-detection of simulated $1/f^3$ noise, which resembles clinical backgrounds. We reported our work along these lines in Original Task 4.

Inclusion of eye-model characteristics: Yet another exciting possibility is to include a realistic vision model in the measurement method. Combined with the proposed extension to anatomic background test-patterns, this would assure that the measurements would correlate optimally with visual mammographer assessments. After all, the SNR of a mathematical observer is less important than the ability to predict how real mammographers perform when using the CRT display. We propose to pursue a future project with Army funding in this area.

Extension to discrimination tasks: The method is extensible to discrimination tasks (so far we focused on detecting the targets) where one has to discriminate between two types of targets. One idea we had was to use a doublet of dots, instead of one dot, as the basic target. One of the dots in the doublet would have a slightly higher contrast than the other. This would be repeated about 600 times in a test pattern analogous to Fig. 5. The measured performance of the ideal observer in this task can be measured (one calculates two cross-correlations, and takes the higher value as corresponding to the brighter dot). The performance in this task may be more relevant to the mammographer's task of discriminating benign from malignant lesions in mammography than measuring SNR. This is an interesting area of research for a future project/

So What: In its present form the proposed method is still too complex for routine QC application. Until we succeed in implementing a practical implementation of the researched measuring method, the full potential of this research will not be realized. Based on our measurements so far we believe we know how to do this. A high performance CCD camera ($20 K) is not needed. We estimate that a good digital camera (about $1 K) and software similar to what we have developed is all that is needed. We intend to pursue this as part of an SBIR phased-innovation award.

REFERENCES

Chakraborty, D. P. and M. P. Eckert (1995). "Quantitative versus subjective evaluation of mammography accreditation phantom images." Medical Physics **22**(2): 133-143.

Chakraborty, D. P. (1997). "Computer analysis of mammography phantom images (CAMPI): An application to the measurement of microcalcification image quality of directly acquired digital images." Medical Physics **24**(8): 1269-1277.

Chakraborty, D. P. (1999). "The Effect of the Anti-Scatter Grid and Target/Filters in Full-field Digital Mammography." SPIE **3659**: 878-885.

Burgess, A. E., Ed. (1990). High level visual decision efficiencies. Vision-Coding and Efficiency, Cambridge University Press.

Burgess, A. E., F. L. Jacobson, et al. (2001). "Human observer detection experiments with mammograms and power-law noise." Med Phys **28**(4): 419-37.

Eckstein, M. P., C. K. Abbey, et al. (2000). A Practical Guide to Model Observers for Visual Detection in Synthetic and Natural Noisy Images. Handbook of Medical Imaging. H. Kundel, J. Beutel and R. Van-Metter. Bellingham, Washington, SPIE: 593-628.

Tapiovaara, M. J. and R. F. Wagner (1993). "SNR and noise measurements for medical imaging: I.

A practical approach based on statistical decision theory." Phys. Med. Biol. **38**: 71-92.

Tapiovaara, M. (1993). "SNR and noise measurements for medical imaging: II.

Application to fluoroscopic x-ray equipment." Phys. Med. Biol. **38**: 1761-1788.

Barrett, H. H., C. Abbey, et al. (1998). "Stabilized Estimates of Hotelling-Observer Detection Performance in Patient-Structured Noise." NA.

Bartroff, J. L., C. A. Morioka, et al. (1999). "Image compression and feature stablization of dynamically displayed coronary angiograms." SPIE 3663: 342-346.

Bochud, F. O., C. K. Abbey, et al. (1999). "Visual Signal Detection in structured backgrounds IV, Calculation of Figures of Merit for Model Observers in Non-Stationary Backgrounds." Journal of the Optical Society of America, A, Optics, Image Science, & Vision 17(2): 206-17.

Bochud, F. O., C. K. Abbey, et al. (2000). "Visual signal detection in structured backrounds. III. Calculation of figures of merit for model observers." Journal of the Optical Society of America, A, Optics, Image Science, & Vision 17(2): 193-205.

Eckstein, M., C. K. Abbey, et al. (1999). "Visual signal detection in structured backgrounds (IV) Figures of merit for model performance in multiple alternative forced choice detection tasks with correlated responses."

Eckstein, M. P., A. J. Ahumada, et al. (1997). "Visual detection in structured backgrounds. II Effects of contrast gain control, background variations, and white noise." Journal of the Optical Society of America 14(9): 2406-2419.

Eckstein, M. P., J. L. Bartroff, et al. (1999). "Feature stabilized digital x-ray coronary angiograms improve hman visual detection in JPEG compressed images." Optics Express 4(6).

Eckstein, M. P., A. C.K., et al. (2000). A Practical Guide to Model Observers for Visual Detection in Synthetic and Natural Noisy Images. Handbook of Medical Imaging. H. L. Kundel, J. Beutel and R. L. Van-Metter. Bellingham, Washington, SPIE: 593-628.

Eckstein, M. P. and J. S. Whiting (1996). "Visual detection in structured backgrounds I. Effect of number of possible spatial locations and signal contrast." Journal of the Optical Society of America 13(9): 1777-1787.

Eckstein, M. P. and J. S. Whiting (1998). "Why Do Anatomic Backgrounds Reduce Lesion Detectability?" Investigative Radiology 33(4): 203-208.

Eckstein, M. P., T. D. Wickens, et al. (1998). "Quantifying the limitations of the use of consensus expert committees in ROC studies." SPIE 3340(Image Perception): 128-134.

Morioka, C., M. P. Eckstein, et al. (1999). "Observer performance for JPEG vs. Wavelet image compression of x-ray coronary angiograms."

Sandrik, J. M. and R. F. Wagner (1982). "Absolute measures of physical image quality: measurement and application to radiographic magnification." Med Phys 9(4): 540-9.

APPENDICES

1. Typical calibration data for a monitor (P-45 in this case), that allowed the CCD values to be converted to DDL values prior to analysis. Also included is MTF and NPS data.

2. DP Chakraborty, M Sivarudrappa and H Roehrig, "Computerized measurements of mammographic display image quality"; SPIE, 3659, page 131-141, 1999.

3. Chakraborty DP, Kundel HL: Anomalous nodule visibility effects in mammographic images, Proc. SPIE Vol. 4324, p. 68-76, Medical Imaging 2001: Image Perception and Performance, Elizabeth A. Krupinski; Dev P. Chakraborty; Eds., Publication Date: 6/2001.

4. Chakraborty, D. P., J. Fan, et al. (2003). "Measuring CRT display image quality: effects of phosphor type, pixel contrast and luminance." SPIE Proc, Medical Imaging 5034.

5. CV s of students who were trained.

APPENDIX 1

The following data are for Siemens P45 high resolution monitor.

1. Here is the list of the corresponding CCD images and CRT images:

CCD_Images	CRT_Images
000.img	BLANK00-B0055.img
001.img	BLANK00-B0127.img
002.img	BLANK00-B0200.img
003.img	BLANK01-B0055.img
004.img	BLANK01-B0127.img
005.img	BLANK01-B0200.img
006.img	BLANK02-B0055.img
007.img	BLANK02-B0127.img
008.img	BLANK02-B0200.img
009.img	BLANK03-B0055.img
010.img	BLANK03-B0127.img
011.img	BLANK03-B0200.img
012.img	BLANK04-B0055.img
013.img	BLANK04-B0127.img
014.img	BLANK04-B0200.img
015.img	BLANK05-B0055.img
016.img	BLANK05-B0127.img
017.img	BLANK05-B0200.img
018.img	BLANK06-B0055.img
019.img	BLANK06-B0127.img
020.img	BLANK06-B0200.img
021.img	BLANK07-B0055.img
022.img	BLANK07-B0127.img
023.img	BLANK07-B0200.img
024.img	BLANK08-B0055.img
025.img	BLANK08-B0127.img
026.img	BLANK08-B0200.img
027.img	BLANK09-B0055.img
028.img	BLANK09-B0127.img
029.img	BLANK09-B0200.img
030.img	BLANK10-B0055.img
031.img	BLANK10-B0127.img
032.img	BLANK10-B0200.img
033.img	BLANK11-B0055.img
034.img	BLANK11-B0127.img
035.img	BLANK11-B0200.img
036.img	BLANK12-B0055.img
037.img	BLANK12-B0127.img
038.img	BLANK12-B0200.img
039.img	BLANK13-B0055.img
040.img	BLANK13-B0127.img
041.img	BLANK13-B0200.img
042.img	BLANK14-B0055.img
043.img	BLANK14-B0127.img
044.img	BLANK14-B0200.img
045.img	R0030-P0077-B0055-BD0010.img
046.img	R0030-P0158-B0127-BD0010.img
047.img	R0030-P0255-B0200-BD0010.img
048.img	R0050-P0063-B0055-BD0020.img
049.img	R0050-P0138-B0127-BD0020.img

050.img	R0050-P0243-B0200-BD0020.img
051.img	R0070-P0059-B0055-BD0020.img
052.img	R0070-P0133-B0127-BD0020.img
053.img	R0070-P0222-B0200-BD0020.img
054.img	SQ13-P0057-B0055-HL1.img
055.img	SQ13-P0058-B0055-HL2.img
056.img	SQ13-P0058-B0055-VL1.img
057.img	SQ13-P0059-B0055-DP1.img
058.img	SQ13-P0059-B0055-HL3.img
059.img	SQ13-P0059-B0055-HL4.img
060.img	SQ13-P0061-B0055-VL3.img
061.img	SQ13-P0062-B0055-DP2.img
062.img	SQ13-P0062-B0055-VL2.img
063.img	SQ13-P0062-B0055-VL4.img
064.img	SQ13-P0063-B0055-DP3.img
065.img	SQ13-P0067-B0055-DP4.img
066.img	SQ13-P0085-B0055-1HL.img
067.img	SQ13-P0085-B0055-1VL.img
068.img	SQ13-P0129-B0127-HL1.img
069.img	SQ13-P0132-B0127-DP1.img
070.img	SQ13-P0132-B0127-HL2.img
071.img	SQ13-P0132-B0127-HL3.img
072.img	SQ13-P0132-B0127-VL1.img
073.img	SQ13-P0133-B0127-HL4.img
074.img	SQ13-P0137-B0127-DP2.img
075.img	SQ13-P0137-B0127-VL2.img
076.img	SQ13-P0138-B0127-VL3.img
077.img	SQ13-P0139-B0127-VL4.img
078.img	SQ13-P0140-B0127-DP3.img
079.img	SQ13-P0147-B0127-DP4.img
080.img	SQ13-P0157-B0127-1HL.img
081.img	SQ13-P0157-B0127-1VL.img
082.img	SQ13-P0208-B0200-VL1.img
083.img	SQ13-P0209-B0200-HL1.img
084.img	SQ13-P0216-B0200-VL2.img
085.img	SQ13-P0218-B0200-HL2.img
086.img	SQ13-P0219-B0200-HL4.img
087.img	SQ13-P0220-B0200-DP1.img
088.img	SQ13-P0221-B0200-VL4.img
089.img	SQ13-P0222-B0200-HL3.img
090.img	SQ13-P0222-B0200-VL3.img
091.img	SQ13-P0230-B0200-1HL.img
092.img	SQ13-P0230-B0200-1VL.img
093.img	SQ13-P0240-B0200-DP2.img
094.img	SQ13-P0255-B0200-DP3.img
095.img	SQ13-P0255-B0200-DP4.img

2. Exposure time

2200ms: All the images with 55 ADU as background.
460ms: All the images with 127 ADU as background.
80ms: All the images with 200 ADU as background.

3. CRT input (ADU) vs. CCD output (ADU)

Exposure time: 2200ms	
CRT input(ADU)	Luminance (CCD ADU)
0	108.916
5	238.216
10	389.292
15	568.708
20	772.525
25	1016.95
30	1309.15
35	1598.39
40	1971.40
45	2359.18
50	2824.38
55	3305.35
60	3861.58
65	4479.15
70	5087.97
75	5887.89
80	6723.69
85	7639.41
90	8652.32
95	9684.25
100	10928.1
105	12225.0
110	13702.9

Exposure time: 460ms	
CRT input(ADU)	Luminance (CCD ADU)
0	26.6195
12	113.552
24	238.472
36	404.471
48	640.499
60	939.756
72	1324.48
84	1808.20
96	2422.18
108	3191.04
120	4165.91
125	4634.84
127	4826.84
130	5113.89
135	5676.59
140	6256.44
145	6939.65
150	7620.56
155	8401.44
160	9273.02
165	10188.2
170	11165.3
175	12299.5
180	13561.2

Exposure time: 80ms	
CRT input(ADU)	Luminance (CCD ADU)
0	7.77093
20	60.3134
40	154.052
60	302.904
80	527.98
100	867.998
120	1349.02
140	2026.82
160	3008.8
180	4374.4
190	5240.93
200	6273.25
210	7477.68
220	8909.88
230	10593.3
240	12563.0
250	14829.8

4. Display Characteristic Data:

Before the experiment:

TYPE = CONF AIM = DICOM
TIME = 2002.01.11-13:23:14 to 2002.01.11-13:24:45
MIN = -1.000 MAX = -1.000
AMBIENT = 0.145 MONITORON
UNIT = cd/m^2
SIZE = 33

0	0.895	0	0
1	1.429	7	1984
2	2.13	15	3520
3	2.994	23	4928
4	4.162	31	6272
5	5.512	39	7552
6	7.235	47	8960
7	9.154	55	10240
8	11.516	63	11584
9	14.174	71	12928
10	17.373	79	14336
11	21.212	87	15808
12	25.395	95	17280
13	30.612	103	18880
14	36.419	111	20480
15	43.211	119	22144
16	51.184	127	23936
17	60.043	135	25728
18	70.476	143	27648
19	81.894	151	29568
20	95.773	159	31680
21	111.029	167	33792
22	129.19	175	36096
23	149.024	183	38400
24	172.401	191	40896
25	199.174	199	43520
26	229.343	207	46208
27	263.4	215	49024
28	303.018	223	52032
29	348.197	231	55168
30	399.184	239	58432
31	457.504	247	61888
32	523.354	255	65472

After the experiment:

TYPE = CONF AIM = DICOM
TIME = 2002.01.11-22:57:42 to 2002.01.11-22:58:54
MIN = -1.000 MAX = -1.000
AMBIENT = 0.145 MONITORON
UNIT = cd/m^2
SIZE = 33

0	0.896	0	0
1	1.429	7	1984
2	2.13	15	3520
3	3.024	23	4928
4	4.134	31	6272
5	5.512	39	7552
6	7.235	47	8960
7	9.154	55	10240
8	11.516	63	11584
9	14.174	71	12928
10	17.373	79	14336
11	21.212	87	15808
12	25.395	95	17280
13	30.612	103	18880
14	36.419	111	20480
15	43.162	119	22144
16	51.135	127	23936
17	60.043	135	25728
18	70.427	143	27648
19	81.845	151	29568
20	95.871	159	31680
21	110.98	167	33792
22	129.042	175	36096
23	149.417	183	38400
24	172.302	191	40896
25	198.928	199	43520
26	229.933	207	46208
27	263.154	215	49024
28	302.624	223	52032
29	348.837	231	55168
30	398.692	239	58432
31	456.914	247	61888
32	523.699	255	65472

5. MTFs

Curves:

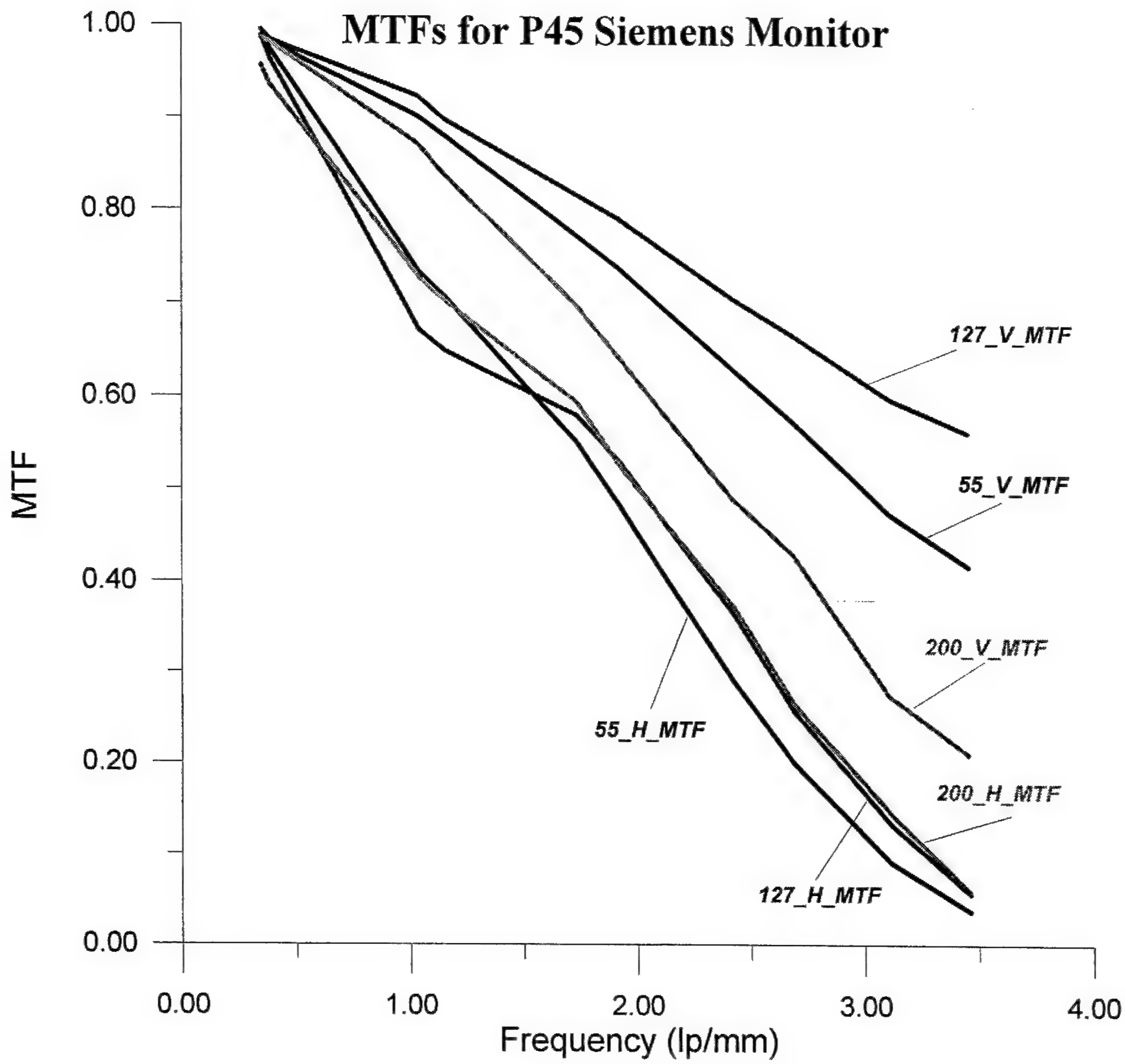

MTF data:

55_v

Frequency lp/mm	Output	Input	MTF
0.345066	623.612244	632.2366452	0.986358903
0.383671	620.207397	632.2366452	0.980973504
1.035197	189.832535	210.7455484	0.900766524
1.151013	185.414383	210.7455484	0.879802133
1.725328	97.820221	126.447329	0.773604486
1.918355	93.250214	126.447329	0.7374629
2.415459	56.956039	90.31952075	0.630606081
2.685697	51.727921	90.31952075	0.572721385
3.10559	33.295696	70.24851614	0.473970097
3.453039	29.289213	70.24851614	0.416937106

55_h

Frequency lp/mm	Output	Input	MTF
0.346141	629.88654	637.95667	0.98735
0.384658	621.39142	637.95667	0.9740339
1.038422	155.98103	212.65222	0.7335029
1.153973	150.28992	212.65222	0.7067404
1.730703	70.374283	127.59133	0.5515601
1.923288	61.449028	127.59133	0.4816082
2.422984	26.430733	91.136668	0.2900121
2.692604	18.173033	91.136668	0.1994042
3.115265	6.445469	70.884075	0.0909297
3.461919	2.608956	70.884075	0.036806

127_v

Frequency lp/mm	Output	Input	MTF
0.345066	595.12744	598.38439	0.9945571
0.383142	588.72168	598.38439	0.983852
1.035197	184.06293	199.46146	0.9227994
1.149425	179.01764	199.46146	0.8975049
1.725328	97.781349	119.67688	0.8170446
1.915709	94.566689	119.67688	0.7901835
2.415459	60.342903	85.483484	0.7059013
2.681993	56.967651	85.483484	0.666417
3.10559	39.783783	66.487154	0.598368
3.448276	37.341915	66.487154	0.561641

127_h

Frequency lp/mm	Output	Input	MTF
0.3465	607.16846	614.49724	0.9880735
0.384658	592.00324	614.49724	0.9633945
1.039501	137.52892	204.83241	0.6714216
1.153973	132.96591	204.83241	0.6491449
1.732502	71.309685	122.89945	0.5802279
1.923288	65.002716	122.89945	0.5289098
2.425503	31.924511	87.785319	0.3636657
2.692604	22.497326	87.785319	0.2562766
3.118503	9.045964	68.277471	0.1324883
3.461919	3.832038	68.277471	0.0561245

200_v

Frequency lp/mm	Output	Input	MTF
0.345066	660.90314	670.09642	0.9862807
0.383671	657.60242	670.09642	0.9813549
1.035197	194.53365	223.36547	0.8709208
1.151013	186.99011	223.36547	0.8371487
1.725328	93.785393	134.01928	0.6997903
1.918355	86.047432	134.01928	0.6420526
2.415459	46.909115	95.72806	0.4900247
2.685697	41.113529	95.72806	0.4294825
3.10559	20.474476	74.455158	0.2749907
3.453039	15.625541	74.455158	0.2098651

200_h

Frequency lp/mm	Output	Input	MTF
0.3465	627.35278	656.00166	0.956328
0.384658	613.60669	656.00166	0.9353737
1.039501	159.04794	218.66722	0.7273516
1.153973	153.59137	218.66722	0.7023978
1.732502	78.014206	131.20033	0.594619
1.923288	68.861107	131.20033	0.5248547
2.425503	34.793785	93.714523	0.3712742
2.692604	24.783945	93.714523	0.2644622
3.118503	10.528934	72.889073	0.1444515
3.461919	4.270566	72.889073	0.0585899

COMPUTERIZED CRT SNR MEASUREMENTS: EFFECT OF PHOSPHORS

Dev P. Chakraborty Ph.D., Jiahua Fan and Hans Roehrig Ph.D.

University of Pennsylvania and University of Arizona

We compared the image quality of two Siemens 5Mega Pixel CRT displays for mammography, one with a P-45 phosphor and the other with a P-104 phosphor, both calibrated according to the DICOM standard for a maximum luminance of 500 Cd/m2. Images (512 x 512 x 8 bits) of computer generated test-patterns were digitized by a CCD camera at a magnification of 8, resulting in 1316 x 1036 x 14 bit image files. The CCD images were analyzed by the template-correlation method suggested by Tapiovaara and Wagner (TW), yielding signal-to-noise ratio (SNR) estimates for the test patterns.

The patterns consisted of targets superposed on uniform backgrounds and uniform fields. Three background values were used with DDL values of 55, 127 and 200, and each uniform field was imaged 15 times by the CCD camera. Each signal image consisted of 25 identical targets, each consisting of a periodic array of target elements, which were dots or horizontal or vertical line-segments. The pixel value difference between the target and the background was varied systematically, as was the spacing between the target elements. Templates were constructed in the manner described by TW except that a special alignment technique was used to account for the scan lines. In all 162 target containing CCD images and 45 uniform field images (for each monitor) were analyzed using the non-prewhitening ideal observer template of TW with a zero frequency filter.

For each test-pattern type and spacing, the dependence of SNR on target contrast was non-linear, and could be well fitted with a 2-parameter exponential rise-to-maximum function, thereby allowing the identification of low-contrast and high-contrast SNR values. For high-contrast signals the P-45 phosphor did better than P-104, except at the highest luminance, where the reverse was true. For low-contrast signals the performance of the two monitors was almost identical across the entire luminance range.

It should be noted that the TW method yielded precise (~2%) SNR measurements quite independent of any assumptions about the MTF, NPS or pixel intensity distribution. We believe this method is ideally suited to the evaluation of the new AMLCD devices that are becoming available, whose evaluation presents special problems to conventional linear system analysis.

Computerized measurement of mammographic display image quality

Dev P. Chakraborty*[a], Mahesh Sivarudrappa[b], Hans Roehrig[b]

[a]University of Pennsylvania, Philadelphia, PA 19104

[b]University of Arizona Health Sciences Center, Tucson, AZ 85724

ABSTRACT

Since the video monitor is widely believed to be the weak link in the imaging chain, it is critical, to include it in the total image quality evaluation. Yet, most physical measurements of mammographic image quality are presently limited to making measurements on the digital matrix, not the displayed image.

A method is described to quantitatively measure image quality of mammographic monitors using ACR phantom-based test patterns. The image of the test pattern is digitized using a charge coupled device (CCD) camera, and the resulting image file is analyzed by an existing phantom analysis method (Computer Analysis of Mammography Phantom Images, CAMPI). The new method is called CCD-CAMPI and it yields the Signal-to-Noise-Ratio (SNR) for an arbitrary target shape (e.g., speck, mass or fiber). In this work we show the feasibility of this idea for speck targets. Also performed were physical image quality characterization of the monitor (so-called Fourier measures) and analysis by another template matching method due to Tapiovaara and Wagner (TW) which is closely related to CAMPI.

The methods were applied to a MegaScan monitor. Test patterns containing a complete speck group superposed on a noiseless background were displayed on the monitor and a series of CCD images were acquired. These images were subjected to CCD-CAMPI and TW analyses. It was found that the SNR values for the CCD-CAMPI method tracked those of the TW method, although the latter measurements were considerably less precise. The TW SNR measure was also about 25% larger than the CCD-CAMPI determination. These differences could be understood from the manner in which the two methods evaluate the noise. Overall accuracy of the CAMPI SNR determination was 4.1% for single images when expressed as a coefficient of variance.

While the SNR measures are predictable from the Fourier measures the number of images and effort required is prohibitive and it is not suited to Quality Control (QC). Unlike the Fourier measures and the TW method, CCD-CAMPI is capable of yielding speck SNR on a single image. This is based on preliminary work and more complete testing is underway. Based on the early promising results, we expect that the CCD-CAMI method can be adapted to routine image QC of monitors using inexpensive equipment.

Keywords: Display Quality Control, Mammography, Digital, ACR phantom, CAMPI, CCD

1. INTRODUCTION

A digital mammography imaging system utilizes an image capture device, usually a flat panel imager, to digitize the post-patient x-ray intensity distribution into a digital matrix. The digital pixel values are processed (e.g., flat field and gain corrected, perceptually linearized, windowed and leveled, etc.) and displayed on a video monitor. The mammographer views the monitors and makes the clinical diagnosis. Most relevant to the mammographer is the quality of the image displayed on the monitor. *Yet, most physical measurements of mammographic image quality are presently limited to making measurements on the digital matrix, not the displayed image.* Since the video monitor is widely believed[1] to be the weak link in the digital mammography imaging chain, it is critical, to include it in the total image quality evaluation.

Most current methods of monitor image quality evaluation involve making *subjective* (human-observer based) measurements using test patterns, e.g., the Society of Motion Picture and Television Engineers (SMPTE) test pattern. These measurements are convenient but suffer from lack of precise quantification. Physical measurements can overcome these limitations, and indeed such measurements are sometimes performed in laboratory settings[2,3,4]. These yield fundamental measures of image quality such as Modulation Transfer Function (MTF), Noise Power Spectrum (NPS) and Detective Quantum Efficiency (DQE). Since they are based on extensive use of the Fourier Transform, they are often collectively referred to as *Fourier Measures*. While the Fourier measures are extremely important for system optimization, they are too complicated and

expensive for routine QC usage. In addition, they do not directly yield a summary task-specific measure. For example, from a QC point of view, it is advantageous to have an image quality measure that is expected to reflect the performance of mammographers on common clinical tasks, e.g., speck, fiber and mass detection and characterization. Such task-specific measures are commonly obtained for analog mammography imaging systems by imaging the American College of Radiology (ACR) accreditation phantom.

Computer Analysis of Mammography Phantom Images (CAMPI) is an image quality evaluation method that we introduced[5,67,8,9,10] several years ago. It yields quantitative image quality measures that are task-specific and relatively simple to calculate. CAMPI software has so far been limited to analyzing the digital matrix. The primary aim of this work was to extend CAMPI to measure image quality of the displayed image. Since it utilizes a CCD device to digitize the monitor image, the new method is called CCD-CAMPI.

The CAMPI method is closely related to a method suggested earlier by Tapiovaara and Wagner[11,12] in the context of fluoroscopic image quality measurement. We propose a variant of this method, which can be used to measure the image quality of monitors. The second aim was to apply the Tapiovaara and Wagner (TW) and the CCD-CAMPI methods to a common image set and do a preliminary comparison of the two.

2. EXPERIMENTAL METHODS AND ANALYSIS

CAMPI Methodology

Early applications of CAMPI were to analog screen-film mammography systems, but recent work has extended these measurements to digital mammography with small-field-of-view biopsy machines[14]. The method requires obtaining several *insert images* of the phantom wax insert, the extraction of regions-of-interest (ROIs) containing the target structures from these images, registering the ROIs corresponding to a given target to each other, and averaging them. For each target type, the final averaged ROI (*template*) is used to calculate the image quality indices for the actual images to be evaluated (*test images*). The CAMPI indices are defined in our previous publications (see Ref. 6). Of interest is the speck Signal-to-Noise-Ratio (SNR) measure, which is defined as the ratio of two cross-correlation values, the *signal* and the *noise* respectively. Each cross correlation value is measured with an aperture having the same size and shape as the speck. The *noise* is defined as the standard deviation of the cross correlation values measured at background (noise) locations. The *signal* is defined as the incremental cross correlation value measured at the speck (signal) location. Formally, SNR = signal/noise. Note that this analysis does not require the target objects to have a particular well-defined shape. The reason for the focus on the SNR measure is the fact that this measure correlates well with the observer's perception of speck visibility[13].

CCD-CAMPI

The adaptation of CAMPI to monitor evaluation, called *CCD-CAMPI* analysis, consists of new pre- and post- acquisition procedures followed by normal CAMPI analysis. For this investigation we limited ourselves to measuring the speck SNR. The pre-acquisition procedures were as follows. For each speck in the first-three microcalcification groups (M1, M2 and M3 using our past notation) we averaged the extracted ROIs from x-ray images of an ACR phantom insert. The averaged ROI pixels were contrast diluted and added to a noiseless image. The resulting image was used as an *intermediate template image* of the CCD/CAMPI method. Separate templates were created in this manner for M1, M2 and M3. Each template was displayed on the monitor to be evaluated and the resulting luminance distribution was digitized with a CCD camera. The post acquisition steps consisted of dimensionally scaling each template so that it had the same geometry as the acquired CCD images. ROIs extracted from the former were the *final templates*, which were used to calculate the SNR of the actual CCD images by running the usual CAMPI analysis. Since the input test pattern is noise free, an ideal monitor is expected to yield an infinite SNR. The SNR values as measured by this method (CCD-CAMPI) are being proposed as image quality metrics for evaluating monitors.

The x-ray images of the ACR phantom insert were obtained at 20 kVp and 8 mAs with a Min-R screen-film system. The images were digitized at 12-bits per pixel with a Lumisys LS-100 digitizer operating at 50-micron pixel size. Using the CAMPI 'average' mode[14], speck regions from 15 such images were averaged. This yielded 18 ROIs, each containing 31 x 31 x 12-bit pixels. As part of the averaging, an extrapolated bilinear background term was subtracted from each speck region to remove the effect of the varying background intensities. For the resulting ROI a typical *minimum* speck pixel value was about -500, which rises to 0±10 as one moves away from the minimum intensity region of the speck. To suppress noise in the background region, all digital values in the ROIs whose magnitudes were below 30 were replaced with zeroes. A 525 x 525 x 12- bit non-target image was created, in which all pixels were initialized to a pixel value of 2047. Adding a diluted version of a speck group created the target image. The *dilution factor* (d) is defined as the number by which the pixel values are diluted

(i.e., divided) before addition to the noiseless image. All images to be displayed on the monitor were transformed to 8-bits by dropping the 4 least significant bits. Therefore, the noiseless background value was 127 on the 8-bit image. The notation for the 12-bit templates is illustrated with two examples: M2-01 is an intermediate template created from the M2 specks by superposing them directly (d = 1) on a noiseless background of pixel values equal to 2047. Likewise, M1-05 is created from M1 by first dividing the pixel values of the original averaged ROI by a factor of five (d=5) and then superposing on a noiseless background of pixel values equal to 2047 (see Fig. 1, top panel).

The 8-bit images were displayed unaltered on a MegaScan display monitor at the University of Arizona. The camera magnification was adjusted so that there were 9 CCD pixels per CRT pixel, corresponding to a linear magnification of 3. For each input image the CCD camera acquired ten 1317 x 1035 x 14-bit images. An example is shown in the bottom panel of Fig 1, for M1-05-CCD, which is the CCD image corresponding to M1-05. This CCD image was displayed under high contrast conditions prior to printing. Note that unlike the input image, this one has a finite signal-to-noise ratio. The exact magnification was modeled as 3f, where the correction factor f was calculated by determining the speck coordinates in an 8-bit template and the corresponding CCD image. Linear regression was applied to the distances between pairs of specks in the two images. This yielded the appropriate correction factor f. We obtained f = 1.0157±0.0004 for the three templates. Thus each 8-bit template image was magnified (bilinear interpolation was used to scale the image) by a factor of 3f to mimic the geometry of the CCD acquisition. The scaled image is a *test pattern* for CAMPI analysis. Speck ROIs extracted from this test pattern served as the final CAMPI templates. Note that no further averaging was needed, as the test pattern *is* the truth.

The calculated SNR values were corrected by multiplying the measured value with the dilution factor. For example, for M1-05 the measured value was multiplied by 5. The SNR values reported below are *corrected* values. Also calculated as part of CAMPI analysis is a quantity called the speck normalization (NORM) which is the standard deviation of all pixel values within the speck ROI. This is a measure of total speck intensity and we have observed in the past that the SNR values are linear with NORM. The measured NORM values were similarly corrected for the difference in dilution factors.

Tapiovaara and Wagner (TW) Methodology and its adaptation

The TW method was originally developed for fluoroscopy. One acquires a series of images (typically several hundred fluoroscopic frames) of the phantom background plus the target object, and averaging them to form the TW template. To evaluate a particular fluoroscopic imaging condition one acquires two sets of images under that condition: a set of images of the background plus the target object, followed by a set of images of the background only. Typically 180 frames might be obtained in each case, for a total of 360. Next one calculates the cross correlation (CC) of the template image with each of these 360 frames. The average μ and standard deviation σ of the CC values for the two phantom configurations are calculated. We denote these quantities by (μ_{target} , σ_{target}) and (μ_{bkgnd} , σ_{bkgnd}) for the target plus background and background, respectively. The SNR-TW of the target is then given by

$$SNR - TW = \frac{\mu_{target} - \mu_{bkgnd}}{\frac{\sigma_{target} + \sigma_{bkgnd}}{2}}$$

Equation 1.

In the proposed adaptation of the TW method to monitor image quality evaluation, we used an 8-bit template described above for CCD/CAMPI. An additional 8-bit noiseless test pattern, in which all pixels were initialized to a pixel value of 127 served as the background (non-target) test pattern. The two patterns were individually displayed on the MegaScan monitor and 10 CCD images were acquired in each case. Ten images were also acquired of the two other 8-bit templates used, for a total of 40 CCD images. The 8-bit truth templates described above for CCD-CAMPI were used to calculate the appropriate cross-correlation values on these images. On the target images the cross-correlation was calculated at the appropriate speck locations. On the background images the cross-correlation was calculated at the *same* locations.

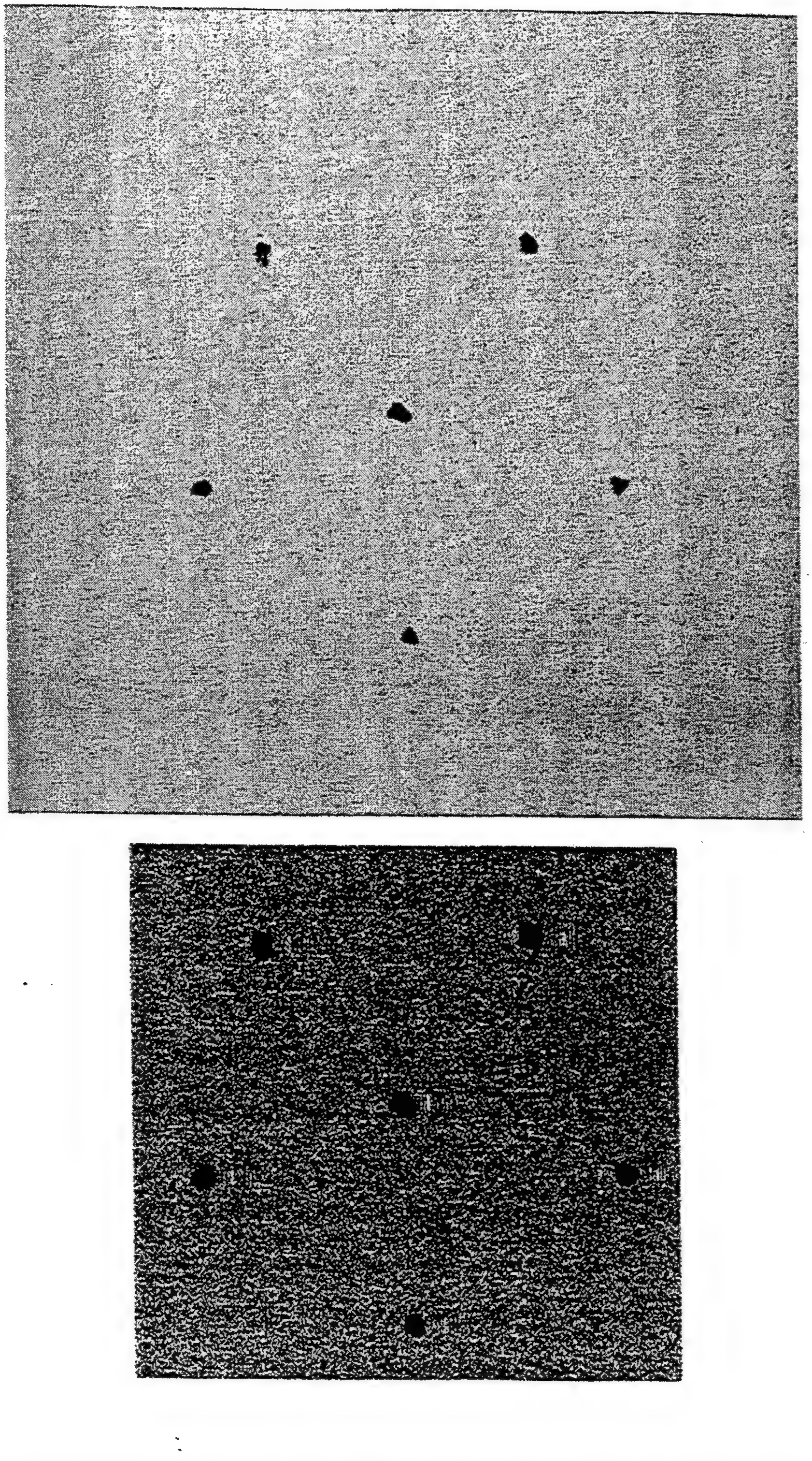

Figure 1: The top panel is an intermediate template image, M1-05, of the 5-times diluted M1 specks superposed on a noiseless background. The bottom panel is the corresponding CCD image (M1-05-CCD) obtained from the MegaScan monitor. The 14-bit CCD image was displayed at very high contrast (window = 10, level = 12,018) to visualize the noise. Faint ringing artifacts are seen along the scan-line direction to the right of each speck. For the CCD-CAMPI analysis only one image like the bottom panel is needed. For the TW analysis, ten images like the bottom panel and 10 of a noiseless image are needed. Note that unlike the top panel image, the bottom panel image has a finite signal-to-noise-ratio.

Details of image acquisition

A high performance digital camera, based on a Fairchild-Loral CCD was coupled to a monitor via a 35-mm photographic lens. Fig. 1 shows the image acquisition set-up. A laptop computer controls the camera. A small portion of the CRT is imaged onto the CCD and one attempts to over-sample the image (to avoid interference with the scan lines). To capture a complete microcalcification group, for this project the magnification was set to 3 CCD pixels per CRT pixel linear dimension. The specific CRT under test was a MegaScan monitor operated by a Dome display controller (MD-4) at 1723 x 2304 pixels. The low noise of the CCD camera was achieved by thermoelectric cooling to -10 degrees Celsius. The CCD pixel x-direction was closely aligned with the raster lines. The camera was read out at 500 kHz. The contrast resolution of the camera is nominally 14 bits. A flat fielding procedure corrects spatial non-uniformity of the CCD camera (spatial pixel noise) and vignetting of the coupling lens. The pixel matrix is 1317 x 1035, the pixel size is 0.0068 mm. The imaging optics is a Nikon Macro lens with a focal length of 55 mm. The f - stops of the lens range from f/2.8 to f/16. The curvature of the monitor was not a problem as the displayed field was small and the depth of focus was sufficiently large. An iris in front of the lens serves as baffle and assures optimum rejection of stray light and consequently assures reduction of veiling glare by the lens.

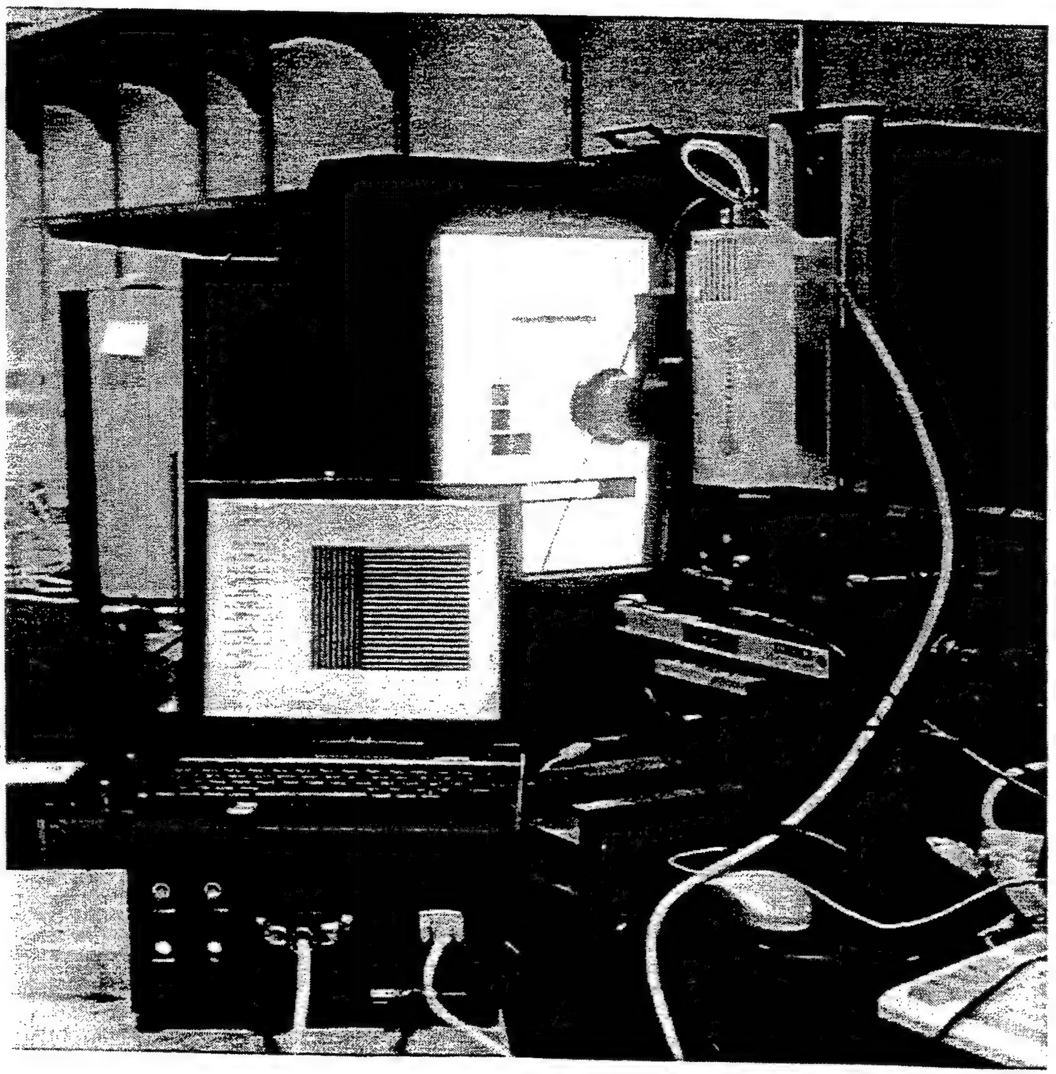

Figure 2: This shows the CCD measurement set-up. Shown are the monitor to be tested, the CCD camera, the x-y-z-positioning device and the laptop computer. In practice a hood is present between the monitor faceplate and the camera lens, which blocks ambient light.

Fourier Measurements

The software used to analyze the images from the CCD camera is based on the Interactive Data Language (IDL, Research Systems Incorporated) software. Programs were written to perform a variety of image analysis tasks, like determining Noise Power Spectra using 1-D and 2-D Fourier Transform, MTF from the Line Spread Function, mean and standard deviation, statistics, making horizontal and vertical profiles and so on. The brightness and contrast controls of the CRTs were adjusted using the SMPTE pattern[15,16]. The display luminance transfer function was determined following the recommendations of the DICOM standard[17]. This specifies that the display function is to be measured by displaying a square with area 10% of the display area in the center of the CRT, on a background with a luminance of 20 % of maximum luminance. Using a Minolta Spot Photometer LS-110 we measured the luminance in the center of the square target at about 30-command levels resulting in 30 equal luminance steps over the whole luminance range of the monitor.

To evaluate the NPS we captured flat field images, i.e. noiseless fields on the monitor set to 5%, 15%, 25%, 50%, 85%, 90%, and 100% of maximum luminance with the CCD camera, using imaging times from 0.5 to 1.5 sec. The Noise Power Spectra was determined from the 2-D Fourier Transform of the flat images after subtraction of the mean value in the image in order to avoid large offset values at zero spatial frequency.

The square wave response (SWR) was measured. Square waves were displayed on the display by setting a CRT line to 'on' and a CRT line to 'off' in horizontal or vertical directions. To satisfy the linear CRT assumption, we used small signal excursions (10% modulation). Rectangular fields were filled with square wave patterns. The fields were approximately 130 x 512 CRT pixels, for measurements in vertical direction, and 512 x 130 CRT pixels for the horizontal direction. Also, a flat field set to 20% of maximum luminance surrounded them. The SWRs were measured for +/-10% input Michelson-contrast in luminance around 4 different luminance levels of 15%, 25%, 50%, and 85% of the maximum luminance. MTFs were calculated from the SWRs, using standard methodology based on the Fourier decomposition of square waves.

3. RESULTS

CCD-CAMPI and TW

The CCD-CAMPI analysis resulted in 180 SNR values in all, corresponding to the 10 CCD images and the 18 specks. The TW analysis resulted in 18 eighteen additional SNR-values, one for each speck. A summary of these results is given in Table 1. This lists the template image name, the speck location as seen on Fig. 1; the NORM quantity; the speck SNR, the coefficient of variance (CV) of the SNR values calculated over the 10 CCD camera images, and the SNR as calculated by the TW method. Location '0' is the central speck, location '1' is the one at the 6 O' Clock position, and the count proceeds clockwise. Shown in Figure 3 is a plot SNR (CCD-CAMPI) vs. NORM. There are 18 points in all, corresponding to the three speck groups studied. A systematic upward shift of the M1-SNR values of about 25% is evident. The straight line fitted *after excluding these points* has excellent correlation ($r^2 = 0.9989$). It is remarkable that scaling the M1-SNR values down by 25% (i.e., assuming a dilution factor of 4 rather than 5) leads to a regression fit to *all* points in Fig. 3 with $R^2 = 0.9989$. The regression line has a small positive intercept, whose significance is not clear. The reasons for the systematic error are discussed later. Also listed in Table 1 are the coefficients of variances of the CCD-CAMPI measurements, approximately 4%. Figure 4 shows a plot of SNR (TW) vs. SNR (CCD-CAMPI). The regression is constrained to pass through the origin. The two methods are seen to track each other and the TW method yields about 24% higher SNR values than CCD-CAMPI. Comparison of this plot to Fig. 3 suggests that the TW method is fairly noisy when only 20 images are used. This is discussed later.

Fourier Measurements

Fig. 5 is a plot of the display luminance transfer characteristic. The luminance to digital value plot (CCD sensitivity) is highly linear over 4 orders of magnitude. Nominally, the CCD digital value was equal to 1308 times the luminance in foot-lamberts. Fig. 6 is the NPS in the scan-line (horizontal) direction for the case that the input to the CRT was 180 ADU. The MTF at 2 lp/mm was about 0.12 in the horizontal direction and 0.18 in the vertical.

Table 1: This table summarizes the CCD-CAMPI results. It lists the template image name, the speck location as seen on Fig. 1; the NORM quantity; the speck SNR, the coefficient of variance (CV) of the SNR values calculated over the 10 CCD camera images, and the SNR as calculated by the TW method. Location '0' is the central speck, location '1' is the one at the 6 O' Clock position, and the count proceeds clockwise.

Image	Speck Location	NORM	SNR CCD-CAMPI	CV CCD-CAMPI	SNR TW
M1-05	0	12.22	2503.1	0.043	3081
M1-05	1	8.32	1717.2	0.037	2641
M1-05	2	9.50	1957.9	0.037	2461
M1-05	3	9.28	1886.1	0.043	1747
M1-05	4	12.81	2537.9	0.039	2975
M1-05	5	9.31	1914.8	0.039	2438
M2-02	0	8.13	1358.3	0.050	1818
M2-02	1	7.13	1192.8	0.055	1524
M2-02	2	5.50	973.8	0.049	913
M2-02	3	5.84	1034.5	0.045	1407
M2-02	4	6.43	1101.7	0.046	1707
M2-02	5	7.58	1277.5	0.040	1553
M3-01	0	4.24	786.2	0.036	822
M3-01	1	3.27	646.4	0.034	808
M3-01	2	3.49	667.1	0.032	706
M3-01	3	3.25	625.4	0.034	772
M3-01	4	4.06	759.5	0.027	1306
M3-01	5	4.29	793.1	0.045	971

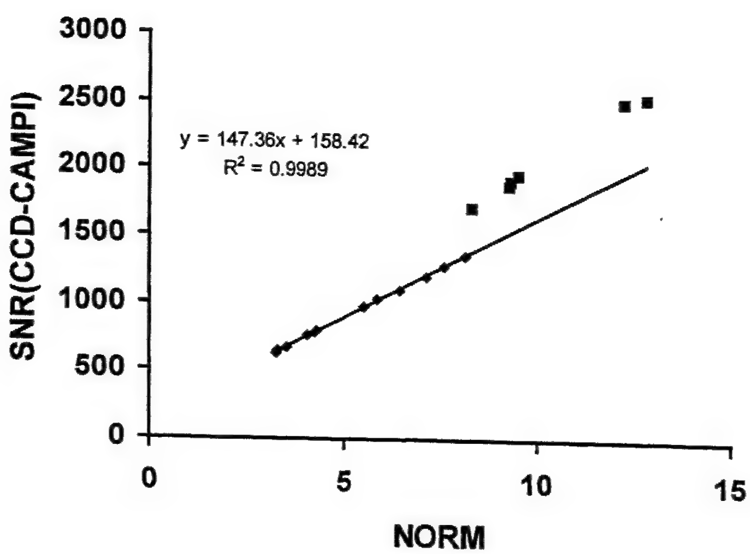

Figure 3: Shown is a plot SNR (CCD-CAMPI) vs. NORM. There are 18 points in all, corresponding to the three speck groups studies. A systematic upward shift of the M1-SNR values of about 25% is evident. The straight line fitted after excluding these points has excellent correlation ($r^2 = 0.9789$). Possible reasons for the systematic error are discussed later. It is remarkable that scaling the M1-SNR values down by 25% leads to a regression fit to *all* points with $R^2 =$ 0.9989.

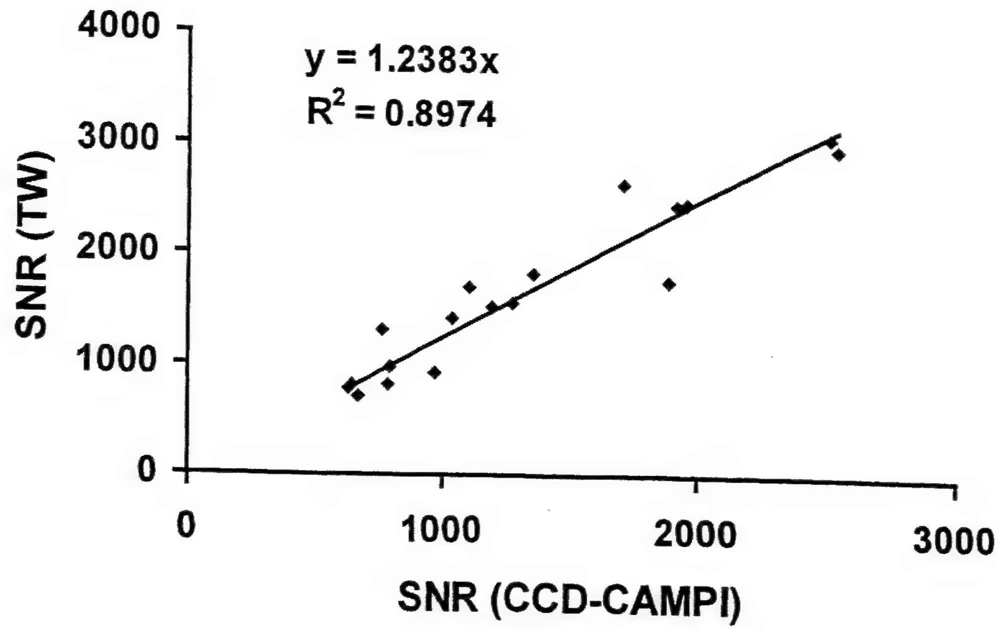

Figure 4: Shown is a plot SNR (TW) vs. SNR (CCD-CAMPI). The regression is constrained to pass through the origin. It is seen that the two methods track each other and the TW method yields about 24% higher SNR values than CCD-CAMPI. Comparison of this plot to Fig. 3 suggests that the TW method is fairly noisy when only 20 images are used.

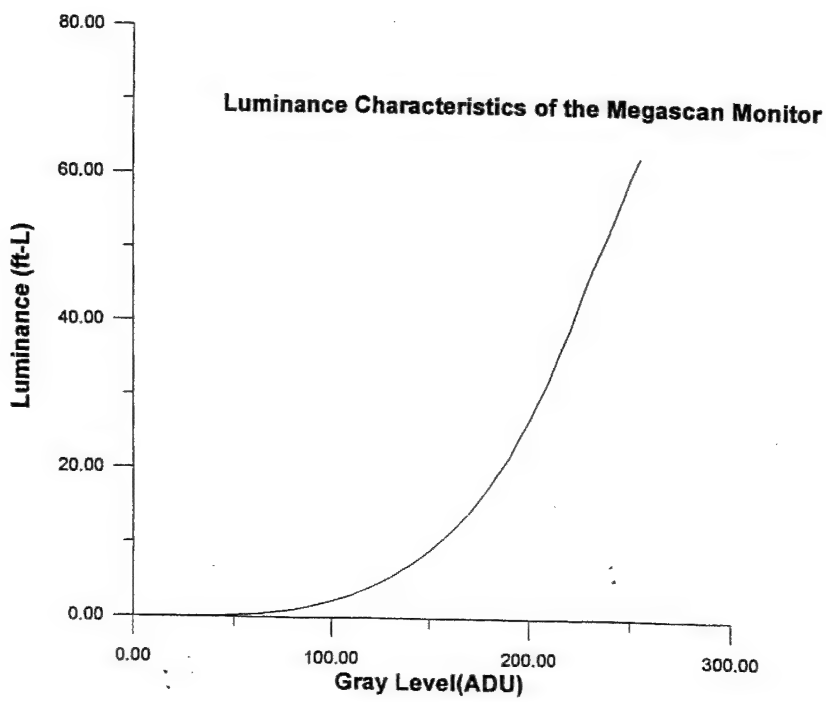

Figure 5: This figure shows the luminance transfer characteristic of the MegaScan monitor used in this study. The CCD-CAMPI test patterns we used had an average value of 127. The CCD digital output was closely linear with the luminance. Nominally, the CCD digital value was equal to 1308 times the luminance in foot-lamberts.

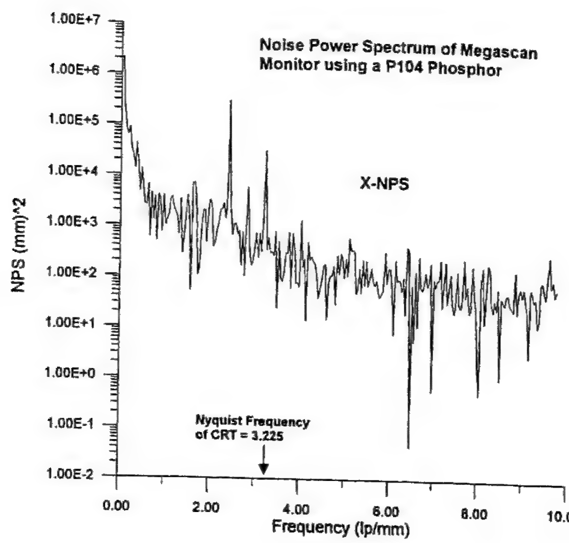

Figure 6: This figure shows the NPS of the MegaScan monitor used in this study. The measurement was in the scan-line (horizontal) direction for the case that the input to the CRT was 180 ADU.

4. DISCUSSION

Note that the CAMPI method can calculate SNR for individual images. It samples one target point for the numerator and approximately 300 non-target points, *on the same image*, for the denominator. The TW method cannot be applied to single images. For reasons of practicality we obtained 20 images in all, leading to 10 samples for the numerator and 10 for the denominator. Also, note that in the TW method the noise sampling is of *different images* at the same physical location. This means that image spatial noise does not contribute as much to the noise determination by the TW method. In fact static structure mottle on the CRT screen would be suppressed in the TW method. In CCD-CAMPI such spatial noise would increase the noise variance and suppress the SNR. We believe this is the reason why the TW method yields a SNR about 25% larger that the CCD-CAMPI method. From a practical point of view we believe that the image spatial noise should be included in the noise determination, as it detracts from the observer's ability to detect the target. From Table 1 it is seen that the intrinsic accuracy of the CCD-CAMPI method is about 4.1% for individual images. This accuracy is affected by actual image-to-image variability of the monitor, variability of the CCD-digitizer and variability due to the CCD-CAMPI algorithm. The accuracy for groups of 10 images would be $\sqrt{10}$ times smaller, i.e., 1.3%. This result and the close correspondence of SNR (CCD-CAMPI) with NORM suggests that the scatter shown in Figure 4 is mainly due to the TW method. It is well known that noise is especially difficult to assess accurately. In Fourier measurements one averages many images to obtain the NPS. The reason for the larger noise in the TW method is due to the much smaller number of noise samples being obtained, i.e., one noise sample per image as compared to over 300 in the CCD-CAMPI method.

It is not clear to us what is the reason for the systematic error observed in Fig. 3 for the M1-specks. A sudden change in the monitor or CCD electronics could have caused this effect. Alternatively, the low pixel value change (7 out of 127) in the M1 specks could have led to a measurement artifact. The pixel value swing was larger for the less diluted M2 and M3 specks. In fact, due to the limited availability of gray levels, the M1 speck template file displayed noticeable contouring effects. The effect could also be due to CRT non-linearity, see Fig. 5. We plan to repeat some of the measurements and test the different theories. Other planned measurements are a systematic evaluation of the effect of CCD imaging parameters (magnification, aperture settings, exposure time, CCD matrix orientation with respect to the raster, etc.). Other planned measurements are to fiber and mass targets and different monitors. As regards the effects of the non-linear monitor response (see Fig. 5), we expect to correct for this in the future by transforming the CCD pixel value to the digital driving level of the monitor (using Fig. 5) and making CCD-CAMPI measurements on the transformed pixels.

While the present work was limited to specks, we could just as well have used other target objects (e.g., fibers and masses) and calculated the equivalent SNR measures. Also, we are not restricted to target objects that are *physically realizable*. For example, we could digitally design different types of target objects that may be more sensitive to discrimination tasks that are

important in mammography, e.g., discriminating benign from malignant specks. The CCD-CAMPI *test pattern* is similar in principle to other test patterns (e.g., the SMPTE). Like the SMPTE, the precise pixel values in the test pattern are known exactly. The essential difference is that the target objects in the test pattern are not bar patterns or step wedges, rather they are clinically significant objects (i.e., specks, fibers and masses) whose visibility is of direct relevance to mammographers. Since these objects can be small and of irregular shape, conventional densitometric measurement techniques are not suited to them. CAMPI is well suited to calculating the SNR of these arbitrarily shaped objects.

The SNR image quality metric has the following advantages over visual evaluation of test patterns, such as the SMPTE. It is objective and more precise and it results in task specific metrics. For example, the speck SNR is expected to closely mimic the performance of the monitor for visualizing specks. The Fourier measures require sophisticated analysis and many images. In principle it should be possible to calculate the SNR based on the physical measurements. The SNR depends on the template, the MTF, the contrast transfer function, the measured signal and the NPS[18]. The relationship can be evaluated numerically and we expect that this will confirm the CCD-CAMPI measurements. Indeed, we plan to conduct such "bridging" measurements in the future. However, we believe that the CCD-CAMPI method represents a more convenient and cheaper way of obtaining this information directly, without having to go through the complete imaging chain analysis. Like the TW method the Fourier measurements cannot be applied to single images. Of the three methods, CCD-CAMPI is by far the most convenient. With adaptation to inexpensive CCD devices that are becoming available, we expect that a low-cost device can be produced that will allow the measurements of image quality of a mammography monitor in less than 15 minutes.

With adaptation to inexpensive CCD devices that are becoming available, we expect that a low-cost device can be produced that will allow the Technologist to measure the image quality of a mammography monitor in less than 15 minutes. Such a device would work in conjunction with template files stored locally on the workstation to produce a complete QC report of monitor image quality. The assessment would cover speck, mass and fiber image quality and their variation over the monitor display area. By comparison, present monitor QC activities are limited to measuring display luminance levels and visual inspection of a SMPTE test pattern.

In conclusion, we have shown the feasibility of measuring video display image quality for digital mammography using the CCD-CAMPI method. The method could be used to measure *relative* performances on different monitors. Work is also underway to characterize the image quality loss introduced by the CCD camera and perform absolute measurement of CRT image quality with other CCD cameras, e.g., a digital camera.

5. ACKNOWLEDGMENTS

This work was supported in part by the US Public Health Service's Office on Women's Health, Department of Health and Human Services, under contract number RFP 282-97-0077 and by a grant from the Department of Health and Human Services, National Institutes of Health, National Cancer Institute, RO1-CA75145.

REFERENCES

[1] Working Group on Digital Mammography. Meeting held in Washington DC, March 9-10, 1998. Sponsored by the US Public Health Service's Office of Women's Health and the National Cancer Institute.

[2] Roehrig H, Blume H, Ji T-L, Browne M. Performance Test and Quality Control of Cathode Ray Tube Displays. J Digital Imaging, 3: 134-145, 1990.

[3] Ji T-L, Roehrig H, Blume H, Seeley G, Browne M: Physical and Psychophysical Evaluation of CRT Noise Performance. *Proceedings of the SPIE*, 1444: 136-150, 1991.

[4] Roehrig H, Dallas W, Ji T-L, Lamoreaux RD, Oikawa C, Vercillo R, Yocky D. Physical evaluation of CRTs for use in digital radiography. *Proceedings of the SPIE,* 1091: 262-278, 1989.

[5] Chakraborty DP, Eckert MP: Quantitative versus Subjective Evaluation of Mammography Phantom Images. Medical Physics, 22: 133-143, 1995.

[6] Chakraborty DP: Computer Analysis of Mammography Phantom Images (CAMPI): An Application to the Measurement of Microcalcification Image Quality of Directly Acquired Digital Images, Medical Physics. 24 (8), 1269-1277, 1997.

[7] Eckert MP, Chakraborty DP: "Quantitative Analysis of Phantom Images in Mammography", *SPIE Proceedings on Image Processing 2167-88*, Newport Beach, CA, 1994.

[8] Chakraborty DP, Eckert MP: "Quantitative versus Subjective Evaluation of Mammography Phantom Images", *Medical Physics* **22**: pp. 133-143, 1995.

[9] Chakraborty DP: "Physical measures of image quality in mammography", *Proceedings of the SPIE, Medical Imaging, Image Display*, **2708**, pp. 179-193, 1996.

[10] Chakraborty DP: "Computer analysis of mammography phantom images (CAMPI)", *Proceedings of the SPIE, The Physics of Medical Imaging*, **3032**, 292-299, 1997.

[11] M. J. Tapiovaara and R. F. Wagner, "SNR and noise measurements for medical imaging: I. A practical approach based on statistical decision theory," Phys. Med. Biol. 38:71-92, 1993.

[12] M. J. Tapiovaara, "SNR and noise measurements for medical imaging: II. Application to fluoroscopic x-ray equipment," Phys. Med. Biol. 38:1761-1788, 1993.

[13] Chakraborty DP: "Comparison of computer analysis of mammography phantom images (CAMPI) with perceived image quality of phantom targets in the ACR phantom", *Proceedings of the SPIE, Image Perception Conference,* **3036**:160-167, 1997.

[14] Chakraborty DP and Fatouros PP: An Application of CAMPI Methodology: Comparison of two Digital Biopsy Machines, *Proceedings of the SPIE*, Medical Imaging, vol 3336, 618-628, 1998.

[15] Gray J.E., Stears J., Wondrow M. Quality Control of Video Components and Display Devices. *Proceedings of the SPIE,* 486:64-71, 1984.

[16] Lisk, K.G. SMPTE Test Pattern for Certification of Medical Diagnostic Display Devices. *Proceedings of the SPIE,* 486:79-82, 1984.

[17] Blume H: The ACR/NEMA Proposal for a Grey-scale Display Function Standard. *Proceedings of the SPIE,* 2707: 344-360, 1996.

[18] D. P. Chakraborty, G. T. Barnes, "Signal-to-noise-ratio considerations in radiographic imaging," Med. Phys. 10:467-469 (1983).

Anomalous Nodule Visibility Effects in Mammographic Images

Dev P. Chakraborty and Harold L. Kundel, University of Pennsylvania, Philadelphia

ABSTRACT

This study was undertaken to further investigate recent reports of unusual contrast-detail (CD) behavior in images with mammographic backgrounds, namely threshold contrast for detection increased with nodule size for Gaussian nodules. In this work we investigated the effects on the CD curve of allowing differently shaped nodules, in particular nodules with sharper edges. The following types of nodules/disks were studied: Gaussian shaped nodules and blurred disks, the latter characterized by a radius and an independent edge sharpness parameter. In a second type of disk the edge blur was held proportional to the disk radius. Ideal Observer detection thresholds were calculated for different nodule/disk radii ranging from 1.5 to 15 mm and observer performance studies were conducted. Noise power spectra (NPS) measurements confirmed the frequency dependence previously reported, NPS $\propto 1/f^{3.1}$. For the Gaussian nodules we confirmed the reported CD behavior, with threshold contrast $\propto$ radius$^{0.2}$. However, for the disk nodules with fixed blur edges we observed different behavior (larger objects required less contrast), with threshold proportional to radius $^{-0.28}$. For the disk nodules with variable blur the threshold contrast was almost independent of radius. In summary while we duplicated the reported CD diagrams for Gaussian nodules, different behavior was observed for nodules with edges. We conclude that in addition to considering the details of the noise, it is necessary to consider the signal properties in more detail.

Keywords: Mammography, nodules, detection threshold, ideal observer models.

1.INTRODUCTION

The threshold contrast for detection is defined as that contrast that yields a specified detection rate. Most imaging physicists are familiar with contrast-detail (CD) diagrams, which show the threshold contrast necessary for detection as a function of size of the object to be detected. In this paper we define the CD diagram to be a plot of the logarithm of threshold lesion amplitude vs. the logarithm of the radius. This plot typically has negative slope, as larger objects generally require less contrast to detect them. In fact, based on a Rose model [1] calculation for white (i.e., uncorrelated) noise one expects a slope of -1 on a log-log plot. The negative slope appears to be reasonable since one expects a larger object to produce a larger measured signal, thereby increasing the numerator of the signal-to-noise-ratio (SNR). Also the associated noise generally decreases with the size of the object to be detected, since more pixels are being averaged. It is less well known that the expected CD diagram depends critically on the nature of the background noise. It has been shown recently [2, 3] that if the noise power spectrum has an inverse power law dependence on spatial frequency, i.e., $1/f^{\beta}$ with $\beta > 2$, as is true for mammographic backgrounds, qualitatively different behavior was observed, namely the threshold contrast increased with lesion size.

Burgess' calculations [3] were made for a class of nodules termed 'scalable' in the sense that they could be characterized by functions of r/a, where **r** is the distance from the center and **a** is the nodule radius. For example, for Gaussian nodules the function is $\exp(-r^2/2a^2)$. For scalable nodules he showed that the slope **m** of the CD diagram on a log-log plot was $m = (\beta-2)/2$. Note that with scalable nodules it is not possible to independently specify the sharpness of a nodule's edges. The scalability criterion represents an assumption that real nodules may not satisfy. An example is a nodule characterized by both a size parameter (the lateral extent of the nodule) and an independent edge-sharpness parameter, namely how rapidly the x-ray transmission changes near the edge. Since the human visual system tends to accentuate edges [4], the CD behavior could change significantly based on the presence or absence of such edges. The objective of this study was to test the effects of deviations from scalability, specifically to investigate the influence of including an independent edge parameter on nodule detection in mammographic backgrounds.

Presented in the following sections are details of the nodules and disks studied, the ideal observer methodology used to calculate threshold amplitudes and the noise power spectra measurement. These are followed by details of the observer experiments and the results.

Image Perception and Performance, Elizabeth A. Krupinski, Dev P. Chakraborty, Editors, Proceedings of SPIE Vol. 4324 (2001)

2.METHODS

2.1 ANALYTICAL

2.1.1 IDEAL OBSERVER MODEL: In order to understand human observer performance it has proven useful to study a variety of model observers, also called numerical observers, which are algorithms for calculating the SNR for specified signal and noise statistics [2, 5, 6]. The model observers differ from each other in how much use is made of information regarding the imaging task. In this work we used the Fisher Hotelling (FH) observer, sometimes called the pre-whitening matched filter, which takes into account knowledge of both the signal and the noise statistics, and the non-prewhitening matched filter with eye-filter (NPWE). Observer internal noise was neglected. Following Ref. 3 we describe a nodule profile by specifying its amplitude rather than its contrast, the two approaches being equivalent. Fourier methods were used to calculate the threshold amplitude for a given signal and noise [7] for the Fisher- Hotelling (FH) numerical observer. Two classes of cylindrically symmetric nodules were generated for this study: blurred disks (BD) and Gaussian nodules (GN) see Figure 1. The amplitude of the Gaussian nodule $S_{GN}(r, a)$ is defined by

$$S_{GN}(r, a) = A \exp\left[-\frac{r^2}{2a^2}\right], \qquad \text{Eqn. 1}$$

where **A** is the peak nodule amplitude. The blurred disk amplitude function $S_{BD}(r, a, \sigma)$ is defined as a two-dimensional convolution of the Rectangle function $\Pi(r/2a)$ (= 1 if $r < a$ and = 0 otherwise) and the Gaussian function $\phi(r, \sigma)$:

$$S_{BD}(r, a, \sigma) = A\,\Pi(r/2a) \otimes \phi(r, \sigma), \qquad \text{Eqn. 2}$$

where σ is the edge-blur parameter and

$$\phi(r, \sigma) = \frac{1}{2\pi\sigma^2} \exp\left[-\frac{r^2}{2\sigma^2}\right]. \qquad \text{Eqn. 3}$$

The Fourier Transform (FT) of a radially symmetric two-dimensional function is a Hankel transform. Using results from [8], the Hankel transform of the blurred disk amplitude function is given by

$$\tilde{S}_{BD}(f, a, \sigma) = A\,\frac{a\,J_1(2\pi a f)}{f} \times \exp[-2\pi^2\sigma^2 f^2], \qquad \text{Eqn. 4}$$

where J_1 is the Bessel function of order 1, and f is the radial frequency. The Hankel-transform of $S_{GN}(r, a)$ is given by

$$\tilde{S}_{GN}(f, a) = A\,e^{-2\pi a^2 f^2}. \qquad \text{Eqn. 5}$$

In either case the SNR of the Fisher-Hotelling (FH) numerical observer is given by

$$SNR^2(A) = \int_0^\infty 2\pi f\,\frac{\tilde{S}^2(f, a)}{NPS(f)}\,df, \qquad \text{Eqn. 6}$$

where NPS is the Noise Power Spectrum of the background and $\tilde{S}(f, a)$ is the relevant Hankel transform. The SNR is equivalent to the detectability index d' measured with a Two-Alternative Forced Choice (2AFC) experiment[9]. Since SNR is proportional to A, one has SNR(A) = A SNR(1). The threshold amplitude A_T, defined by $SNR(A_T) = 1.0$ is given by $A_T = 1/SNR(1)$. The integral in Eqn. 6 was evaluated numerically using 20th-order Romberg integration as implemented in the Interactive Data Language (IDL) development system (Research Systems Inc., Boulder, CO). All calculations were also repeated with the NPWE observer using the formula given in Ref. 3.

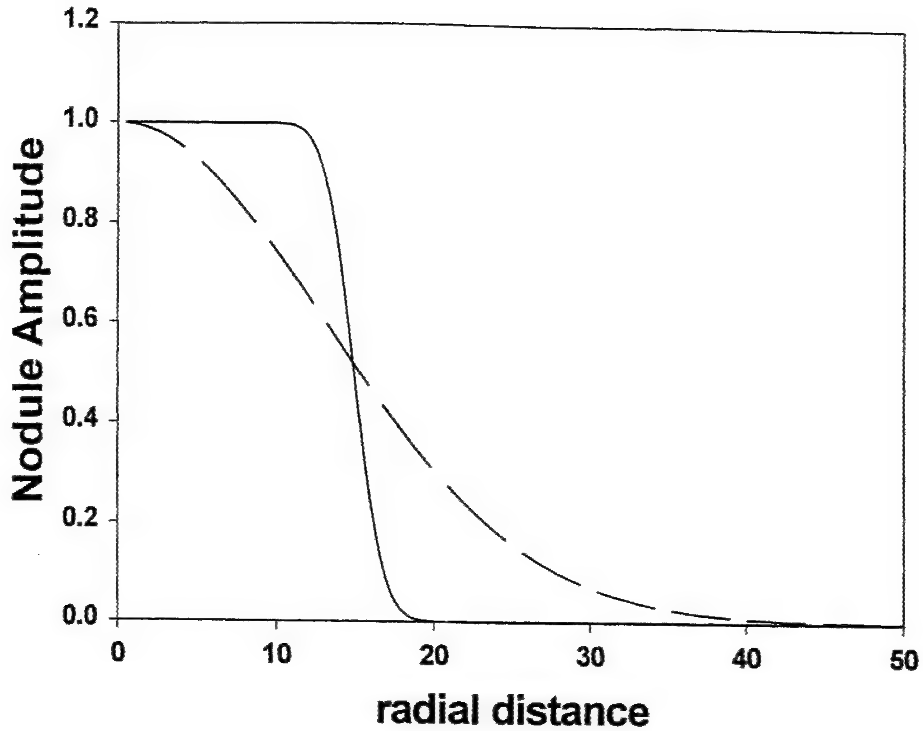

Figure 1: The solid line shows the radial profile of a blurred-disk nodule, with radius a = 15, edge blur parameter σ = 1.5, and the dashed line is for a Gaussian nodule with radius a = 13.

In addition to the blurred-disk model with fixed edge blur described above, we also studied nodules in which the edge-blur parameter was proportional to the nodule radius, $\sigma = 0.3$ a. These will be referred to as VB (variable blur) disks to distinguish them from the previously described FB (fixed blur) disks.

2.1.2 NPS MEASUREMENTS: The Noise Power Spectrum (NPS) of mammographic backgrounds was measured using 256 x 256 ROIs (regions-of-interest) randomly rotated, using nearest-neighbor interpolation, and extracted from digitized mammograms. The rotation served to average over any non-cylindrically symmetric asymmetry present in the images and to be consistent with the subsequent NPS analysis. A larger (by a factor of 1.414) square ROI was extracted around an operator chosen point in a relatively homogeneous region of the image. This ROI was randomly rotated around the center and the 256 x 256 ROI was then extracted. By choosing to rotate the larger ROI we eliminated the possibility that missing or invalid pixels would contaminate the smaller one.

We followed the Digital Fourier Transform (DFT) convention given in [10]. Before taking the DFT it is necessary to apply a window function to prevent leakage of power between frequency channels[11]. We used the Hanning window function H_{jk} ($0 < j,k < N-1$, where N is the number of pixels per square ROI-edge) defined by [12]:

$$H_{jk} = w_j \, w_k, \qquad \text{Eqn. 7}$$

and

$$w_j = \frac{1}{2} \left| 1 - \cos\left(\frac{2\pi j}{N-1}\right) \right|. \qquad \text{Eqn. 8}$$

The window normalization factor W_{ss} is defined by

$$W_{SS} = \sum_{j,k=0}^{N-1} w_j^{2} \; w_k^{2} \qquad \text{Eqn. 9}$$

With these definitions the NPS, in units of mm^2, is given by

$$NPS = \frac{|\, DFT\ (H_{jk}\, I_{jk})\ |^2\ P^2}{W_{SS}}, \qquad \text{Eqn. 10}$$

where I is the average-subtracted ROI and P is the monitor pixel size, equal to 0.15 mm in our case. As a check on the normalization the sum of the NPS values divided by the area of the ROI, should yield the variance of the pixel values.

Finally a radial-frequency average was performed by averaging all pixels in the 2-dimensional NPS matrix at a fixed distance from the origin in frequency space. The measurement was repeated for 60 images, and the individual-image NPS functions were averaged. In this manner we determined the NPS (f) function of spatial frequency. The NPS function was fitted to the following empirically determined form (all logarithms are with respect to base 10):

$$\log\,(NPS\,(f)) = A + B\,f - \log\,(D + f^{\beta}), \qquad \text{Eqn. 11}$$

where A, B and β were treated as fitting parameters and D was fixed at $(1/256)^3$ to prevent the NPS from going to infinity at zero frequency [3]. The NPS algorithm was also tested on simulated Gaussian noise images and images of an ACR phantom. In our experience the effect of the Hanning window was fairly significant. Without it the phantom NPS also showed unrealistic $\sim 1/f^3$ frequency dependence, which disappeared on use of the filter.

2.2 OBSERVER STUDIES

2.2.1 NODULE GENERATION: Gaussian nodules of unit amplitude were generated using Eqn. 1. To generate blurred-disk nodules we convolved a Rectangle function of suitable radius with the Gaussian function defined in Equation 3. Six (6) nodule sizes with radii ranging from 1.5 mm < a < 15 mm were generated and the blur parameter σ was held at 5 pixels (0.75 mm) for the FB disks and 0.3 a for the VB disks. The display window (512 pixels square) was not large enough to accommodate the largest disk in the VB condition. We did not employ a look-up-table to linearize the display as recommended in Reference 3). Linearizing the display and physical imaging chain may be insufficient since a significant source of uncorrected non-linearity, the human observer, exists beyond it.

2.2.2 IMAGES: Fifty (50) screen-film mammograms were digitized (Lumisys LS-100) at 100-micron spot size for this study. Note that the digitizer pixel size is irrelevant to this study – it is the monitor pixel size (0.15 mm) that enters the formulae. Typically twenty to forty 512 x 512 ROIs were extracted from each image with the constraints that (1) the ROIs were separated by at least 100 monitor pixels (1.5 cm) in the horizontal or vertical direction, and (2) the ROIs were extracted from areas of reasonably uniform breast thickness. ROIs from different images were displayed in pairs on a 2048 x 2560 monitor (BARCO MGD-5, Clinton Electronics, Rockford, IL) driven by a DOME MD-5PCI display card (Dome Imaging Systems, Inc, Waltham, MA) using a Dell Optiplex computer running the Windows NT 4.0 operating system. A simulated nodule, as described above, was randomly superposed (i.e., added) at the center of one of the image-pairs. An algorithm using histogram analysis, applied separately to each image of the pair, was used to determine linear look-up-tables to display the images at optimal contrast and brightness. The region used to determine the histogram was confined to the central 256x256 region of the image.

2.2.3 READERS: Figure 2 shows the user interface for the human reader studies. The readers for this study were paid subjects (university students and staff) with good vision. They were told that a nodule was always present at the center of one of the image pairs. Their task was to indicate with a pointing device which side (left-or-right) was more likely to contain the superposed nodule. A modified QUEST algorithm [13] was used that utilized all preceding observer responses to

determine the amplitude of the nodule for the next presentation, to achieve a target detection rate of 92% (corresponding to a d' of 2.0). QUEST also calculated the maximum likelihood estimate (MLE) of the threshold amplitude and its uncertainty. The experiment was terminated after 512 image pairs had been viewed. The MLE value of the nodule amplitude at that point was defined as the threshold amplitude.

The readers were trained on 200 ROI pairs randomly drawn from the set described above, and these results were not scored. Following each response the software indicated if the reader's selection was correct or incorrect. The continuous feedback condition was maintained for the duration of the studies. A total of 6 readers performed the experiment for six nodule-radii and three nodule types (Gaussian, fixed and variable blur disks). The viewing distance was not restricted.

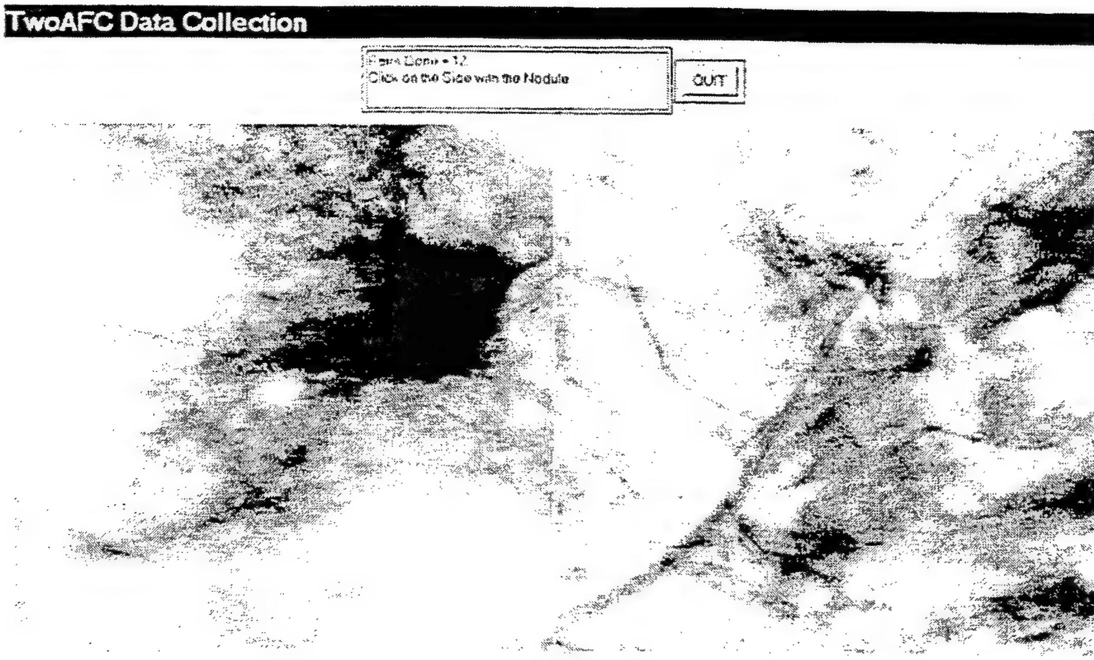

Figure 2: The user interface for the 2AFC human reader experiments. The two regions shown are 512 x 512 ROIs extracted from mammographic images. At the center of the left ROI is a 3 mm (20 pixel) radius blurred pixel disk with edge blur = 1 mm. Reference examples of the disks at three different contrasts were displayed below this window.

3.RESULTS

3.1 NPS Measurements

Figure 3 shows the NPS data plotted as $\log_{10}$(NPS) vs. frequency and the fitted function according to Eqn. 11. The fitting parameters were A = -2.0, B = 0.4 and β = 3.1. The parameter β is, of course, the exponent of the inverse power law dependence of NPS on frequency, i.e., if the constant D in Eqn. 11 is neglected, then for small frequencies NPS ~ $1/f^{\beta}$. All curve fitting was done using Sigma Plot software (SPSS, Chicago, IL). The fitted NPS function was used to calculate the threshold amplitudes of the nodules, as shown in Eqn. 6.

3.2 Analytical Threshold Results

3.2.1 Gaussian nodules: In Figure 4 the logarithm of the amplitude threshold is shown versus the logarithm of the radius in mm. This is seen to be similar to Figure 1 in Reference 3, the differences could be accounted for by the differing noise power spectra used. The peak threshold occurs at radius = 29.8 mm. Also shown is a straight line with slope 0.5, which is the limiting behavior at small radius. It is seen that for the Gaussian nodules our results confirmed the findings reported in the earlier study.

3.2.2 Blurred Disks: For the blurred disks with fixed edge blur of 0.75 mm, we found different behavior, as shown in Figure 5. For the range of nodule sizes studied, the threshold amplitude decreased as the radius increased, with an approximate $a^{-0.5}$ dependence. Finally, as shown in Figure 6, for the blurred disk with variable edges we found behavior similar to that for Gaussian nodules. The results shown here are for $\sigma = ka$, with $k = 0.3$. The peak occurs at radius $a = 49.5$ mm. For the NPWE numerical observer we obtained qualitatively similar results. The only substantive difference was that the thresholds were somewhat higher as compared to the FH observer. This is consistent with the fact that the NPWE observer is necessarily less efficient in detecting signals than the FH observer.

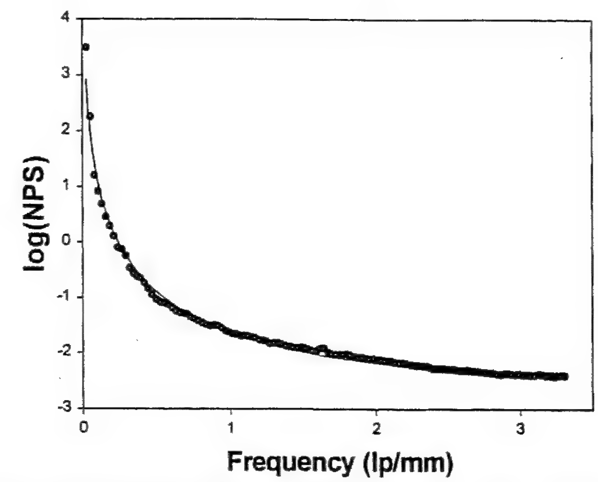

Figure 3: This shows Noise Power Spectra (NPS) results for mammographic backgrounds plotted as $\log_{10}$(NPS) vs. frequency. The solid line is the empirically determined fitting function described in Eqn. 11.

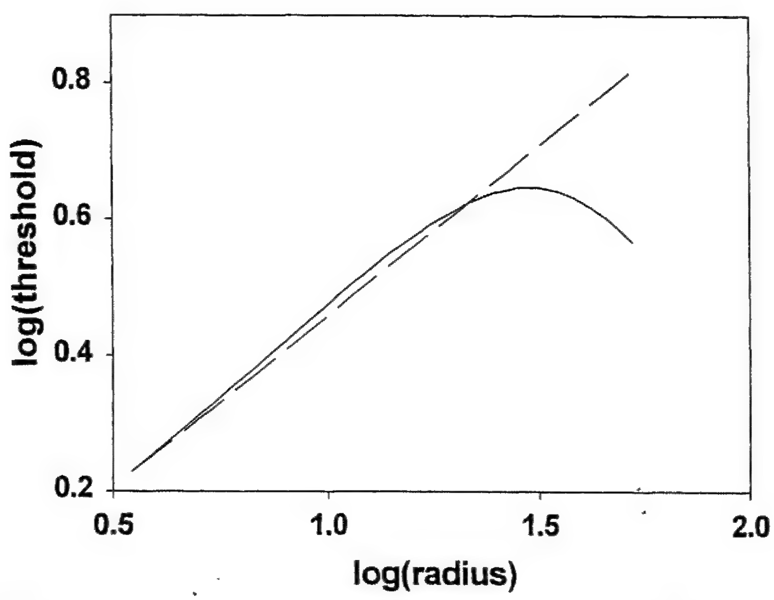

Figure 4: Contrast-detail plot for the Fisher-Hotelling numerical observer, showing the variation of threshold with radius (in mm) for Gaussian nodules. Note the increase in threshold with radius for radius less than 29.8 mm. Also shown is a straight line with slope 0.5, which is the predicted behavior at small radius.

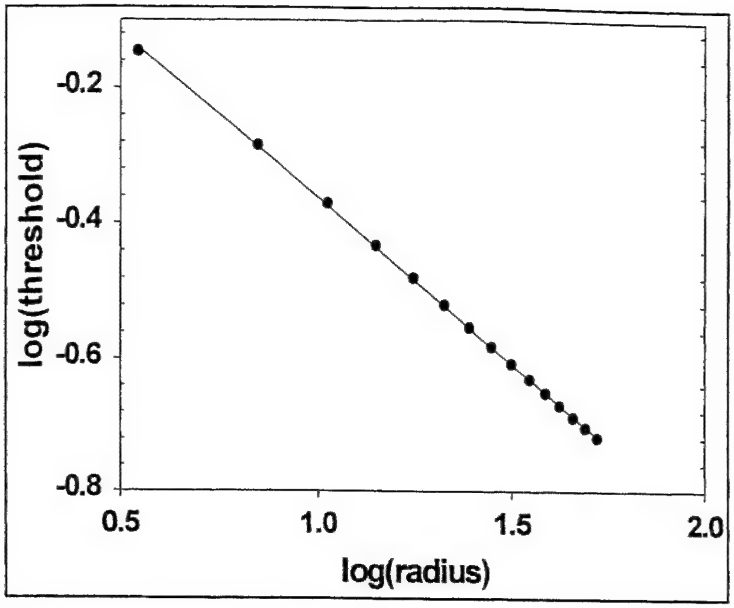

Figure 5: A contrast-detail plot for the Fisher-Hotelling numerical observer, showing the variation of threshold with radius (in mm) for fixed blur disks with $\sigma = 0.75$ mm. Note the uniform decrease of threshold with radius. The straight line is a regression fit to the data points with slope = -0.5, which is the predicted slope.

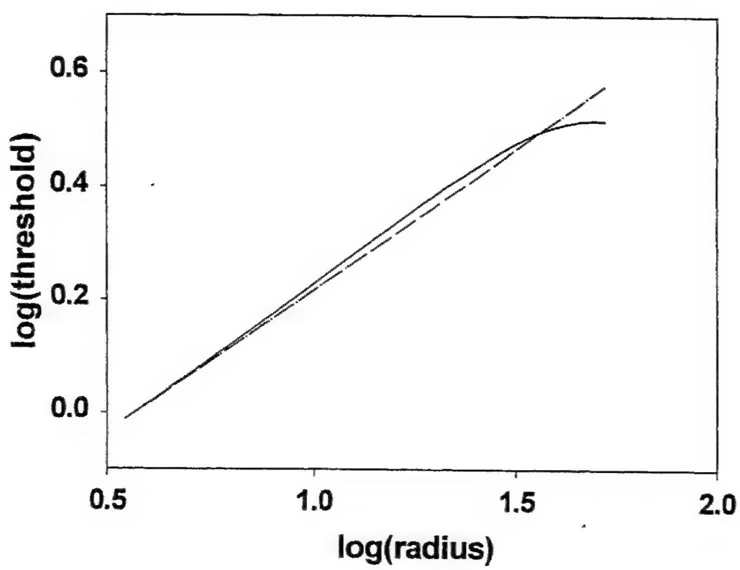

Figure 6: Contrast-detail plot for the Fisher-Hotelling numerical observer, showing the variation of threshold with radius (in mm) for variable blur disks with $\sigma = 0.3$ a. Note the resemblance of the behavior to that shown in Figure 4 for Gaussian nodules. The straight line, the limiting behavior at small radius, has slope = 0.5. The maximum occurs at a = 49.5 mm.

3.3 Human Observer Threshold Results

3.3.1 Gaussian nodules: Figure 7 shows the measured thresholds vs. radius, on a log-log plot, for the Gaussian nodules. The observed slope was 0.2 ± 0.09, which should be compared to the predicted value of 0.5. The standard deviation of each data point is about 10%, of which roughly 4% is the case sampling error, and the rest is inter-and intra- reader variability.

3.3.2 Disk nodules: Figure 8 shows the measured thresholds vs. radius for the FB disks with $\sigma = 0.75$ mm. The observed slope was -0.28 ± 0.06, which should be compared to the predicted value of 0.5. Similar results were observed for other values of σ in the range $0.075 < \sigma < 5.00$. As σ becomes smaller, the threshold amplitude drops. This is consistent with the notion that the increased edge information decreases the need for the observer to rely on amplitude to detect the nodule. For the variable blur disks the threshold data were observed to be constant to within the experimental uncertainty (5%), indicating that one is near the peak of the CD curve whose general form is shown in Fig. 4.

3.3.3 Efficiency: The human observer and ideal observer results can be combined to yield the efficiency of the human observer, defined as the square of the ratio of human and ideal observer d's[14]. This reduces to the square of the ratio of the ideal and human observer amplitude thresholds. Typically the efficiencies ranged from 10% to 20% for the FB disks, with the larger disks yielding smaller efficiencies, and 25%-80% for the Gaussian nodules, with larger nodules yielding greater efficiencies, and 15% to 50% for the variable blur disks, with the larger disks yielding greater efficiencies. The uncertainty in the efficiency numbers is considerable, about 30%.

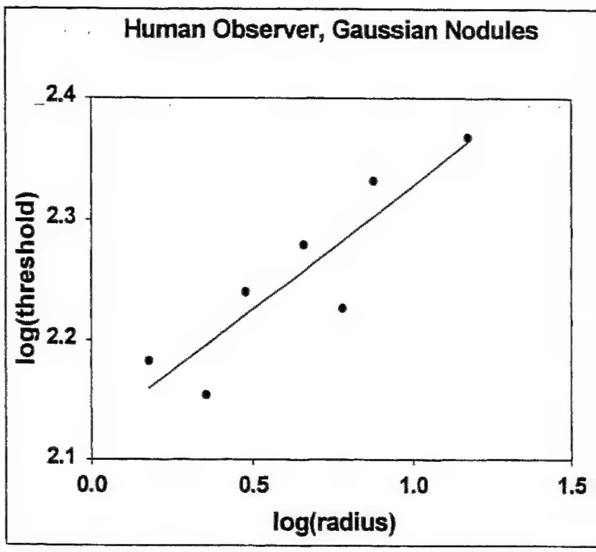

Figure 7: Contrast-detail plot for the average of six human observers showing the variation of threshold with radius for Gaussian nodules. The regression line has a slope of 0.20±0.09, which should be compared to the predicted value of 0.5 for the FH observer.

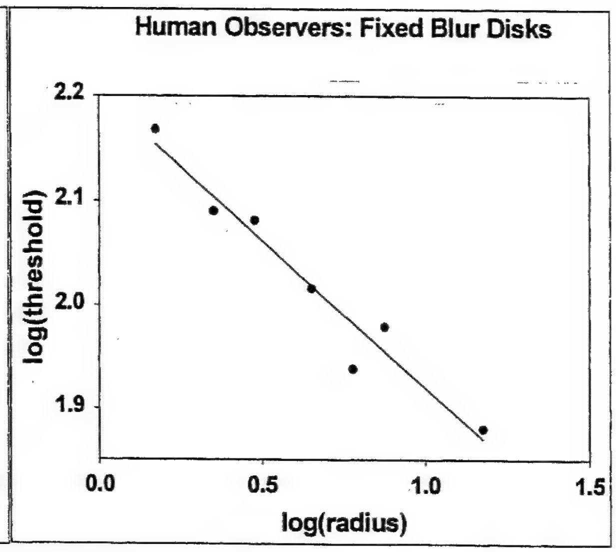

Figure 8: Variation of threshold with radius for the average of six human observers for fixed blur disks with $\sigma = 0.75$ mm. The regression line has a slope of -0.28 ± 0.06, which should be compared to the predicted value of -0.5 for the FH observer.

4. DISCUSSION

As indicated in the Introduction these experiments were undertaken to further investigate an unusual and significant result reported earlier in these proceedings. Our results confirmed the earlier findings for the Gaussian nodules. The NPS measurements, on an independent set of images, are in good agreement with the quoted range of exponents in the earlier studies. The fixed blur results can be understood by noting that as the disk becomes larger the edge information does *not* shift to lower spatial frequencies, as is true for Gaussian nodules. Therefore, the low frequency noise does not interfere with the edge information, leading to increased SNR and decreased threshold. While the shape of clinical nodules is open to question, one may get clues from the field of Computer Aided Detection (CAD) mammography. Researchers in CAD have found it necessary to include other independent features to characterize clinical masses, e.g., edge gradient, spiculation,

texture, etc. Each of these features could result in departures from the scalability assumption and a study of their effects is warranted. We have shown that the presence of an independent edge gradient can significantly change the CD diagram from that expected for scalable nodules, namely one can observe CD curves with negative, positive or near zero slopes as we have demonstrated. In spite of significant departures from the underlying assumptions (linearity and stationarity), the Fourier method appears to be able to qualitatively predict CD behavior (the value of the radius at the peak of the CD curve tends to be overestimated). Lastly, this study emphasizes the need to consider signal properties more accurately. The historical progression in human performance modeling has been from simple phantoms (i.e., flat backgrounds, white noise) to phantoms with more complex backgrounds (structured phantoms with power law noise) and a similar emphasis needs to be given to the complexity of the signal.

ACKNOWLEDGMENTS

We gratefully acknowledge several helpful comments by A. E. Burgess, PhD. This work was partially supported by a grant from the Department of Health and Human Services, National Institutes of Health, National Cancer Institute, RO1-CA75145.

REFERENCES

1. Rose, A., *Vision - Human and Electronic*. 1973, New York: Plenum Press.
2. Bochud, F.O., C.K. Abbey, and M.P. Eckstein, *Visual Signal Detection in structured backgrounds IV, Calculation of Figures of Merit for Model Observers in Non-Stationary Backgrounds*. J Opt Soc of Am A, 1999.
3. Burgess, A., F. Jacobson, and P. Judy, *On the detection of lesions in mammographic structure*. SPIE: The International Society for Optical Engineering, Medical Imaging Conference, 1999. **3663**: p. 304-315.
4. Barten, P.G., *Contrast Sensitivity of the Human Eye and its Effects on Image Quality*. 1999, Bellingham: SPIE Optical Engineering Press.
5. Wagner, R. and D. Brown, *Unified SNR analysis of medical imaging systems*. Physics Medicine Biology, 1985. **30**(6): p. 489-518.
6. Eckstein, M., Abbey CK, Bochud FO, *A Practical Guide to Model Observers for Visual Detection in Synthetic and Natural Noisy Images*, in *Handbook of Medical Imaging*, H.L. Kundel, J. Beutel, and R.L. Van-Metter, Editors. 2000, SPIE: Bellingham, Washington. p. 593-628.
7. Burgess, A., Li, X, Abbey CK, *Visual signal detectability with two noise components: anomalous masking effects*. Journal Opt. Soc. Am. A, 1997. **14**(9): p. 2420-2442.
8. Bracewell, R.N., *The Fourier Transform and Its Applications*. 2nd ed. 1986, New York: Mcgraw-Hill. 474.
9. Burgess, A., *Comparison of receiver operating characteristic and forced choice observer performance measurement methods*. Medical Physics, 1995. **22**(5): p. 643-655.
10. Cunningham, I.A., *Applied Linear-Systems Theory*, in *Handbook of Medical Imaging*, H.L. Kundel, J. Beutel, and R.L. Van-Metter, Editors. 2000, SPIE: Bellingham. p. 79-159.
11. Bendat, J.S. and A.G. Piersol, *Random Data: Analysis and Measurement Procedures*. second ed. 1986, New York: John Wiley & Sons. 566.
12. Press, W.H., *et al.*, *Numerical Recipes in C: The Art of Scientific Computing*. 1988, Cambridge: Cambridge University Press. 735.
13. Watson, A. and D. Pelli, *QUEST: A Bayesian adaptive psychometric method*. Perception and Psychophysics, 1983. **33**(2): p. 113-120.
14. Burgess, A.E., ed. *High level visual decision efficiencies*. X ed. Vision-Coding and Efficiency, ed. C. Blakemore. Vol. X. 1990, Cambridge University Press. 431-440.

Measuring CRT display image quality: effects of phosphor type, pixel contrast and luminance

Dev P. Chakraborty*, Jiahua Fan, Hans Roehrig (University of Pittsburgh, Department of Radiology, 4200 Magee, 300 Halket Street, Pittsburgh, PA 15213) (JF, HR University of Arizona, 1501 N. Campbell Ave, Tucson, AZ 85724)

ABSTRACT

There is much interest in methodology for accurate measurements of display image quality that is suitable for evaluation and Quality Control purposes. This work aimed to assess the image qualities of two mammography Cathode Ray Tube (CRT) displays for the detection of small targets simulating microcalcifications. Twenty five test patterns containing single pixel targets with variable background values and contrasts, and uniform background test patterns, were generated. Each test pattern was displayed on a P-45 and a P-104 five mega-pixel monitor and images were acquired with a CCD camera. An existing method for measuring Signal to Noise Ratio (SNR) of targets on uniform backgrounds was adapted by including a crucial step to suppress the spurious effects due to the raster lines in the display. It was found that SNR scaled linearly with target contrast and increased with background luminance. The P-45 phosphor was superior at low luminance. Preliminary indications are that this method may be the preferred way to evaluate AMLCD displays.

Keywords: Displays, CRT, measurements, SNR, matched filter, evaluation, test patterns, CRT phosphors

1. INTRODUCTION

The cathode ray tube (CRT) display is recognized as a weak link in the digital mammography imaging chain[1] and consequently there is interest in measuring and optimizing CRT image quality. This work aimed to assess the image qualities of two mammography CRT displays for the detection of small targets simulating microcalcifications. Before describing the application to CRT displays, we summarize the widely accepted Fourier method that is used for assessing the physical image quality of a general imaging system. It involves determining quantities characterizing the input-output characteristics of the imaging device, such as H&D curve for screen film systems, the Modulation Transfer Characteristic (MTF), the Noise Power Spectrum (NPS), and the Detective Quantum Efficiency (DQE). Manufacturers of imaging equipment rely heavily on these measurements for system design and optimization, but these measurements are usually difficult to implement for clinical use or quality control, since they require significant laboratory resources and expertise in interpreting the data. Even if standardized software is made available (e.g., an AAPM Task Group, TG 16, is working on standards for Noise Power Spectrum analysis) it can be difficult to predict the effect on clinical performance of MTF and NPS data. For example, if the MTF curves of two imaging systems cross, then for small objects the system with the higher limiting resolution will be better, whereas for larger objects the opposite may be true. With raster scan displays there are additional problems. For these reasons it is desirable to use a task-specific figure of merit. Some time ago we proposed[2] that the detectability, as quantified by SNR of targets chosen to resemble objects of clinical interest on a uniform background, be used as such metrics. For example, the object to be detected could be a disk of radius R (similar to a microcalcification). One measures the cross correlation (the summed product of corresponding pixel values) of the image of the disk with an aperture, when the latter is aligned with the image of the disk. The aperture function is defined to be unity within a circle of radius R, and zero elsewhere. Similarly, one can measure the noise cross correlation when the aperture is positioned elsewhere, and the ratio of the signal to the standard deviation of the noise cross correlation is the desired SNR for detection of the disk object on a uniform background. Since the SNR can be calculated from the Fourier measurements the two approaches are not fundamentally different. However, the SNR approach has the practical advantage that it can be readily implemented. A formal embodiment of this idea was proposed[3] by Tapiovaara and Wagner (TW) who showed that by using an appropriately blurred target (via the system

* dchakraborty@mail.magee.edu; phone 412-641-2571; fax 412-641-2582

MTF) as the aperture function, one obtains the non-pre-whitening matched filter (NPWMF) SNR, which has been widely used in ideal observer models. This type of model observer is ideal (in the sense of maximum SNR) if the noise is white. For non-white noise, the corresponding filter is the pre-whitening matched filter, implementation of which requires knowledge of the NPS of the imaging system. The TW approach appears to have been neglected. Besides the original application to fluoroscopic image quality[4], we know of only one other application of the TW method to medical imaging, namely the Computer Analysis of Mammography Phantom Images (CAMPI) method developed by us[5,6,7].

In the context of CRT displays there is the additional problem of how to deal with the scan-lines. The presence of the periodic scan-line pattern, even when displaying a uniform field, implies that the NPS and MTF will yield peaks at the corresponding frequency, and possibly at its harmonics. This makes it difficult to interpret measurements near these frequencies[8]. Moreover, the human observer normally views the CRT images at a distance at which the scan-lines cannot be spatially resolved. Therefore, relating the Fourier measurements to the human observer results is difficult for raster scan displays. For these reasons, while we recognize the advantage of the Fourier methods for basic investigations of imaging system performance, there is a need for alternate methods, particularly for raster scan displays, and we believe that the TW method, which does not involve calculations in Fourier space, is a more promising approach.

This work sought to asses the image quality of two mammography CRT displays, with different phosphors, for the detection of small targets simulating microcalcifications. Images of computer generated test patterns of single-pixel targets on a uniform background were displayed on the monitor and captured by a charge-coupled-device (CCD) camera. A model observer TW-based method was used to measure the SNR of the targets.

2. METHODS

We followed the method described by Tapiovaara and Wagner (TW) with an important modification. In the TW method one starts with a set of independently acquired images of a fixed background with a superimposed target (referred to as background + target), and a set of background-only images. Random imaging system noise is present in each of these images, which ultimately limits the detectability of the target. In the TW method one subtracts pairs of background + target and background images to estimate the target, along with residual subtraction noise. An average over all such subtracted pairs is performed to minimize the subtraction noise. This yields an estimate of the target, appropriately blurred by the system spatial resolution loss, which is referred to as the template. The process of determining the template will be referred to as the training step, which needs to be performed only once for a target. If a second set of independently acquired background + target and background images is available, and assuming that the pixel noise is "white", one can compute the NPWMF-SNR for the detection of the target in the second set of images by calculating the cross-correlation between the template and each registered image in the second set. The mean of the background + target and background cross correlations are calculated, which are denoted by μ_s and μ_n respectively, as well as the corresponding standard deviations, denoted by σ_s and σ_n respectively. The final SNR is given by $SNR = (\mu_s - \mu_n) / \sqrt{((\sigma_s^2 + \sigma_n^2)/2)}$.

In the case of a CRT display it can be seen that, unless special precautions are taken, the estimate of the template can be contaminated by the scan lines, which will generally not cancel out in the subtraction step. Use of the scan-line contaminated template will lead to incorrect SNR estimates. Accordingly we devised a scan-line suppression step that is necessary when the TW method is applied to displays such as CRTs that have an underlying raster structure.

2. 1 Test Patterns

Eight (8) bit 512 x 512 digital test patterns consisting of a regular array of single pixel targets ("dots") on a uniform background, were generated. The dot spacing was 6 pixels and the uniform background pixel value was set to one of three values, 55, 127 or 200. The pixel value difference between the target and the background, referred to as "dot-contrast", was varied in steps of 10 between 0 and a maximum value, where the maximum value was typically 100, excepting when the background was 200, when it was restricted to 50 to satisfy the 0-255 pixel value range imposed by the 8-bit display. Note that images with zero dot-contrast were also generated; these are the background images. The non-zero contrast images are the target + background images.

2.2 Image Acquisition

Studied were two 5-megapixel (2048 x 2560 x 8 bits) monitors manufactured by Siemens, which were identical in all respects except that one had a P-45 phosphor and the other had a P-104 phosphor. Each was calibrated according to the DICOM standard[9] to a maximum luminance of 500 Cd/m^2. The calibration curve of each monitor (i.e., luminance as a function of display driving level) was recorded. Each 8-bit test pattern was displayed as Display Driving Level (DDL) values, i.e., without any further look-up-table modifications. Three CCD camera images (each 1316 x 1036 x 14 bits) of the central region (164 x 129) of each test pattern were acquired at a magnification factor of 8. Each CCD image of target containing test patterns contained about 27 x 22 imaged dots. To avoid problems near image edges we restricted analysis to the 500 (25 x 20) central dots. Representative portions of the images are shown in Fig. 1. Care was taken to align the CCD camera with respect to the test-pattern so that the dots on a row of the test-pattern were aligned with a row of the CCD image matrix. The camera was shielded from extraneous light with an opaque drop-cloth, and ambient illumination of the room was minimized. For a particular monitor the camera acquisition set-up was undisturbed for the duration of the image acquisition. The CCD image acquisition procedure was repeated for the different test patterns and for both monitors.

The monitor luminance calibration data was fitted to an analytical function to allow the luminance data to be readily interpolated to DDL values. To correct for monitor luminance non-linearity, each CCD image was converted to DDL values via this function (i.e., it was linearized).

2.3 SNR Calculation

Corresponding background + target and background CCD image pairs (training images), were used to estimate the TW template.

2.3.1 Locations of the target dots

For a given monitor and for a particular high dot-contrast image, the location of the top-left-corner dot in the CCD image was manually determined using a mouse and cursor. Since the acquisition geometry was undisturbed, and we knew the approximate distance between any two neighboring dots (i.e., 6x8=48 pixels, ignoring geometric distortion effects), this one measurement sufficed to estimate the approximate locations of all target-dots in all images originating from this monitor. Each approximate dot location was a pair of integer valued pixel coordinates. A pair of correction values for each dot location was found by an alignment procedure that involved estimating an intermediate template (48 x 48 pixels, see Step 2.3.2), specifying a trial shift value (generally a small fractional number), extracting a 48 x 48 region surrounding the shifted location (all pixel shifting was done using bilinear interpolation), calculating the linear correlation coefficient between the extracted region and the intermediate template, and repeating the procedure for different trial shifts (in both x and y directions) until the correlation was maximized, at which point the shift parameters were the desired corrections. These values were saved and the procedure was repeated for all dots, all test patterns and both monitors.

2.3.2 Intermediate template

This was the average of ten 48 x 48 dot-regions calculated as follows. The starting template, assumed to be a two-dimensional Gaussian with standard deviations, along the raster and perpendicular directions, of 3 and 2 pixels, respectively, was realized on a 48x48 matrix. Using correlation coefficient maximization, this template was used to sequentially register the first ten dots along the raster direction. At each registered location we extracted a 48x48 dot-containing region, and calculated the cumulative average of the extracted regions (the first extracted region replaced the Gaussian, and each succeeding region was added with appropriate weight). This template was used for the alignment of all the dots as described in Step 2.3.1.

2.3.3 TW Template

Unlike the intermediate template used in Steps 2.3.1 and 2.3.2, the TW template was obtained by averaging 500 dot-regions in the CCD image <u>after</u> applying a scan line suppression algorithm at each region.

a) A 240 x 240 pixel region S_1, which was sufficient to encompass a 5 x 5 array of dots, was extracted from a target image (Fig. 2 shows a schematic of the process). To accentuate the scan lines a 3x3 kernel smoothed version was

subtracted from S_1. A similar region N_1 was extracted from the corresponding location from the background image of the training image pair, and similarly scan-line accentuated. A small vertical shift was applied to S_1 to register the scan lines in the two images (in our notation the scan lines are running in the x-direction, see Fig. 2). The necessary vertical shift was estimated by maximizing the correlation coefficient of two one-dimensional arrays obtained by averaging N_1 and S_1, respectively, along the horizontal direction. To allow for differences in scan line intensities between S_1 and N_1, we calculated $D_1 = N_1 - f_1 S_1$, where f_1 is a scale-factor, initially set to unity, which was varied to minimize the standard deviation of D_1. The factor f_1 was necessary to allow for differences in scan line intensities between target and background images, which could occur due to temporal fluctuations between acquisitions. For example, if the scan lines in S_1 have lower amplitude than those in N_1, f_1 will need to be greater than 1 to obtain scan-line cancellation and consequent minimization of the standard deviation of D_1.

b) The region D_1, containing the 5 x 5 array of scan-line-suppressed-dots, was analyzed at each dot location using the location information saved in Step 2.3.1. At each location we extracted a 48 x 48 region that was locally-registered (using two dimensional pixel shifting) to the most recent TW template estimate (the initial TW template estimate was the intermediate template determined in Step 2.3.2). After each location was registered, the TW template was updated by the corresponding extracted 48 x 48 region, in other words a 'running' average was performed on the TW template.

c) When all 25 dots in the 240 x 240 region D_1 were used up, the analysis in Steps 2.3.3(a) and 2.3.3 (b) was repeated with a new 240 x 240 background + target region S_2, containing a fresh array of 5 x 5 dots, and the corresponding background region N_2, and D_2 was computed using $D_2 = N_2 - f_2 S_2$, and so on. The running average on the TW template was continued until all 500 dots were used up. The final TW template was therefore the result of averaging 500 dot-regions obtained from a target + background and background image pair.

2.3.4 Zero frequency correction of TW template

This was accomplished by subtracting the mean value of the TW-template from the template. The difference was used in the subsequent SNR calculation in Step 2.3.5. This subtraction has the effect that average brightness information in the image yields zero cross-correlation, and therefore does not contribute to the SNR. It is believed to yield SNR values that correlate better with human observer detectability of the targets than using the uncorrected template.

2.3.5 SNR Computation

Since three CCD images were acquired for each test pattern, there were two background + target and two background images that were not used in the training step described above. These images, referred to as the Testing Images, were used along with the TW-template determined in Step 2.3.3 and 2.3.4, to calculate the SNR. The cross correlations between the TW - template and the 1000 registered target locations (500 per background + target image), and with the corresponding 1000 locations on background images (500 per background image) were calculated. Note that no scan line suppression was used in this step, as we wished to measure the total detectability, which may be influenced by the presence of the scan lines.

2.4 Training and Testing Image Combinations

The calculations were repeated for 2 other choices of training and testing image pairs. For example, with three repeated acquisitions per test pattern, denoted by 1, 2 and 3, we trained on 1 (containing a background + target and background image pair) and tested on 2 and 3 (containing two background and two background + target image pairs). Likewise we trained on 2 and tested on 1 and 3, and finally we trained on 3 and tested on 1 and 2. The final 3 values of SNR were averaged to obtain a grand mean, and the corresponding standard deviation of the SNR values was also calculated. The last quantity yielded a measure of SNR variability, $\sigma(SNR)$, resulting from the method.

The above analysis was repeated for all test patterns and both monitors.

3. RESULTS

The top-left figure in Fig. 3 shows the first extracted 48 x 48 region obtained in Step 2.3.3(a), i.e., before application of the scan line suppression procedure. It shows that the scan-lines are easily visible. The top-right figure in Fig. 3 shows the effect of applying the scan-line suppression step. Note the partial suppression of the scan lines. The last figure in Fig.

3 shows the effect of averaging 500 regions like that shown in top-right. Note the near elimination of the scan lines. With a base-line shift, the last figure in Fig. 3 bottom is the final template used in the analysis for this CCD image-pair.

Fig. 4 shows the dependence of the measured SNR on dot-contrast, for the P-45 monitor (left column), for three values of background pixel value (from top to bottom, 55, 127 and 200 respectively). The dot-contrast was defined above as the difference between the dot and background pixel values. Figure 4 right column shows the corresponding plots for the P-104 phosphor.

The slopes of the regression straight-lines in Fig. 4 (denoted by m) were used to define measures of image quality that were independent of the dot-contrast. Both m and its standard deviation $\sigma(m)$ were calculated using a weighted least squares fitting procedure (REG in SAS) with weights $\sigma(SNR)$. Figure 5 shows a summary plot of the SNR of targets at equal Michelson contrasts – obtained by multiplying m by the corresponding pixel value. The multiplication is necessary as m represents the SNR per unit dot contrast. This is because Michelson contrast equals dot-contrast per background pixel value.

4. DISCUSSION

Note the close linearity of the plots in Figure 4. If the monitor linearization correction was not used, then the plots were systematically nonlinear, typically increasing to a maximum and subsequently decreasing. Once the signal has been linearized, one expects SNR to be proportional to dot-contrast. The observed high degree of linearity confirms this expectation and moreover, is an indication of the overall accuracy of the SNR measurements (estimated to be about 2%). Note that the template is measured under identical conditions as the test images. This has the advantage that non-linearity and beam spreading effects that affect the template are automatically included in the measurements.

The reason for using the larger (480 x 480) region to align the scan lines is that an ROI that is too small (e.g., 48 x 48) will yield a small and noisy correlation between the two-sets of scan-lines in background + target and background images respectively), which cannot be accurately maximized. With the larger region there are more pixels within the scan-lines, so that a larger and more sharply peaked correlation is obtained. If the region is too large then the geometrical distortion introduced by the monitor will yield a point of diminishing returns. Also it is desirable to exclude the region of the dots from contributing to the correlation coefficient, as spurious low values will result due to the absence of dots in the background images. In practice an equivalent effect was obtained by enhancing the scan lines in both images (by un-sharp masking), as this suppresses the dot regions.

It should be noted that the P-45 phosphor is not normally calibrated at such high maximum luminance (500 Cd/m^2). A more typical value for this type of monitor is 300 Cd/m^2. Therefore it is not surprising that the P-45 monitor deteriorated at the highest luminance. The P-104 phosphor is designed for higher luminance applications, so as to be less sensitive to ambient lighting conditions.

5. CONCLUSIONS

A model observer method was used to calculate the NPWMF SNR of the targets. Investigated were the effects of target contrast, background luminance and phosphor type. It was found that the SNR was linear with pixel contrast, SNR decreased with increasing background luminance and, for the target studied, the P-45 phosphor was superior to the P-104 phosphor for luminance less than 200 Cd/m2, above which the measured performances were equivalent.

6. ACKNOWLEDGEMENTS

This work was supported in part by a contract from the US Army Medical Research and Materiel Command under DAMD 17-99-1-9347, and in part by a grant from the Department of Health and Human Services, National Institutes of Health, R01-CA87935.

7. REFERENCES

1. Working Group on Digital Mammography. Meeting held in Washington DC, March 9-10, 1998. Sponsored by the US Public Health Service's Office of Women's Health and the National Cancer Institute.
2. DP Chakraborty and GT Barnes, "Signal-to-noise ratio considerations in radiographic imaging." Medical Physics 10(4): 467-469, 1983.
3. MJ Tapiovaara and RF Wagner, "SNR and noise measurements for medical imaging: I. A practical approach based on statistical decision theory", Phys. Med. Biol. 38: 71-92, 1993.
4. M Tapiovaara, "SNR and noise measurements for medical imaging: II. Application to fluoroscopic x-ray equipment." Phys. Med. Biol. 38: 1761-1788, 1993.
5. DP Chakraborty and MP Eckert, "Quantitative versus subjective evaluation of mammography accreditation phantom images." Medical Physics 22(2): 133-143, 1995.
6. DP Chakraborty, "Computer analysis of mammography phantom images (CAMPI): An application to the measurement of microcalcification image quality of directly acquired digital images." Medical Physics *24(8)*, 1269-1277, 1997.
7. DP Chakraborty, "The Effect of the Antiscatter Grid on Full-Field Digital Mammography Phantom Images." J of Dig Imag, *12(1)*, 12-22, 1999.
8. PC Bunch and RL Van Metter, "Interpreting the noise power spectra of digitally printed images." Proc. SPIE *914*, 813-828, 1988.
9. NEMA Publication, PS 3.14-2000, "Digital Imaging and Communications in Medicine (DICOM) Part 14: Grayscale Standard Display Function", National Electrical Manufacturers Association, Rosslyn, Virginia. Draft viewable at http://medical.nema.org/dicom/2000/draft/00_14DR.PDF.

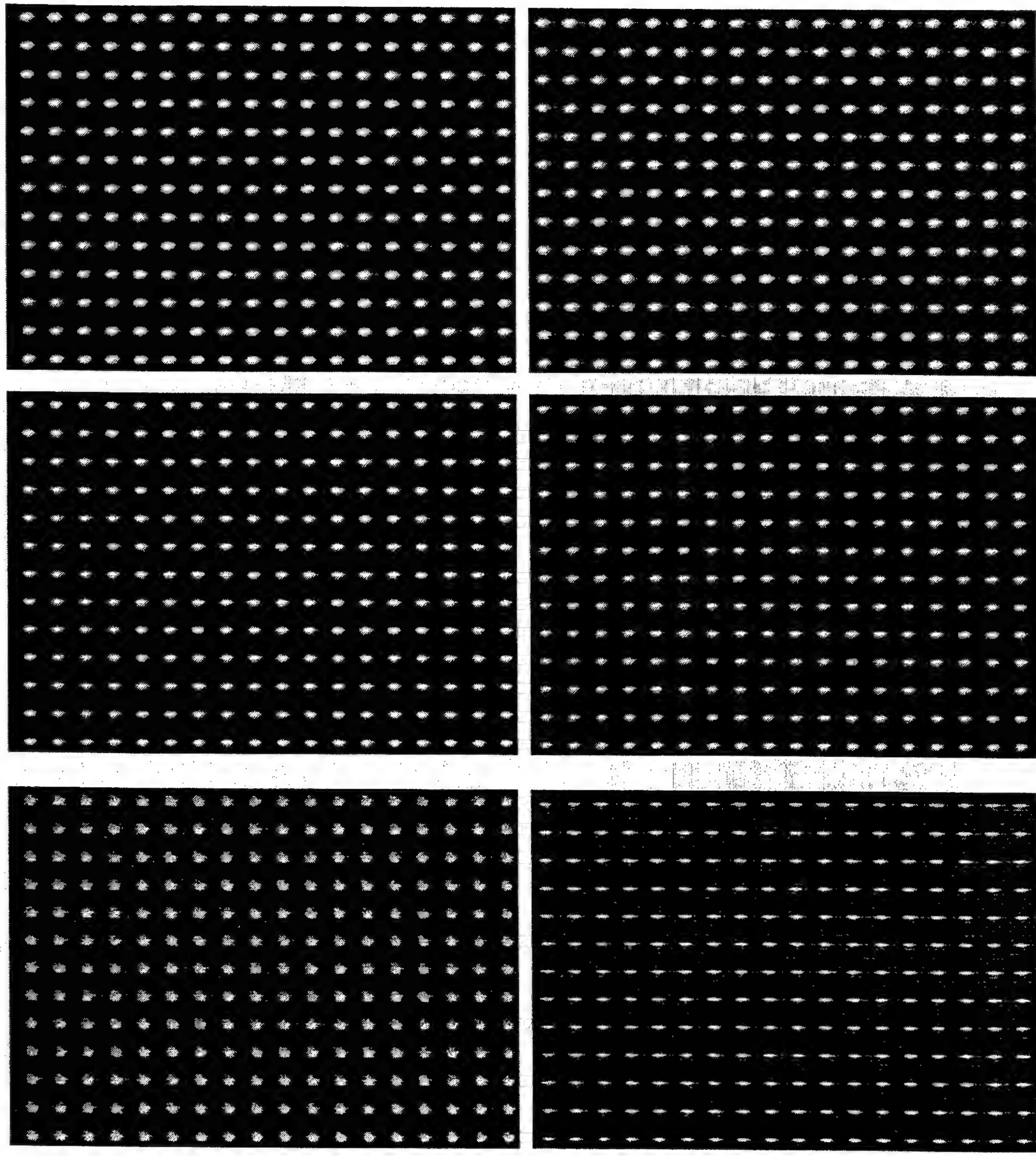

Figure 1: Shown are representative CCD images of the test patterns for the P-45 monitor (left column) and the P-104 monitor (right column) at three background pixel values: 55 (top row), 127 (middle row) and 200 (bottom row) respectively. The target test patterns consisted of single pixel "dots" spaced by 6 pixels in each direction and were imaged at a magnification of 8.

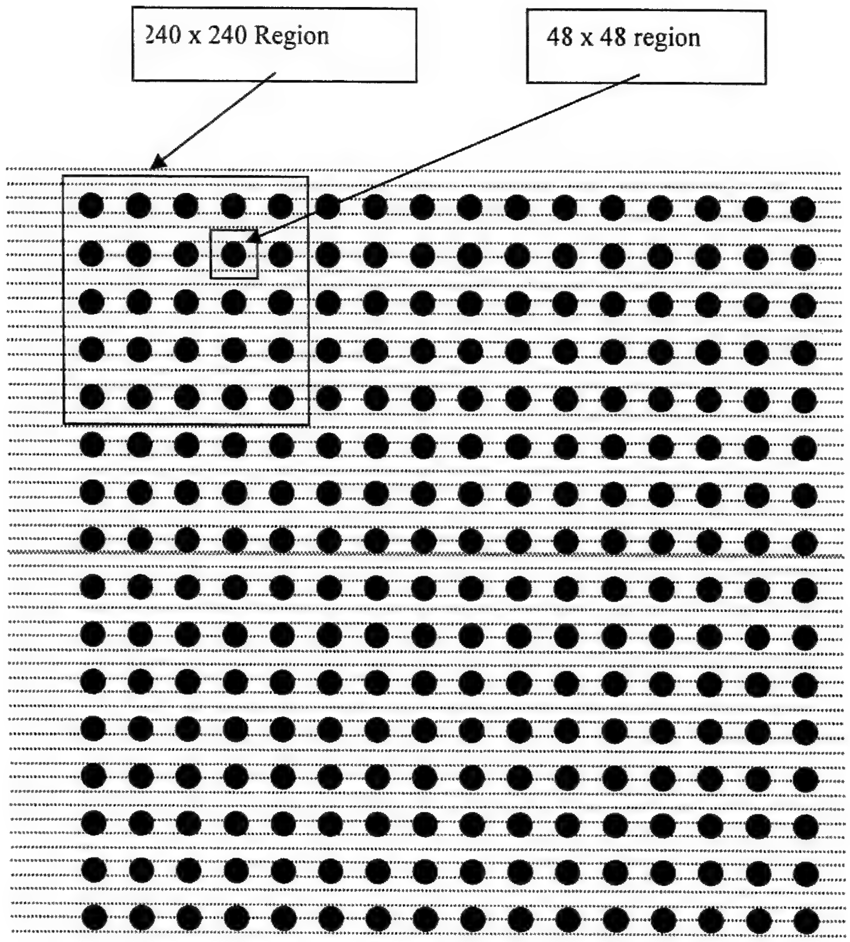

Figure 2: Template estimation: shown is a schematic of the dot-targets (shown as filled circles) and the scan-lines (shown as dotted lines), superimposed on which is a 240 x 240 region of interest S_1. The scan-lies in S_1 were aligned to a similar region N_1, extracted from a background image. The two were then subtracted, following which smaller square regions (48 x 48, one of which is shown) were extracted and averaged. The diagram is not to scale.

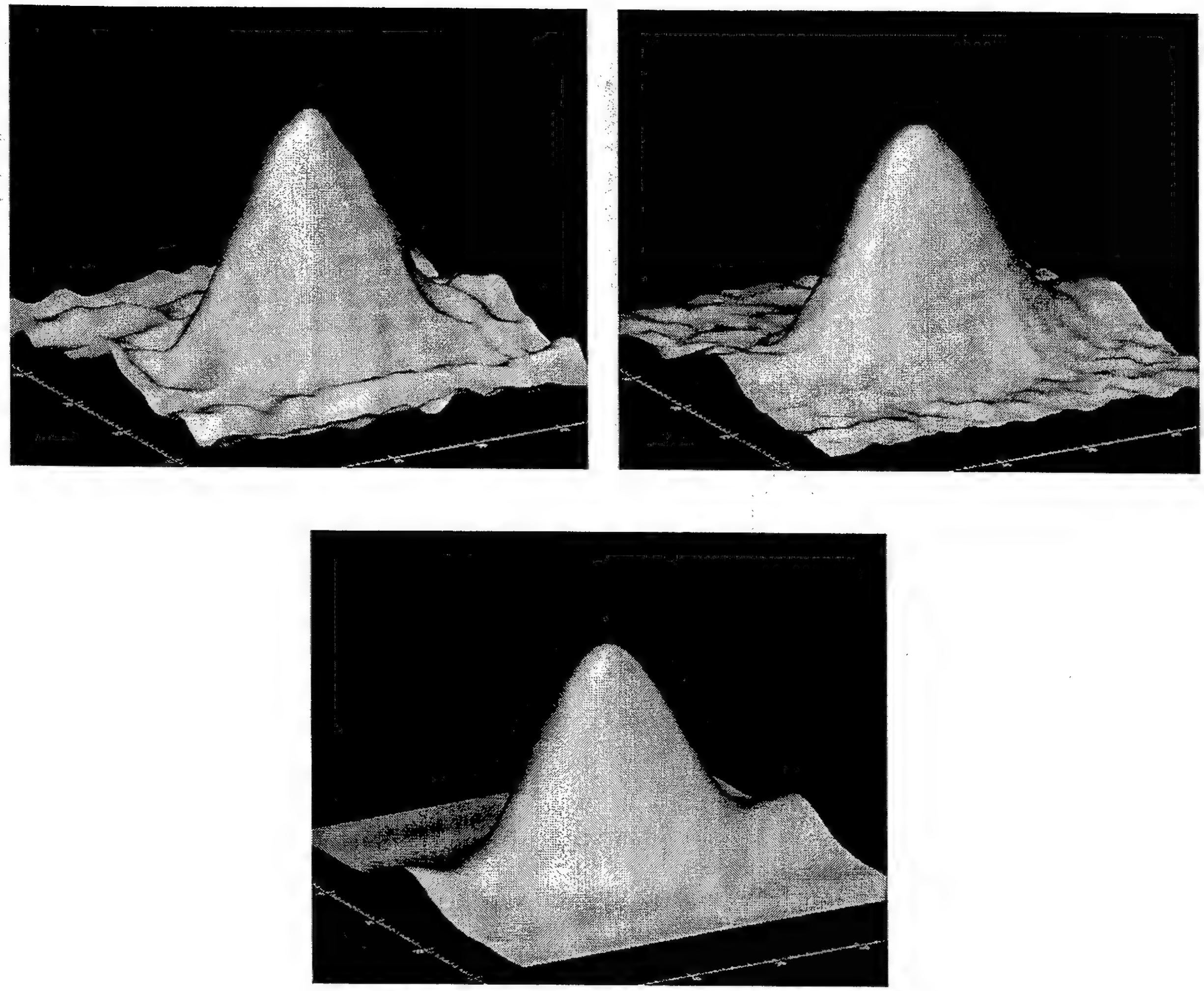

Figure 3: TW template estimation procedure: the top-left figure shows a 48 x 48 pixel region S_1, extracted as shown in Fig. 2. The top-right figure shows the effect of aligning and subtracting the scan lines from a background image – note the suppression of the scan lines. The bottom figure shows the result of averaging 500-regions like the top-right figure – note the near elimination of the scan lines. This was the TW template for this test-pattern.

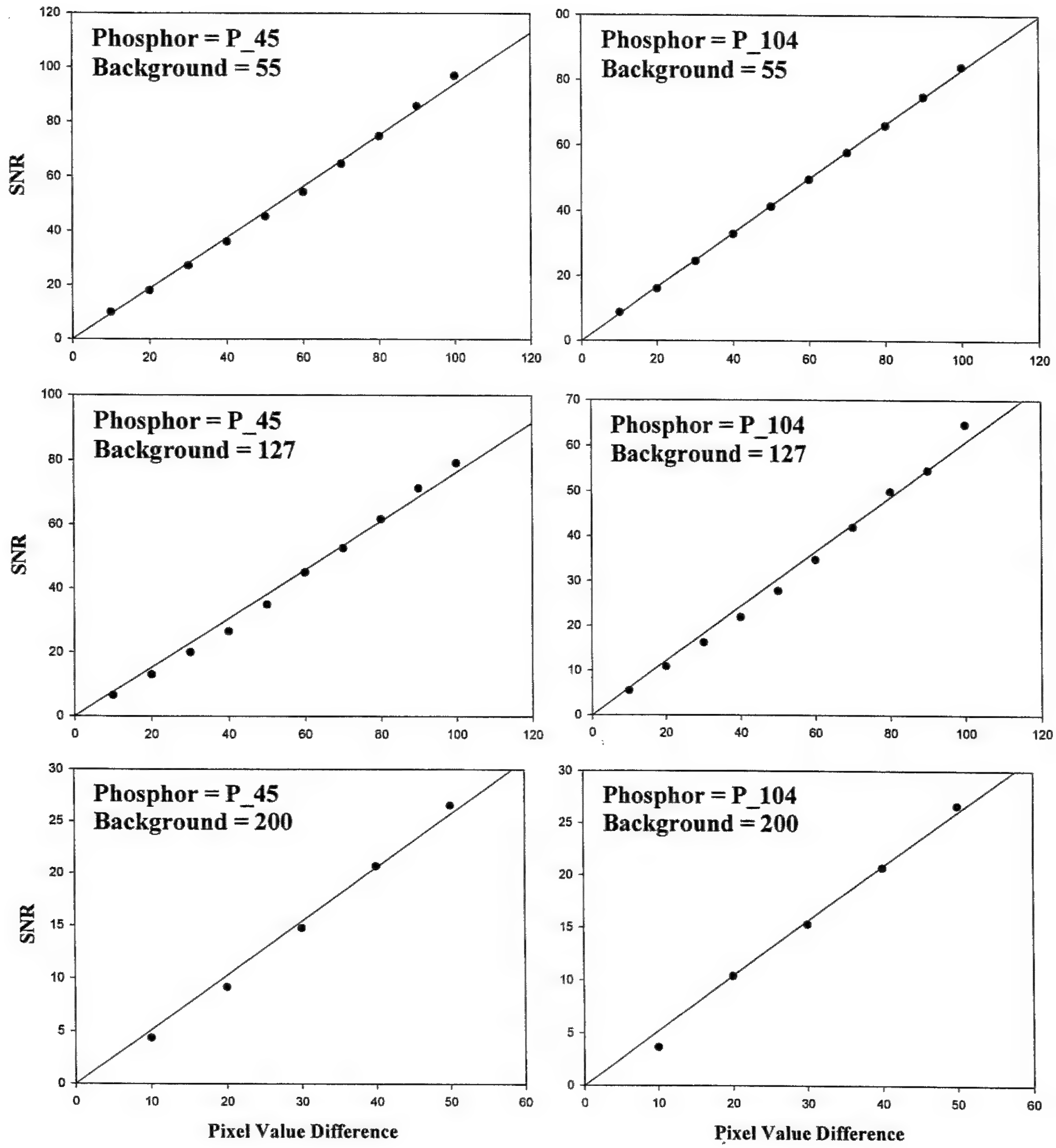

Figure 4: Contrast dependence of SNR: The left column shows the dependence of the measured SNR on dot-contrast, for the P-45 monitor, for three values of background pixel value, 55, 127 and 200 respectively. The right column shows corresponding plots for the P-104 phosphor. The slopes of the regression straight-lines in this figure were used to define measures of image quality that were independent of the dot-contrast, see Fig. 5.

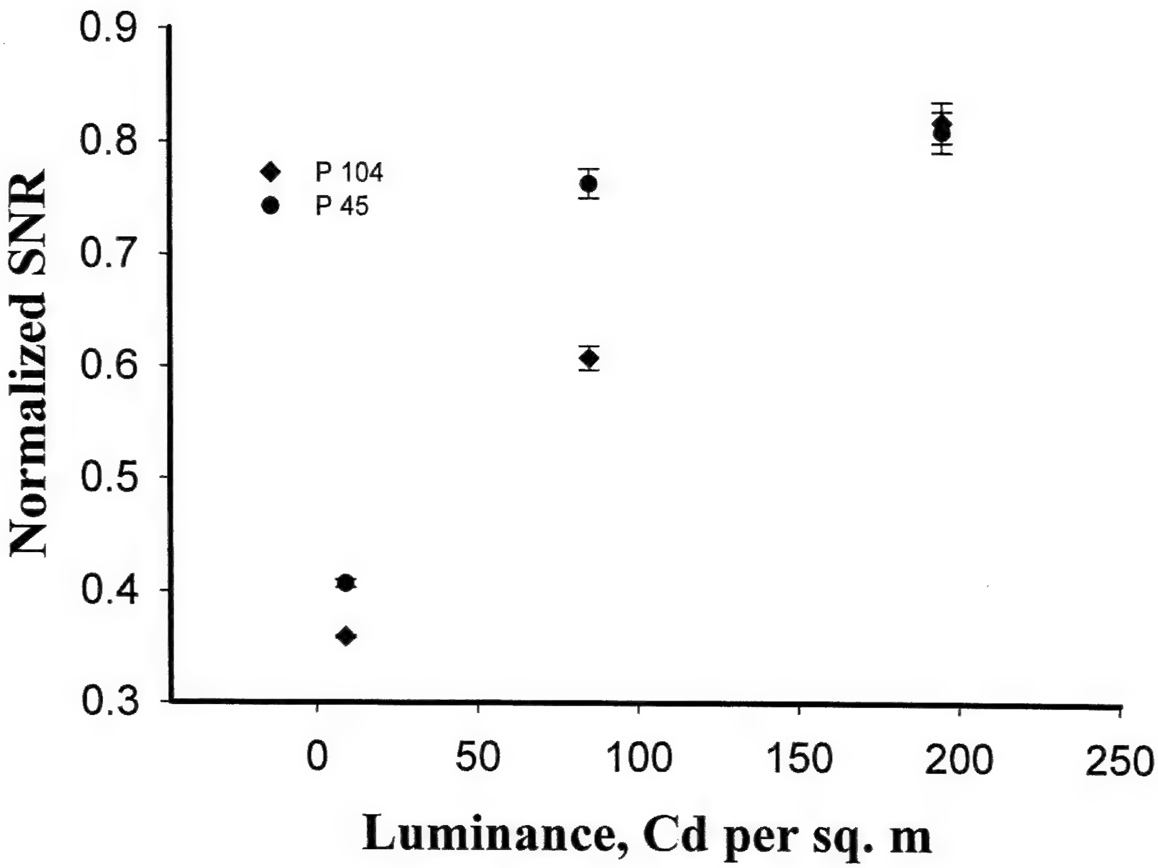

Figure 5. This shows a plot of the SNR of targets at equal Michelson contrasts as a function of background luminance. It was obtained by multiplying the slopes of the straight lines in Fig. 4 by the corresponding background pixel values. Note the superiority of the P-45 monitor at luminance below 100 Cd/m^2.

RESUME

Name: **Fan, Jiahua**
Sex: Male
Current Status: PhD candidate, Dept. of Electrical and Computer Engineering, Univ. of Arizona
Research Associate, Dept. of Radiology, Univ. of Arizona
Address: 1214 E 8TH ST, Tucson, AZ, 85719, USA
Telephone: Home: (1-520) 8849367
Office: (1-520) 6267854
FAX: (520) 6264376
Email: fanjh@ece.arizona.edu

Education

08/00 ~ present University of Arizona, Arizona, USA
Major: Electrical and Computer Engineering
Minor: Optical Science
GPA: 4.0/4.0
Degree: **PhD**

09/94 ~ 03/97 Tianjin University, Tianjin, China
Major: Electronic Engineering - Signal and Information Processing
Degree: **MS**

09/90 ~ 07/94 Tianjin University, Tianjin, China
Major: Electronic Engineering - Telecommunication Technology
Degree: **BS**

Professional Experience

08/01 ~ present **Research Associate**
Department of Radiology, University of Arizona, USA
- Medical image processing and medical image display evaluation

08/00 ~ 07/01 **Research Assistant**
Department of Radiology, University of Arizona, USA
- Medical image evaluation and processing

05/99 ~ 07/00 **Research Assistant**
Image Processing Lab, Dept. of Electronic Engineering, City University of Hong Kong, Hong Kong
- Designed and setup a Beowulf class supercomputer dedicated to image processing
- Developed a parallel image retrieval algorithm based on DCT coefficients histogram
- Developed a novel image retrieval algorithm using wavelet-fractal based similarity measurement

04/97 ~ 04/99 **Assistant Professor**
Advanced Technology Research Center, School of Information Engineering, Shenzhen University, China
- Research on image and video processing
- Earned the "Meridian 1 Technician" certificate given by TongGuang-Nortel Comp.
- Earned the "Certificate of IPP" given by Fluke Comp.

09/94 ~ 03/97 **Graduate student**
Department of Electronic Engineering, Tianjin University, China
In the TD951 CATV system,

- Developed the digital scrambling and descrambling hardware unit
- Developed the central controlling software
- Developed the encryption and decryption software based on a three-level cipher scheme
- Developed an address-locating software in the descrambling unit

In the SCM (SubCarrier Multiplexing) system,
(Sponsored by Chinese National Science Fund)

- Developed a frequency optimization software
- Designed and adjusted some hardware of the system

10/95 ~ 12/95 **Lecturer** (part time)
Tianjin University, China

- Taught database management system

07/95 ~ 08/95 Worked for Merchants Anjuwuye Co., Ltd. in Shenzhen city (part time)

- Developed a mansion pay-managing system
- Developed a salary management software

09/94 ~ 11/94 Worked for Jinke Electronic Co., Ltd. (part time)

- Designed and adjusted part of microwave communication system circuits

Honors

2003 Graduate Tuition Scholarship, Graduate Research Assistantship, University of Arizona
2002 Graduate Tuition Scholarship, Graduate Research Assistantship, University of Arizona
2001 Graduate Tuition Scholarship, Graduate Research Assistantship, University of Arizona
2000 Graduate Tuition Scholarship, Graduate Research Assistantship, University of Arizona
2000 Graduate Research Assistantship, City University of Hong Kong
1999 Graduate Research Assistantship, City University of Hong Kong
1997 "Analysis and Application of Nonlinear Noise in the High Capacity Multichannel FDM Analogical Modulation System", Second Prize on the forum of Tianjin University 100th anniversary celebration
1996 Huawei Scholarship, Tianjin University
1996 Tianjin University Scholarship: Second Prize
1995 Tianjin University Scholarship: Second Prize
1994 Motorola Scholarship
1994 As top student, entered the Graduate School of Tianjin University without taking the entrance examination
1993 Tianjin University Scholarship: First Prize
1992 Tianjin University Scholarship: Second Prize
1992 Wang Kechang Scholarship, Tianjin University
1991 Third Prize in the Chinese National Physics Competition for non-physics-major college students
1991 Motorola Scholarship
1990 Tianjin University Scholarship: First Prize
1990 Highest score among the students from Tanggu District in the National Entrance Examination for Universities, won the Special Prize for freshmen

Publications

1. Jiahua Fan, Willian J. Dallas, Hans Roehrig and Elizabeth Krupinski, "Improving Visualization of Digital Mammograms on the CRT display system", Medical Imaging 2003, Proceedings of SPIE (accepted for publication).
2. Dev P. Chakraborty, Jiahua Fan and Hans Roehrig, "Measuring CRT Display Image Quality: effects of phosphor type, pixel contrast and luminance", Medical Imaging 2003, Proceedings of SPIE (accepted for publication).
3. H. Blume, P. Steven, M. Cobb, A. Ho, F. Stevens, S. Muller, H. Roehrig and J. Fan, "Characterization of liquid-crystal displays for medical images – Part 2", Medical Imaging 2003, Proceedings of SPIE (accepted for publication).
4. Dev P. Chakraborty, Jiahua Fan and Hans Roehrig, "Computerized CRT SNR measurements: effect of phosphor types", Era of Hope, The Department of Defense Breast Cancer Research Program Meeting, Proceedings, Vol. II, Digital Imaging, P28-4, Orlando, Florida, USA, Sep. 2002.
5. Hans Roehrig, Dev P. Chakraborty, Jiahua Fan, A. Chawla and K. Gandhi, "The modulation transfer function (MTF) of CRT display systems", Era of Hope, The Department of Defense Breast Cancer Research Program Meeting, Proceedings, Vol. II, Digital Imaging, P28-3, Orlando, Florida, USA, Sep. 2002.
6. H. Roehrig, J. Fan, A. Chawla, K. Gandhi, "The liquid crystal display (LCD) for medical imaging in comparison with the cathode ray tube display (CRT)", (Invited Paper), Penetrating Radiation Systems and Applications IV, Proceedings of SPIE, Vol. 4786, pp.114 ~131, Seattle, Washington, USA, July 2002.
7. H. Blume, P. Steven, M. Cobb, A. Ho, F. Stevens, H. Roehrig and Jiahua Fan, "Comparison of liquid crystal and CRT displays for medical images".
8. Hans Roehrig, William J. Dallas, Elizabeth Krupinski, Jiahua Fan, Amarpreet Chawla and Kunal Gandhi, "Display of mammograms on a CRT", 6th International Workshop on Digital Mammograhpy (IWDM 2002), Bremen, Germany, June 2002.
9. H. Roehrig, J. Fan, T. Furukawa, M. Ohashi, A. Chawla and K. Gandhi, "Performance Evaluation of LCD displays", Computer Assisted Radiology and Survey, Proceedings of the 16th International Congress and Exhibition, pp. 461~466, Paris, France, Jun. 2002.
10. H. Blume, P. Steven, M. Cobb, A. Ho, F. Stevens, H. Roehrig and J. Fan, "Characterization of Physical Image Quality of a 3-Million-Pixel Monochrome AMLCD: DICOM Conformance, Spatial MTF, and Spatial NPS", 2002 SID International Symposium Digest of Technical Papers, Vol XXXIII, No. 1, pp. 86~89, San Jose, CA, USA, May 2002.
11. H. Roehrig, W. J. Dallas, H. R. Blume, E. A. Krupinski, M. M. Rogulski, J. Fan and K. Gandhi, "Evaluation of plain-film digitizers: a comparison of different systems and models", Medical Imaging 2002, Physics of Medical Imaging, Proceedings of SPIE, Vol. 4682, pp.694~703, San Diego, USA, Feb. 2002.
12. H. R. Blume, P. M. Steven, M. E. Cobb, A. M. Ho, F. Stevens, S. Muller, H. Roehrig and J. Fan, "Characterization of high-resolution liquid crystal displays for medical images", Medical Imaging 2002, Visualization, Image-Guided Procedures, and Display, Proceedings of SPIE, Vol. 4681, pp.271~292, San Diego, USA, Feb. 2002.
13. Jiahua Fan, Shun-Tat Yiu and Laiman Po, "Image Retrieval Using Parallel Algorithm on the Beowulf Class Supercomputer", 2000 International Workshop on Multimedia Data Storage, Retrieval, Integration and Applications, Hong Kong, Jan. 2000.
14. Fuyun Guo, Guowei Liu, Wei Zheng and Jiahua Fan, "Model TD-951 Addressable Scrambling/Descrambling Pay TV System", Television Technology, Sep. 1997.
15. Jiahua Fan, Fuyun Guo and Zhaohua Wang, "Research on the Conditional Access Technology of Pay TV System", Youth Academic Proceedings, Broadcast and Television Technology Branch, The Chinese Electronic Society, Aug. 1997.
16. Jiahua Fan, Fuyun Guo and Zhaohua Wang, "Research on the Application of Random Line-Reverse-Scanning Digital Scrambling and Descrambling Technology in the Pay TV Communication System", Tianjin Telecommunication Technology, Jan. 1997.

17. Jiahua Fan, Guiyun Liu, Tianhai Wang and Jufeng Dai, "Analysis of Nonlinear Noise and Arrangement of the Subcarrier in the Multichannel Fiber Communication System", China Twelve Conference on Circuits and Systems Proceedings, The Chinese Electronic Society, July 1995.

Main Courses Taken

University of Arizona, Arizona, USA (PhD program)

	Course Name	Grade
Major: ECE	Random Processes for Engineering Applications	A
	Digital Image Analysis	A
	Synthesis of Control Systems	A
	Advanced Digital Signal Processing	A
	Digital Image Processing	A
	Fundamentals of Computer Networks	A
	Digital Communication Systems	A
	Data Compression	Audit
	Neural Networks	
Minor: Optical Science	Linear Systems, Fourier Transforms	A
	Probability and Statistics in Optics	A
	Photoelectronic Imaging Devices	A
	Noise in Image Systems	A
	Mathematical Methods for Optics	A

Tianjin University, Tianjin, China (MS program)

	Course Name	Grade
Major: EE	Applied Mathematics	84
	Computer Science and Application	80
	Intelligent System Design	95
	Random Digital Signal Processing	90
	Nonlinear Signal Processing	85
	Image Coding	82
	Advanced Digital Circuit	83
	Digital Image Processing	88
	Technology of Digital TV	90
	Statistical Pattern Recognition	90

Language Proficiency

English:
GRE: 2130 (V: 580/80%, A: 750/94%, Q: 800/99%), Apr. 10, 1999.
TOEFL: 620 (60/63/63), TWE: 4.5, Oct. 23, 1999.
Once worked as an oral translator for an American merchant

Japanese: Took one year course, learned as the second foreign language

Amarpreet S. Chawla

841, E. Drachman Street
Tucson, AZ 85719

Email: achawla@ece.arizona.edu
Tel: (520) 626 5876(W)
623 6658(H)

Education

Master of Science in **Electrical and Computer Engineering,** University of Arizona, Tucson
(Expected Graduation – December 2002) **GPA: 3.84/4.0**

Bachelor of Engineering-Electrical, Indian Institute of Technology, Roorkee (formerly, University of Roorkee), India (Spring 2000), **GPA equivalent to 3.9/4.0**

Graduate Course Work
Signal Theory, Advanced (Statistical) Digital Signal Processing, Digital Image Processing, Introduction to Fourier Optics, Digital Image Analysis, Random Processes in Engineering Application, Stochastic Processes, Linear System Theory, Decentralized Control and Large-Scale System, , Principles of Operating System, Analog Signal Processing, Digital Communication Systems

Relevant Experience

Department of Radiology, University of Arizona, Tucson **Spring 2001-Present**
Graduate Research Assistant

Working on the project titled '*Soft Copy Analysis of Mammograms*', in a team of four. Quality evaluation of various displays (flat/curved CRTs and LCDs) is being performed. The focus of research is on the measurement of spatial resolution properties, conformance to the concept of perceptual linearization and finally, analysis of spatial and temporal noise and its effect on image perception.

The project has been supported by a grant from the National Institute of Health

Department of Electrical Engineering, Instrumentation and Signal Processing Laboratory, University of Roorkee, India **January-May 2000**
(B.E. Senior year major project)

Comparative study of various transformative techniques like DCT, FFT and Wavelet Transformation for compression of ECG data was done.

Department of Electrical Engineering, Biomedical Eng. Laboratory, Indian Institute of Science (IISc), Bangalore June-July 1999
Undergraduate Research Assistant

Worked on the project titled *'Compression of ECG by Average Normalized Beat Subtraction'.* Compression of ECG signals (MIT/BIH database) was accomplished by downsampling the non-QRS complex of the average PAN (Period and Amplitude Normalization) beats, followed by Huffman coding and upsampling which resulted in a low NRMSE of 2.05% (as compared to 9.9% achieved by many other compression techniques).

Department of Electrical Engineering, Instrumentation and Signal Processing Laboratory, University of Roorkee, India **June-July1998**
Undergraduate Research Assistant

Developed software for a *'Dedicated system for vibration Testing of EM and STATIC meters on PLC based on 8032 microcontroller implementing closed loop control law',* in a team of two. Implemented a closed loop digital control software using the C-51 Archimedes cross compiler and A8051 Assembler.

A.G Measuramatics Private Ltd., Roorkee, India **January-May 1998**
Volunteer

Programmed in assembly language of 8086 to interface the microprocessor to serial/parallel interfaces to initialize a

• complete CPU

Class Projects

- Designed and implemented a kernel of an operating system on USLOSS simulator.
- Developed a face recognition system based on Principal-Component Analysis and DCT
- Implemented a noise-canceling system by Adaptive FIR filter using the LMS algorithm.
- Class presentation on *'Approximation of FIR by IIR digital filters based on Balanced Model Reduction'*
- Worked in Yacsim to implement Fair Queuing and First Come First Serve Scheduling Algorithm

Paper Presentations/Publications

- Chawla A., Roehrig H., Fan J., Gandhi K., *'Real-time evaluation of displays in the clinical arena'*, submitted to SPIE's conference on Medical Imaging, San Diego, Feb. 15-20, 2003
- Roehrig H., Krupinski A., Chawla A., Fan J., Gandhi K., *'Spatial Noise and Threshold Contrasts in LCD Displays'*, submitted to SPIE's conference on Medical Imaging, San Diego, Feb. 15-20, 2003
- Roehrig H., Fan J., Furukawa T., Chawla A., Gandhi K., *'Performance evaluation of LCD displays'*, Computer Assisted Radiology and Surgery (CARS) 2002, Proceedings of the 16th International Congress and Exhibition, Paris, pp. 461-466.
- Roehrig H., Fan J., Chawla A., Gandhi K., *'The Liquid Crystal Display(LCD) for Medical Imaging in Comparison with the Cathode Ray Tube Display(CRT)'*, Invited paper, Proceedings of SPIE, Seattle, Vol. 4786, pp 114-131, July 9-11, 2002
- Roehrig H., Chakraborty D.P., Fan J., Chawla A., Gandhi K., *'The Modulation Transfer Function (MTF) of CRT display systems'*, Proceedings of the Department of Defense Breast Cancer Research Program Meeting-ERA OF HOPE, Florida, Vol. 2, Poster Session 28, Sept. 25-28, 2002
- Chawla A.S, *'Wavelets and Multiresolution Analysis'*, INFLUX 1999, Department of Electrical Eng., University of Roorkee
- Chawla A.S and Joshi K.K, *'Solar Power Satellites- a solution to our power problems'*, INFLUX 1997, Department of Electrical Eng., University of Roorkee

Computer and Programming Skills

- ***Languages***
  C, Data Structures with C, Assembly of 8085/8086/8032, FORTRAN, HTML
- ***Tools***
  MATLAB, IDL (Interactive Data Language), Visual C++, USLOSS (Unix Software Library for Operating System Simulation), Archimedes Cross Compiler For 8051 Family (Archimedes Software Inc.), Yacsim (a process oriented discrete event simulation package based on the C programming language)
- ***Environments***
  UNIX, LINUX, MS Windows

Academic Achievements

- **First Prize** at the IEEE recognized all India Students' Technical Symposium-INFLUX '97 organized by the Department of Electrical Engineering, University of Roorkee for my paper entitled *'Solar Power Satellites- a solution to our power problems'*
- Selected for Co-op with *Advanced Micro Devices Inc.* (Fall Rush 2001)
- Been a recipient of the **University Merit Scholarship** for outstanding undergraduate academic performance

Professional Affiliation

Student member of the IEEE and SID (Society for Information Display).

Kunal Gandhi

819, East Drachman Street
Tucson, AZ 85719.

kgandhi@ece.arizona.edu
Phone: (520) 624 4467

Education:

Masters in ECE, University of Arizona, *Tucson* *(August 2000- present)*
GPA = 3.6/4.0
MSEE, University of Memphis *(August 1999-May 2000)*
Completed two semesters of graduate study (GPA= 3.75/4.0)
Bachelor of Engineering in Biomedical, *Bombay, India (June 1995- June 1999)*
Rank: 5/100

Relevant Courses Taken:

Random Processes in Engineering Applications	Image Analysis
Digital Communication Systems I	Digital Signal Processing
Digital Communication Systems II	Digital Image Processing
Information Theory	Channel Coding

Projects:

- **Soft-Copy Analysis of Mammograms:**
  - Quality evaluation of various CRTs/LCDs.
    Ex: *Modulation Transfer Function; Conformance to the DICOM curve.*
  - Analysis of spatial and temporal noise of the displays.
- **Digital Communication Systems:**
  - Designed a ***Viterbi Equalizer*** that gives hard decisions and reliability outputs for different types of partial response channels ***(Soft Output Viterbi Algorithm).***
  - Simulating a ***Satellite Communications Channel*** using PSK and QAM modulation techniques and calculate the SNR and the probability of error.
  - Implemented ***Reed-Muller Codes*** for Image Restoration.
- **Image Segmentation Using Genetic Algorithms**: Implemented Edge Detection using the *Simple Genetic Algorithm(SGA).*
- **Image Super-resolution:** Co-developed a package in VC++ wherein all algorithms developed in the IPDSL lab are integrated.
- **PC- based Cardio-Respiratory Analyzer at Bhabha Atomic Research Center, India** The project involved detection of heart rate variability and peripheral blood flow, non-invasively.
- **555- based Transcutaneous Nerve and Muscle Stimulator:** The instrument produced controlled pulses of current which, when used to stimulate nerves and muscles, helps in easing pain.

Technical Skills:

- ***Programming Languages:*** C
- ***Operating Systems:*** Windows 95/98/NT, Linux RH 7.x, Unix, SunOS
- ***Development/Design Tools:*** MATLAB , IDL

Work Experience:

- **Research Assistantship** *June 2001-present*
  The Department of Radiology, University of Arizona
  Working on improving displays of Mammogram devices.
- **Research Assistantship** *August 2000 – June 2001*
  The Information Processing and Decision Systems Laboratory, Department of ECE, University of Arizona
  Worked on Super-resolution Algorithms for restoration of PMMW Images

Publications:

- H.Roehrig, J.Fan, T.Furukuwa, A.Chawla, *K.Gandhi*, **"Performance Evaluation of LCD Displays"**, *Computer Assisted Radiology and Surgery, CARS 2002, pp 461-466.*
- H.Roehrig et al, **"Evaluation of Plain-Film Digitizers: A Comparison of Different Systems and Models"**, *Proc. SPIE, Medical Imaging pp 694-703.*

Honors and Awards:

- 1993 Recipient of National Talent Scholarship awarded by the Central Board of Education of India

References: Available on request